NONLINEAR FINFITE ELEMENT ANALYSIS OF REINFORCED CONCRETE CYLINDRICAL SHELLS AND FOLDED PLATES WITH EDGE BEAMS

A THESIS
SUBMITTED TO THE COLLEGE OF ENGINEERING OF THE UNIVERSITY OF BABYLON IN FULFILLMENT OF PARTIAL REQUIREMENTS FOR THE DEGREE OF MASTER OF SCIENCE
IN
CIVIL ENGINEERING
(STRUCTURAL ENGINEERING)

By

Maitham Karim Al-Tae'y

B.Sc. ٢٠٠٠

Shawal ١٤٢٤ December ٢٠٠٣

التحليل اللاخطي بالعناصر المحددة للقشريات الاسطوانية والصفائح المطوية من الخرسانة المسلحة مع أعتاب طرفية

رسالة

مقدمة إلى كلية الهندسة في جامعة بابل كجزء من متطلبات نيل درجة ماجستير علوم في الهندسة المدنية (هندسة إنشائية)

ميثم كريم الطائي

بكالوريوس هندسة مدنية

٢٠٠٠

شوال ١٤٢٣ **كانون أول ٢٠٠٣**

بسم الله الرحمن الرحيم

قَالُواْ سُبْحَانَكَ لاَ عِلْمَ لَنَا إِلاَّ مَا عَلَّمْتَنَا إِنَّكَ أَنتَ الْعَلِيمُ الْحَكِيمُ

صدق الله العلي العظيم

سورة البقرة – الآية (٣٢)

الخلاصة

تتناول هذه الدراسة التحليل اللاخطي للازاحات الكبيرة للقشريات الاسطوانية والالواح المطوية الكونكريتية بطريقة العناصر المحددة. تم استخدام العناصر الطابوقية ثلاثية الابعاد ذات الثمانية والاربعة عشر والعشرين عقدة لتمثيل الكونكريت. اما بالنسبة لحديد التسليح فقد تم تمثيله كعناصر محوريه مطمورة داخل العنصر الطابوقي ثلاثي الابعاد مع فرض وجود ترابط تام بين بين الخرسانة وحديد التسليح.

أعتبر تصرف الخرسانة تحت تأثير اجهادات الإنضغاط تصرفا مرنا-لدنا يتبعه تصرف لدن تام ينتهي عند تهشم الخرسانة. اما بالنسبة للمنطقة الواقعة تحت تأثير اجهادات الشد فقد تم أستخدام أنموذج الشق المنتشر (Smeared Crack Model) لتمثيل تصرف الخرسانة مع اعتماد أنموذج تصلب الشد (Tension-Stiffening Model) لتمثيل الاجهادات المتبقية بعد مرحلة التشقق.

تم حل معادلات التوازن اللاخطية باستخدام طريقة تزايدية-تكرارية (-Incremental Iterative Technique) اعتمادا على الطريقة المعدلة لنيوتن-رافسون. تمت السيطرة على اقتراب الحلول من خلال استخدام معيار الاقتراب المبني على أساس القوى.ثلاثة انواع من التكاملات العددية (٢٠ , ١٥a , ٨) تم استخدامها لتحليل التطبيقات الموجودة في هذه الاطروحة .

اللاخطية الهندسية (Geometrical Nonlinearity) تم حلها بالاعتماد على أسلوب لاجرانج (Lagrange) الكلي مع الخذ بعين الاعتبار فرضيات(Von Karman) .

تم تطبيق الدراسة على المنشئات القشرية ذات التقوس باتجاه واحد (Cylindrical Shell) بالاضافة الى الالواح المطوية (Folded Plate) التي تحتوي على أعتاب طرفية لمعرفة قابلية البرنامج على تحليلها. كانت النتائج المحصلة متوافقة بشكل جيد مع النتائج العملية والنظرية المنشورة لهذه الامثلة.

كما تضمنت الدراسة تاثير بعض العوامل على تصرف المنشئات التي استخدمت في هذه الرسالة. هذه العوامل هي : تغير السمك، ارتفاع العتب الطرفي، تغيير نسبة حديد التسليح، بالاضافة الى بعض العوامل الاخرى.

بالاعتماد على نتائج هذه الدراسة، فان حمل الفشل القصى كان حساسا جدا للتغيير في زاوية المنشا القشري. فقد ادت زيادة الزاوية من ٨٠° الى ١٨٠° الى زيادة في حمل الفشل من ٤٩.٣kN الى ١٥٩.٣kN . وبالاعتماد على تلك النتائج، فقد زاد الحمل الاقصى ٢.٨٩ مرة عند زيادة سمك القشرة من ١٠mm الى ٣٠mm .كما كانت هناك زيادة ملحوظة في مقدار الحمل الاقصى عند زيادة نسبة حديد التسليح.

بالنسبة للالواح المطوية، كانت زاوية الميلان عاملا مؤثرا في تحديد مقدار الحمل الاقصى للفشل. لقد كان هناك تناقص في مقدار حمل الفشل مقداره ٠.٧٣ عند زيادة زاوية

الميلان من ٣٠° الى ٦٠° . ادت الزيادة في نسبة الحديد بالاتجاه القصير(التسليح الرئيسي) والتي مقدارها ٢٠٠٪ الى زيادة تحمل المنشا الى ١٥٢٪ .

تم اقتراح معادلتين لحساب مقدار التحمل الاقصى للقشريات الاسطوانية والالواح المطوية لحالات مختلفة وكما موضحة في الفصل الخامس.

ABSTRACT

This study deals with nonlinear large displacement analysis of reinforced concrete shells and folded plates by the finite element method. The ٨, ١٤ and ٢٠-node brick element have been used to model the concrete. The reinforcing bars are modeled as axial members embedded within the brick element. Perfect bond between the concrete and the reinforcing bars was assumed to occur.

The elasto-plastic strain hardening model followed by perfectly plastic response is used to simulate the compressive behavior of concrete. This response is terminated at the beginning of crushing. In tension, linear elastic behavior prior to cracking is assumed. A smeared crack model with fixed orthogonal cracks is adopted to represent the fracture of concrete.

The nonlinear equations of equilibrium have been solved by using an incremental-iterative technique operating under load control. Modified version of the Newton-Raphson method has been employed. Various integration rules (٢٠, ١٥a and ٨points) have been used in the analysis of the applications presented in this study.

A nonlinear geometrical model based on the total Lagrangian approach and taking into account Von Karman assumptions is considered.

The study was applied on reinforced concrete shell structures and folded plates including edge beams to test the validity of the program in the analysis. A good agreement has been achieved between the examples analyzed in this research work and their published experimental and theoretical results.

Also the study included effect of some parameters on the behavior of shell and folded plate structures. The parameters include; change of the thickness, edge beams height, change of the reinforcement ratio and some other parameter.

Based on the results of this work, the ultimate collapse load was very sensitive to the variation in the angle of shell. When the shell angle (θ) increased from ٨٠° to ١٨٠°, the failure load increased from ٤٩.٣kN to ١٥٩.٣kN. From the results obtained, it was found that the ultimate load of the cylindrical shell could be increased up to ٢.٨٩ times when the thickness of shell increased from ١٠mm to ٣٠mm. The increase in the height of edge beam gave significant increase in the ultimate load especially when the shell angle is increased. A

noticed enhancement is gained from increasing the steel reinforcement by increasing the ultimate load carrying capacity and the ultimate deflection.

For The folded plate, the inclination angle has also significant effect on increasing or decreasing the ultimate load. The ultimate load is decreased ٠.٧٣ times, when the inclination angle is increased from ٣٠^{o} to ٦٠^{o}. The increasing in the percent of short direction steel reinforcement to ٢٠٠٪ an increase in the failure load equals to ١٥٢٪.

Two simplified equations to determine the ultimate collapse load for cylindrical shells and folded plates were suggested to calculate the collapse load of these structures for different cases which were explained in chapter five.

ACKNOWLEDGEMENT

Praise be to ALLAH, most gracious, and most merciful, who gave me the ability and desire to complete this research work.

The author wishes to express his cordial thanks and deepest gratitude to his supervisors ***Dr. Nameer A. Awash*** and ***Dr. Mustafa Balasim*** for their generous guidance, valuable suggestions and active interest in the author's work.

The author also wishes to express his special thanks to ***Dr. Ihsan Al–Shaarbaf*** for his appreciable assistance in conducting the computer program.

A special words of thanks due to ***Mr. Usama Al–Safar, Mr. Ahmed Zeki Mohammad*** ,and ***Mr. Haider Abdul–Ameer Baka*** who supported me through the preparation of this work.

I wish to express my deepest thanks for all my friends who supported me thought the preparation of this work.

The author would likes to express his thanks to the ***AL-Ajial Computer Center*** for their financial support to this research.

Finally, the author wishes to express his deepest thanks to his family for all the love and support during the preparation of this research.

CERTIFICATION

We certify that this thesis titled **Nonlinear Finite element Analysis of Reinforced Concrete Cylindrical Shells and Folded Plates With Edge Beams** was prepared by **Maitham Karim Hamza Al-Tae'dy** under our supervision at Babylon University in partial fulfillment of the requirement for the degree of Master of Science in Civil Engineering.

Signature:	**Signature:**
Asst. Prof. Dr. Nameer A. Alwash	**Asst. Prof. Dr. Mustafa B. Dawood**
(Supervisor)	**(Supervisor)**
Date: / /٢٠٠٤	**Date**: / /٢٠٠٤

EXAMINING COMMITTEE CERTIFICATE

We certify that we have read this thesis, titled **Nonlinear Finite element Analysis of Reinforced Concrete Cylindrical Shells and Folded Plates With Edge Beams**, and as examining committee examined the student **Maitham Karim Hamza Al-Tae'y** in its contents and in what is connected with it, and that in our opinion it meets the standard of a thesis for the degree of Master of Science in Civil Engineering.

Signature:
Asst. Prof. Dr. Ali Al-Athary
(Member)
Date: / /٢٠٠٤

Signature:
Asst. Prof. Dr. Mahdi S. Essa
(Member)
Date: / /٢٠٠٤

Signature:
Prof. Dr. Husain M. Husain
(Chairman)
Date: / /٢٠٠٤

Signature:
Asst. Prof. Dr. Nameer A. Alwash
(Supervisor)
Date: / /٢٠٠٤

Signature:
Asst. Prof. Dr. Mustafa B. Dawood
(Supervisor)
Date: / /٢٠٠٤

Approval of the Civil Engineering Department
Head of the Civil Engineering Department

Signature
Asst. Prof. Dr. Ammar Yaser Ali
Date: / /٢٠٠٤

Approval of the Deanery of the College of Engineering
Dean of the College of Engineering

Signature
Asst. Prof. Dr. Haron A. Shahad
Dean of the College of Engineering
University of Babylon
Date: / /٢٠٠٤

LIST OF CONTENTS

CHAPTER FOUR: APPLICATIONS, RESULTS AND DISCUSSION

CHAPTER FIVE: PARAMETRIC STUDY

CHAPTER SIX: CONCLUSIONS AND RECOMMENDATIONS FOR FURTHER WORKS

NOTATIONS

$[A]$	**Matrix which contains the differential operators**
$\{a\}$	**Displacement vector**
$\{a\}^e$	**Nodal displacements**
As	**Cross-sectional area of steel**
B	**Body forces**
$[B]$	**Strain – displacement matrix**
$[B_o]$	**Linear strain – displacement matrix**
$[B_{nl}]$	**Nonlinear strain – displacement matrix**
$[B']$	**Strain – displacement matrix of bar element**
$[B'_o]$	**Linear strain – displacement matrix of bar element**
$[B'_{nl}]$	**Nonlinear strain – displacement matrix of bar element**
C_p	**Plasticity coefficient**
$[D]$	**Constitutive matrix**
$[D]^e$	**Elastic constitutive matrix**
$[D']$	**Constitutive matrix of the bar element**
D_{cr}	**Cracked material stiffness in the local axis**
E_1	**Reduced modulus of elasticity**
$\{f\}$	**Applied load vector**
$f'c$	**Ultimate compressive strength of concrete**
f_t	**Maximum tensile strength of concrete**
G	**Shear modulus of elasticity**
H'	**Hardening parameter**
I_1	**First stress invariant**
$\bar{I}_1$	**First strain invariant**
$[J]$	**Jacobian matrix**
J_2	**Second deviatoric stress invariant**
$\bar{J}_1$	**Second deviatoric strain invariant**
$[k]$	**Stiffness matrix**
$[\bar{k}]$	**Stiffness matrix of the concrete element**
$[k]_\sigma$	**Geometric stiffness matrix**
$[\bar{k}']$	**Stiffness matrix of the bar element**
$[k']_\sigma$	**Geometric stiffness matrix of the bar element**
i, m, n	**Directional cosines in the x, y, z directions respectively**
$[N]$	**Matrix containing interpolation functions**
N_i	**Shape function at the ith node**
$\{P\}$	**Internal force vector**
$\{u\}^e$	**Displacement vector at any point within the element**

u, v, w	**Displacement components in x, y and z – direction respectively**
$u_{i,}$ v_i, w_I	**Nodal displacement**
V	**Volume**
W_{ext}	**External work**
W_i	**Weight of the sampling point**
W_{int}	**Internal work**
x, y, z	**Global or Cartisian coordinates**
x_i, y_i, z_I	**Global coordinates of ith node**
α, β	**Material parameters**
α_1	**The rate of stress release as the crack widens**
α_2	**Sudden loss of stress at instant of cracking**
$\beta_{\backslash}$	**Reduction factor**
ε	**Strain**
ε_c	**Total effective strain of concrete**
ε_{cr}	**Cracking strain**
ε_{cu}	**Ultimate concrete strain**
ε_e	**Elastic component of total effective strain of concrete**
ε_p	**Plastic component of total effective strain of concrete**
$\{\varepsilon\}$	**Strain vector**
$\{\varepsilon'\}$	**Strain vector of bar element**
$\{\varepsilon_p\}$	**Effective accumulated plastic strain vector**
$\{\varepsilon_{nl}\}$	**Nonlinear component of strain vector**
$\{\varepsilon'_{nl}\}$	**Nonlinear component of strain vector of embedded steel bar**
$\{\varepsilon'_o\}$	**Linear component of strain vector of embedded steel bar**
λ	**Compression reduction factor**
γ_1	**Rate of decay of shear stiffness as the crack widens**
γ_2	**Sudden loss in shear stiffness at the instant of cracking**
γ_3	**Residual shear stiffness due to the dowel action**
σ	**Stress**
$\bar{\sigma}$	**Equivalent uniaxial stress**
σ_{cr}	**Cracking stress of concrete**
σ_o	**Equivalent effective stress at the onset of plastic deformation**
$\{\sigma\}$	**Stress vector**
ξ, η, ζ	**Local coordinate system**

CHAPTER ONE

INTRODUCTION

١.١ General

Reinforced concrete is the one of the most commonly used construction material. It is a composite material consisting of concrete and steel reinforcement. The two materials have widely different properties. The properties of reinforcing steel are generally known and well understood. On the other hand, the properties of concrete under various stress combinations have not been fully interpreted.

For concrete, it is well known that the mechanical properties depend upon particular condition of mixing, placing, curing, nature and rate of loading and environmental influences. Extensive experimental studies have been undertaken to study the response of ultimate strength of plain concrete under multiaxial stress state [Bresler and Pister (١٩٥٨), Tasuji, Slate and Nelson (١٩٧٨)]. Considerable scattering of results have been observed and collaborative studies have been undertaken to identify the principal factors influencing this variation [Neville (١٩٨١), Mirza, Hazinikdas and McGregor (١٩٧٩)].

Research and experimental data have been achieved on the behavior and properties of reinforced concrete as a material, and also on reinforced concrete structures. This helps engineers to understand better the nonlinear behavior and encourages them in construction field to increase the use of reinforced concrete as a construction material for different forms and shapes of structures.

An analytical procedure for the prediction of the complete response of such structures through the pre and post – cracking range up to failure is necessary to assess the true factor of safety against collapse and serviceability requirements. At present the finite element method offers a powerful and a general tool to investigate the behavior of such reinforced concrete structures and plays an important role in the analysis and design of these structures (Baka ٢٠٠٢).

In recent years, nonlinear finite element analysis has proven to be an extremely effective means for analyzing concrete structures. The complex behavior of reinforced concrete structures including cracking, crushing, yielding and tension stiffening, (previously treated in a very approximate way) can presently be incorporated into the analysis in a more rational manner. The correct prediction of reinforced concrete structures response can be achieved by using the finite element method. It provides a valuable tool for research as well as offering a basis for codes of practice and building specifications (Thannon ١٩٨٨).

A considerable number of successful theoretical and practical studies have been published on the nonlinear analysis of reinforced concrete stiffened plates and stiffened shells by using degenerated shell element only or by using degenerated shell and curved beam elements. While investigations on stiffened plates and shells by using all types of brick element are still lacking. Attempts to analyze plate and shell with effect of edge beam and end diaphragm by using eight, fourteen and twenty node brick element have proved inadequate to predict the actual behavior of the structure up to its ultimate load.

١.٢ Objective and Scope

The aim of the present study is to investigate the overall structural behavior of reinforced concrete plates and shells with effect of edge beam and end diaphragms. In this study, the behavior of plate and shell is simulated by nonlinear three-dimensional finite element. Both material and geometric nonlinearity are simulated by eight, fourteen, and twenty node brick elements.

The computer program ***P٣DNFEA*** that was originally developed by Al–Shaarbaf (١٩٩٠) uses finite element analysis of reinforced concrete members by eight, and twenty node brick elements with material nonlinearity. The modification to this program that was carried out by Mohammed (٢٠٠١), was the incorporation of the geometrical nonlinearity. The main modifications to the computer program which have been carried out in the present study, was the analysis of reinforced concrete structure by fourteen node brick element in addition to the previous elements. Also, the present study is an attempt to investigate the effect of edge beams on the shell and folded plate behavior.

Many other parameters affect the behavior and load carrying capacity like the amount of reinforcement, the edge beam height, end diaphragm, thickness of plate and shell, and some other parameters. The effect of brick element type is also studied.

١.٣ Layout of The Thesis

This thesis consists of six chapters. Chapter one introduces the problem within hand. Chapter two contains a brief review of the previous studies that are related to the nonlinear finite element analysis of reinforced concrete plates and shells. The formulation of eight, fourteen, and twenty-node brick elements, constitutive relations of concrete and steel also presented in Chapter three. Chapter four contains numerical applications to test the validity of the constitutive relationships and finite element formulation. The parametric study and the empirical equations obtained from this study are given in Chapter five. Chapter six gives a summary of the conclusions that can be drawn from this study and the suggestions for further work.

CHAPTER TWO

REVIEW OF LITERATURE

٢.١ Finite Element Method

The finite element method has become a powerful tool for the numerical solution of a wide range of engineering problems. Applications range from deformation and stress analysis of automotive, aircraft, building, and bridge structures to field analysis of heat flux, fluid flow, magnetic flux, seepage and other flow problems. With the advances in computer technology and computer aided design system, complex problem can be modeled with relative ease (Tirupathi ١٩٩٦).

Basic ideas of the finite element method originated from advances in aircraft structure analysis. In ١٩٤١, Hrennikoff presented a solution of elasticity problems using the “Framework method”. Courant’s paper, using a piecewise polynomial interpolation over triangular subregions to model torsion problems, appeared in ١٩٤٣.

Argyris and Kelsey in ١٩٥٦ developed efficient solution techniques for analyzing complicated structure configuration. These techniques used in the aircraft industry, helped to establish the foundation for further development in the finite element studies.

Turner et al. derived stiffness matrices for truss bar, beam, and other elements and presented their findings in ١٩٥٦. In ١٩٦٠ the term **finite element** was first coined and used by Clough in a paper on plane elasticity problems.

In the early ١٩٦٠s, engineers used the method for approximate solution of problems in stress analysis, fluid flow, heat transfer, and other areas. The first book on finite element by Zienkiewicz and Cheung was published in ١٩٦٧. In the late ١٩٦٠s, and early ١٩٧١s, there was a growing interest in the application of the finite element procedure to the analysis of reinforced concrete structure, particularly with respect to the influence of cracking on the response. In ١٩٧٢ Scordelis wrote a comprehensive survey of finite element analysis of reinforced concrete structure.

Success in developing finite element models for application to reinforced concrete is closely linked to the development of quantitative information concerning the load-deformation behavior of concrete. Formulation of such information in a suitable form for use in the analytical technique is essential.

At present, the development in mainframe computers and availability of powerful microcomputers has brought this method within reach of researchers and engineers working in engineering industrial fields.

٢.٢ Finite Element Method for Analysis of Reinforced Concrete Members

Ahmad et al. in ١٩٧٠ originally produced the degenerated shell element for the linear finite element analysis of thick and thin shell structures. The three dimensional stress and strain conditions were degenerated to a shell behavior by employing isoparametric element with independent rotation and displacement degrees of freedom. The Mindlin's assumption was used in place of Kirchhoff hypothesis. In the formulation of this element only the nodes on the mid-surface of the element were retained. Five degrees of freedom were used at each node (three displacements and two independent rotations).

Zienkiewics et al. in ١٩٧١ achieved a great improvement of this element by using reduced integration techniques in general analysis of plate and shell problems.

In ١٩٧٢, Valliappan and Doolan used the finite element method for determining the stress distribution in reinforced conctere structures not only due to the limited tensile strength of concrete, but also due to the elasto-plastic behavior of concrete and steel. The Von-Mises yield criterion had been used for both steel and concrete. A two-dimensional displacement method of analysis had been used in this study. The triangular elements were used for the concrete, and the bar elements to model the reinforcement. The results of the numerical examples indicated that this type of analysis would be valuable to the design engineer as it offers a complete picture of the stress distribution both in concrete and steel.

Hand et al. in ١٩٧٣ used doubly curved shallow shell layered nonlinear finite element to analyze reinforced concrete plates and shells and obtained the load-deflection history up to failure. The reinforcing steel is assumed to be elastic-plastic and bilinear elasto-plastic behavior is used for concrete. The concrete is assumed to be tension-limited and to yield in biaxial compression in accordance with a yield criterion proposed by Kupfer and Gerstle (١٩٧٣). A comparison of the numerical results obtained from finite element analysis of plate and shell showed a good agreement with experimental results.

In ١٩٧٣, Suidan and Schnobrich presented a finite element analysis of reinforced concrete beams, which utilizes three-dimensional isoparametric ٢٠-node brick elements to simulate the concrete, while, the steel reinforcement was assumed to be smeared throughout the concrete element. An elastic-perfectly plastic behavior for both steel and concrete was assumed. The Von-Mises yield criterion was adopted to indicate yielding condition. Perfect bond between steel and concrete was assumed to occur. Cracking occurred when the principal tensile stress violates the specific tensile strength of concrete and consequently, the stiffness normal to the crack was reduced to zero. The analysis also includes a factor for shear-retention in the cracked planes of concrete. The predicted behavior of reinforced concrete beams analyzed by this manner was compared against the experimentally observed behavior of the same beams. Good agreement has been obtained between the predicted and the experimental behavior.

Mawenya and Davies in ١٩٧٤ used the finite element technique to account for the effect of membrane action in orthotropically reinforced concrete slabs. The analysis included the effects of inplane stresses. The results obtained in this study were compared with the classical thin plate theory solutions.

Review of Literature

Scanlon in ١٩٧٤ presented a finite element model which is capable of simulating the behavior of reinforced concrete slabs at working loads, including the effects of nonuniform reinforcing and tensile cracking. This study concentrates on technique for including the effect of creep and shrinkage.

Also Lin and Scordelis in ١٩٧٥ used triangular finite elements for the nonlinear analysis of reinforced concrete shells of general form. The analysis includes tracing the load-deflection response and the crack prorogation through the elastic, inelastic and ultimate ranges. A layered approach was used to represent both the concrete and the steel. A bilinear state of stress was assumed for both the concrete and the steel, and the tension stiffening effect of the concrete between cracks was included in such study and was found to have significant influence on the post-cracking load-deflection response of under reinforced concrete structures.

In ١٩٧٦, Phillips and Zienkiewicz presented a nonlinear analysis of reinforced concrete structures by using the finite element technique. Nonlinear effects such as cracking, multiaxial compressive behavior of concrete, yielding of reinforcement and to a lesser extent, aggregate interlocking were included. Isoparametric elements, under plane and axisymmetric conditions, were used to represent the concrete, while steel reinforcement was simulated by special line elements embedded within the isoparametric elements. Perfect bond between concrete and steel bars was assumed. A linear elastic-fracture model simulating the behavior of concrete in tension and cracking was handled by adjusting the stress level and material properties in the cracked zone. In compression, two models were adopted to predict the concrete behavior, the first model was based on experimental uniaxial and biaxial stress-strain relationships, and the second model was based on deviatoric and hydrostatic components of stress and strain. Several realistic concrete structures were analyzed and the finite element solutions were compared with experimental evidence. It has been shown that the behavior of reinforced concrete structures was generally well predicted by the method presented. The load-displacement relationships, and the location and direction of tensile cracking were determined with sufficient accuracy.

In his research, Kabir (١٩٧٦) extended the work of Lin and Scordelis to include the time dependent effect of creep, shrinkage and load history for the nonlinear analysis of reinforced concrete shells.

In ١٩٧٧, Buyukozturk used doubly curved isoparametric thin shell finite elements to analyze reinforced concrete deep beams and cylindrical shells subjected to short time loading. A generalization of the Mohr-Coulomb criterion was made in terms of the principal stress invariants. The generalized yield and failure criteria were developed to account for the progressive cracking of concrete in tension, and the nonlinear response of concrete under multiaxial compressive stresses. Using these criteria, incremental stress-strain relationship was established in suitable form for the nonlinear finite element analysis. Equivalent isotropic steel layers represented the actual reinforcing bars. These layers carry uniaxial stresses only in the same direction as the actual bars. The effect of dowel action was neglected in this work.

In ١٩٧٩, Bergan and Holand used the finite element method for the nonlinear analysis of reinforced concrete beams, shear walls, and slabs under short time loading and/or cyclic loading. Simple beam elements with three and four degrees of freedom per node and rectangular elements with four corner nodes, each node has two degrees of freedom were used to simulate the concrete structure. The reinforcement was idealized either by discrete bar elements or smearing out into a steel layer. Full compatibility between concrete and reinforcement displacements was assumed to occur. A smeared crack model was used to simulate the behavior of concrete in tension, while the endochronic theory of plasticity was used to model the behavior of concrete in compression. Geometric nonliearity based on total and updated co-rotational description involving nonlinear strain expressions were considered in this analysis. The results of ultimate loads and deflections show good agreement between the numerical models and the experimental results. It was concluded that the geometric nonlinearity plays an important role for predicting the ultimate strength of the plates.

Bathe and Bolourchi in ١٩٨٠ applied the finite element method for the analysis plates and shells including geometric and material nonlinearity. The element was formulated by interpolating the element geometry using the mid-surface nodal point coordinates and mid-surface nodal point normals. Total and updated Lagrangian formulations are adopted that allow very large displacements and rotations. The element is implemented as a variable-number-nodes element and could be employed as a fully compatible transition element to model shell intersections and shell-solid regions.

In their paper, Arnesen et al. (١٩٨٠) developed a numerical procedure based on the finite element method for the analysis of plane stress problems and plates and shells under monotonically increasing load up to failure. Both the flow theory of plasticity and the endochronic theory of plasticity were used in the constitutive laws for concrete and reinforcement. General ٤-node quadrilateral elements with selective sampling of strain and triangular shell elements were used in the discretization. Geometric nonlinearity was accounted for through updating of coordinates for the shell elements in the analysis of plates and shells. Reinforced concrete beams, corbels, square plates and shells were analyzed and compared with several experimental results. These studies show good agreement with experimental results.

Bathe and Ho in ١٩٨١ adopted a simple flat three-node triangular shell element for linear and nonlinear analysis of general shells. The element stiffness matrix with six degrees of freedom per node is obtained by superimposing its bending and membrane stiffness matrices. An updated Lagrangian formulation was used for large displacement analysis. The application of the element to the analysis of various linear and nonlinear problems was demonstrated also.

Abdel-Rahman and Hinton in ١٩٨٦ presented linear and nonlinear finite element analysis of reinforced and prestressed concrete cellular slabs based on slab-beam model. Mindlin/Timoshenko assumptions are adopted in the slab-beam model which thus allows for transverse shear deformation. A layered approach was used to represent the concrete and steel. The slab-beam model consists of Mindlin plate elements to represent the slab and Timoshenko beam elements to represent the eccentric beam stiffeners. A reference plane at which all degrees of freedom are defined is usually chosen to coincide with plate mid-surface. It is assumed that the stiffeners are monolithically connected to the plate. This assumption implies that identical displacement fields must be produced at the junction between the plate and the beams.

Huang in ١٩٨٧ used the degenerated shell element and improved it by assuming transverse shear and membrane strains. An explanation of the locking behavior and also the location of sampling points for the assumed strains field were given. In order to overcome the shear locking problem of the new element, transverse shear strains in the natural coordinate system were assumed and membrane strains in the orthogonal curvilinear coordinate system were applied to this element to avoid membrane locking behavior. Both linear and nonlinear problems were considered

Thannon, Bicanic and Owen in ١٩٨٧ used degenerated quadratic thick shell element for simulating the behavior of reinforced concrete plates and shells stiffened with eccentric beam systems. The shell elements were employed for the plate and shell body. For the beams, a curved element formulation is adopted based on beam theory with incorporation of transverse shear deformation. A layered approach is used for both shell and beam in order to model the progressive characteristics. The analysis was based on short term loading conditions.

Owen, Thannon and Bicanic in ١٩٨٧ used degenerated quadratic shell element and curved beam element for the analysis of reinforced concrete stiffened shells, including both geometric and material nonlinearities. A layered representation through the depth is employed, in conjunction with a simple nonlinear model of reinforced concrete. The curved beam element exhibits the required displacement compatibility with the degenerated shell element, and the six degrees of freedom are capable of representing torsional and transverse bending behavior. Numerical examples for reinforced concrete funicular shells and folded slabs showed good agreement with the experimental work.

Thannon in ١٩٨٨ applied the finite element method for the nonlinear analysis of reinforced concrete stiffened shells and folded slabs. Degenerated quadratic thick shell elements were employed for the shell. For the beam, a curved element formulation was adopted which was based on the beam theory and incorporating transverse shear deformation. For the stiffened shell, the modification of the degenerated shell element that was needed for the connection with curved beam was made. A layered model was employed with special treatment of the combined torque and bending about the weak axis of the beam. Various reinforced concrete beams, stiffened shells, and folded slabs were analyzed. The numerical results of the structures analyzed showed a good agreement with the experimental results.

Guice et al. in ١٩٨٩ presented a truss-element model, which incorporates nonlinear geometric theory to reinforced concrete slabs response by relating the behavior of the slab to that of shallow shell. A simple truss element model, which is typically used in the stability analysis of thin shells, was used to predict the total load-deflection curve for restrained slabs. The comparison of the results with experimental data suggests that it is a reasonable approach to predict the total load-deflection behavior especially when a single degree of freedom model is considered.

In his thesis, Al-Shaarbaf (١٩٩٠) described a three-dimensional nonlinear finite element model suitable for the analysis of reinforced concrete or steel members under general states of loading. The ٢٠-node isoparametric brick element was used to model the concrete, and reinforcing bars were idealized as axial members embedded within the concrete elements. The behavior of concrete in compression was simulated by an elasto-plastic work hardening model followed by a perfectly plastic response, which is terminated at the onset of crushing. In tension, a smeared crack model with fixed orthogonal cracks was used with the inclusion of models for the retained post-cracking stress and reduced shear modulus. Only material nonlinearity due to concrete behavior in compression, cracking of concrete, yielding of reinforcement was considered. The analysis of reinforced concrete members, which fails in shear or torsion modes, was investigated. The numerical solutions obtained for reinforced concrete panels under pure shear and beams in pure torsion and compound bending and torsion revealed that the inclusion of a model for reducing the compressive strength of cracked concrete can significantly improve the correlation of the predicted post-cracking stiffness and ultimate loads with the experimental results.

In ١٩٩٢, Abbasi et al. applied the finite element method for the nonlinear analysis of reinforced concrete slabs subjected to central patch loads. Using the layered approach, a degenerated quadratic plate element with five degrees of freedom has been employed to model the reinforced concrete slabs. Smeared crack model was used with fixed orthogonal cracking. Several comparisons have been considered in this work. These comparisons are; perfectly plastic models versus hardening models, variation of tension-stiffening parameters, degraded shear modulus and the role of yield criterion.

Review of Literature

Usama in ١٩٩٧ used layered degenerated shell element for the nonlinear finite element analysis of partially restrained reinforced concrete slabs. Perfect bond between the concrete and reinforcement is assumed. The compressive behavior of reinforced concrete is simulated by an elasto-plastic work hardening model. Heterosis isoparametric element has been used to model the concrete. In tension, a smeared crack model with fixed orthogonal cracks has been used with the inclusion of models to account for the retained post-cracking stress and shear modulus. The nonlinear equation of equilibrium has been solved by using an incremental-iterative technique operating under load or displacement control and standard and modified Newton-Raphson solver technique is adopted. Displacement control incrementation scheme is used to trace the falling branch of the load-deflection curve. Good agreement with experimental results for slabs analyzed was gained.

In their paper, Edwards and Billington (١٩٩٨) presented a nonlinear finite element analysis of reinforced concrete hipped hyperbolic paraboloid shell roof. The ٤-node shell elements with six degrees of freedom at each node (three translations, and three rotations) were used to idealize the shell roof. While, the edge beams, columns, and tie beams were modeled by using ٨-node solid elements with three degrees of freedom at each node (three translations). The effects of geometrical nonlinearity and long-term effects of creep and shrinkage were considered in this study. The finite element analysis was based on uncracked materials and assumed that the incremental creep strains were proportional to the stresses and exponentially decaying with time. The finite element results show good agreement with experimental results in terms of failure loads.

In ١٩٩٨, Mohammed investigated the behavior of various ferrocement structures subjected to short time loading, using two-dimensional nonlinear finite element model adopted by Thannon. Both ٨-node Serendipity and ٩-node Lagrangian degenerated quadrilateral shell elements have been used to model the concrete. The reinforcement was idealized as a smeared layer of equivalent thickness throughout the thickness of the shell element. Perfect bond between concrete and steel reinforcement had been assumed. Ferrocement shells, box beams, and slabs were analyzed using the proposed model and showed good agreement with experimental results. A parametric study to investigate the effect of tension-stiffening parameters, effect of number of concrete layers, and the effects of the quadratic Lagrangian elements was also carried out in this work.

In his thesis, Al-Khuza'y (٢٠٠١) used degenerated shell elements for modeling both shells, and edge beams to study different types of concrete shell structures. A layered model is considered in the modeling of the reinforced concrete behavior and a perfect bond between the concrete and reinforcement had been assumed. The compressive behavior of the concrete had been modeled by employing two approaches, both the elastic-strain hardening and elastic-perfectly plastic approach. The nonlinear equations of equilibrium had been solved using the incremental-iterative technique operating under load control. Various integration rules (full, selective, reduced) had been used in the analysis of the applications. A nonlinear geometrical model based on the total Lagrangian approach and taking into account Von Karman assumption is considered. A good agreement with experimental results had been achieved for the used examples. Also the study included the effect of some parameters on the behavior of shell structures.

Mohammed in ٢٠٠١ studied both two and three-dimensional nonlinear finite element models suitable for the analysis of reinforced concrete folded plates. The ٩-node Lagrangian degenerated shell elements and the ٢٠-node isoparametric brick elements have been used to model the concrete. While, the reinforcing bars were modeled as smeared layers of equivalent thickness throughout the shell element or as axial members embedded within the brick elements for the two and three-dimensional models respectively. The finite element results showed good agreement with the experimental results. The influence of simulating the reinforced concrete folded plates by using two or three-dimensional finite elements were also studied. Several parametric studies had been carried like; the influence of increasing concrete compressive strength, amount of reinforcement, plate thickness, span/width ratio, and inclination.

Baka in ٢٠٠٢ applied the nonlinear finite element for the analysis of flat slab and reinforced concrete funicular shell. A layered degenerated quadratic shell elements with five degrees of freedom per node was employed. Both the elastic-perfectly plastic and strain hardening plasticity approach had been employed to model the compressive behavior of the concrete. A smeared fixed cracked approach was used, the reinforcement is represented by equivalent thickness with uniaxial properties. Perfect bond between the concrete and reinforcement has been assumed. The geometric and material nonlinearity were considered in the analysis. Instead of modeling the edge beam in these structures, it was considered as boundary conditions only. Numerical results obtained from the finite element analysis showed good agreement with experimental results.

The present study deals with the case of reinforced concrete shells and folded plates by using three–dimensional nonlinear finite element analysis. Different types of isoparametric brick elements with three degrees of freedom for each node are employed to model the concrete structures. Some parameters affecting the behavior of shells and folded plates are studied herein.

CHAPTER THREE

FINITE ELEMENT MODEL

٣.١ Introduction

The finite element method as a numerical technique for solving complicated boundaries and complex material characteristic problems of solid mechanics offers scope to develop a rigorous and rational analysis of reinforced concrete structures. The method can be thought of as a general method of structural analysis by means of which a solution of a problem in continuum mechanics can be approximated. This can be achieved by analyzing a structure consisting of an assemblage of properly selected finite elements interconnected at a finite number of nodal points.

Nonlinear analysis of reinforced concrete structures has become popular over the last three decades. This approach can be achieved by carrying out a numerical simulation of the complete structural response up to collapse load. In particular, it has proved that it is difficult to describe the highly complex behavior of reinforced concrete within the framework of a unified material law because of its extremely nonlinear response. This nonlinear response involving phenomena like cracking of concrete, yielding of reinforcement, and the nonlinear stress-strain relationship of concrete in compression and interactive effects between the concrete and reinforcement (Bergan and Holand ١٩٧٩). These special properties of reinforced concrete must be considered for material modeling at all stages of loading. Therefore, it is necessary to model the reinforced concrete by considering the constitutive relationships of the composite material. This can be usually achieved by the superposition of constitutive models of the individual material components, concrete and reinforcement (Chen ١٩٨٢).

Structures may exhibit nonlinear behavior due to material or geometric nonlinearities. Geometric nonlinearity is associated only with certain special structural members and systems in which the effect of displacements on initial forces must be considered in the analysis. Long columns, flexible arches, and some thin plate and shell structures are examples of such special structural members. On the other hand, material nonlinearities occur in all reinforced concrete structures and should be considered by using an accurate rational analysis (Nilson ١٩٨٢).

٣.٢ Three – Dimensional Brick Elements

In the ٣D finite element method, the construction of the stiffness matrix of the brick element has been facilitated by three advances in the finite element technology: local coordinates, isoparametric definition and numerical integration (Al – Shaarbaf ١٩٩٠).

These advances revolutionized the finite element field in mid – ١٩٦٠'s, mainly, when the ٨– node linear and the ٢٠ – node quadratic brick elements were presented as shown in Fig. (٣.١c) and (٣.١a) respectively. This two elements were used in representing the three dimensional solid bodies.

Alternatively, Smith and Kidger (١٩٩٢) used a ١٤-node element as shown in Fig. (٣.١b). This element has eight corner and six mid-face nodes.

These elements have been adopted in the present study to show their ability for concrete representation for shell structures and for folded plates.

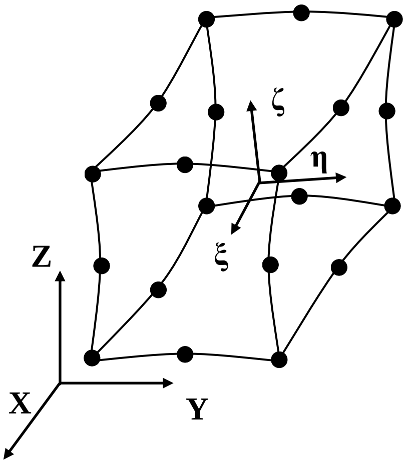

a. Quadratic ٢٠-node brick element

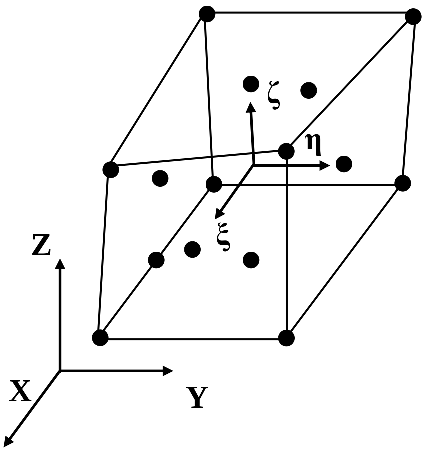

b. ١٤-node brick element

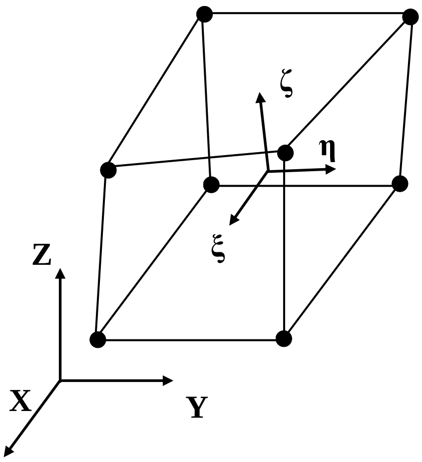

c. Linear ٨-node brick element

Fig. (٣.١) Isoparametric Brick Elements

٣.٢.١ Shape Functions

The natural (local) coordinates system is used to describe the displacement components of a point p (ξ, η, ζ) within the element. These local coordinates (ξ, η, ζ) are scattered in the center of the brick element where the origin point is located as shown in the Fig. (٣.٢)

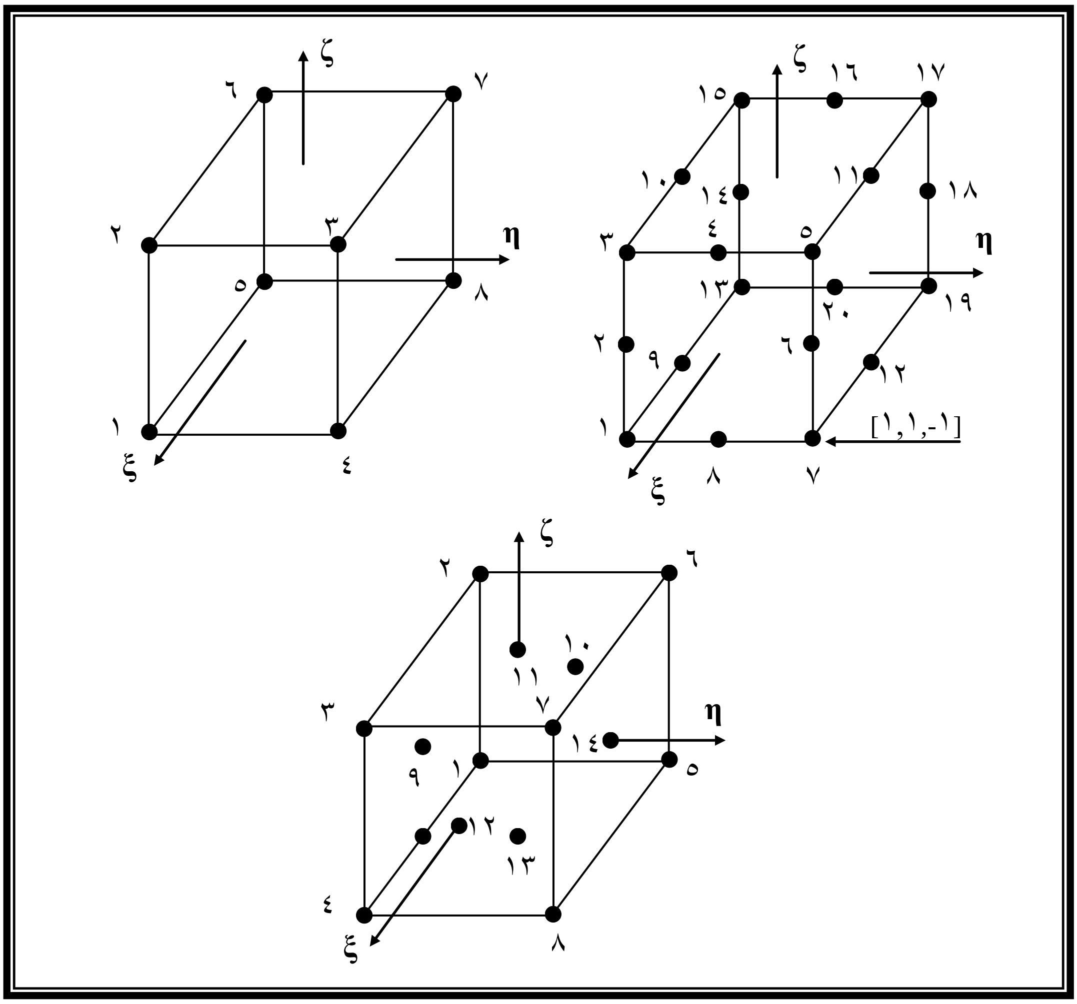

Fig. (٣.٢) Local coordinate system (Smith and Griffiths ١٩٩٨)

Every brick element has ٣ d.o.f per node and bounded by planes with ξ, η, and ζ = ± ١ in ξ, η, ζ space. The starting point for the stiffness matrix derivation is the element displacement field. The isoparametric definition of displacement components is:

$$\left.\begin{aligned} u(\xi,\eta,\zeta) &= \sum_{i=1}^{n} N_i\,(\xi,\eta,\zeta)u_i \\ v(\xi,\eta,\zeta) &= \sum_{i=1}^{n} N_i\,(\xi,\eta,\zeta)v_i \\ w(\xi,\eta,\zeta) &= \sum_{i=1}^{n} N_i\,(\xi,\eta,\zeta)w_i \end{aligned}\right\} \qquad ...(٣.١)$$

where N_i (ξ, η, ζ) is the shape function at the i-th node, n represent the number of nodes per element and u_i, v_i and w_i are the corresponding nodal displacements.

The shape functions of the quadratic ٢٠-node brick element are shown in Table (٣.١)

Table (٣.١) Shape Functions of the Quadratic ٢٠-Node Brick Element (Cook ١٩٧٤)

Location	ξ_i	η_i	ζ_i	Ni (ξ, η, ζ)
Corner nodes	±١	±١	±١	$(١+ \xi \xi_i)(١+ \eta \eta_i)(١+\zeta\zeta_i)\,(\xi \xi_i+ \eta \eta_i + \zeta \zeta_i-٢)/٨$
mid–side nodes	٠	±١	±١	$(١- \xi^٢)(١+ \eta \eta_i)(١+ \zeta \zeta_i)/٤$
mid–side nodes	±١	٠	±١	$(١- \eta^٢)(١+ \xi \xi_i)(١+ \zeta \zeta_i)/٤$
mid–side nodes	±١	±١	٠	$(١- \zeta^٢)(١+ \xi \xi_i)(١+ \eta \eta_i)/٤$

where ξ_i, η_i and ζ_I are local coordinate for i-th node and they are equal ±١.

The shape function, which represents the linear ٨-node brick element, is shown in Table (٣.٢)

Table (٣.٢) Shape Function of the Linear ٨-Node Brick Element

Node no.(i)	ξ_i	η_i	ζ_i	Ni (ξ, η, ζ)

i=١ - ٨	±١	±١	±١	(١+ ξ ξ_i)(١+ η η_i)(١+ζζ_i) /٨

Table (٣.٣) shows the shape functions of the ١٤-node brick element.

Table (٣.٣) Shape Functions of ١٤-Node Brick Element (Smith and Griffiths ١٩٩٨)

Node no.	Ni (ξ, η, ζ)
١	((ξ*η+ξ*ζ+٢*ξ+η*ζ+٢*η+٢*ζ+٢)*(ξ-١)*(η-١)*(ζ-١))/٨
٢	((ξ*η-ξ*ζ-٢*ξ+η*ζ+٢*η-٢*ζ-٢)*(ξ-١)*(η+١)*(ζ-١))/٨
٣	((ξ*η+ξ*ζ+٢*ξ-η*ζ-٢*η-٢*ζ-٢)*(ξ+١)*(η-١)*(ζ-١))/٨
٤	((ξ*η-ξ*ζ-٢*ξ-η*ζ-٢*η+٢*ζ+٢)*(ξ+١)*(η+١)*(ζ-١))/٨
٥	-((ξ*η-ξ*ζ+٢*ξ-η*ζ+٢*η-٢*ζ+٢)*(ξ-١)*(η-١)*(ζ+١))/٨
٦	-((ξ*η+ξ*ζ-٢*ξ-η*ζ+٢*η+٢*ζ-٢)*(ξ-١)*(η+١)*(ζ+١))/٨
٧	-((ξ*η-ξ*ζ+٢*ξ+η*ζ-٢*η+٢*ζ-٢)*(ξ+١)*(η-١)*(ζ+١))/٨
٨	-((ξ*η+ξ*ζ-٢*ξ+η*ζ-٢*η-٢*ζ+٢)*(ξ+١)*(η+١)*(ζ+١))/٨
٩	-((ξ+١)*(ξ-١)*(η-١)*(ζ-١))/٢
١٠	((ξ+١)*(ξ-١)*(η+١)*(η-١)*(ζ+١))/٢
١١	-((ξ+١)*(ξ-١) *(η-١)*(ζ+١) *(ζ-١))/٢
١٢	((ξ+١)*(ξ-١) *(η+١)*(ζ+١) *(ζ-١))/٢
١٣	-((ξ-١)*(η+١) *(η-١)*(ζ+١) *(ζ-١))/٢
١٤	((ξ+١)*(η+١) *(η-١)*(ζ+١) *(ζ-١))/٢

In the isoparametric group of elements, the interpolation shape functions are also used to define the geometry of the element and the global coordinates of any point p(ξ, η, ζ) in the terms of the natural local coordinates by using the relations:

$$\left.\begin{aligned} x(\xi,\eta,\zeta) &= \sum_{i=1}^{20} N_i\,(\xi,\eta,\zeta)x_i \\ y(\xi,\eta,\zeta) &= \sum_{i=1}^{20} N_i\,(\xi,\eta,\zeta)y_i \\ z(\xi,\eta,\zeta) &= \sum_{i=1}^{20} N_i\,(\xi,\eta,\zeta)z_i \end{aligned}\right\} \qquad \text{...(٣.٢)}$$

where x_i , y_i and z_i are the global coordinates of the node i .

٣.٢.٢ Definition of Strain and Stress Fields

In order to take into account the geometrical nonlinearity of the structure, the general strain-displacement equations that are used for small and large deformation problems can be written as (Zienkiewicz ١٩٧٧):

$$\{\varepsilon\} = \begin{Bmatrix} \varepsilon_x \\ \varepsilon_y \\ \varepsilon_z \\ \gamma_{xy} \\ \gamma_{yz} \\ \gamma_{zx} \end{Bmatrix} = \begin{Bmatrix} \partial u/\partial x + \frac{1}{2}\left[\left(\frac{\partial u}{\partial x}\right)^2 + \left(\frac{\partial v}{\partial x}\right)^2 + \left(\frac{\partial w}{\partial x}\right)^2\right] \\ \partial v/\partial y + \frac{1}{2}\left[\left(\frac{\partial u}{\partial y}\right)^2 + \left(\frac{\partial v}{\partial y}\right)^2 + \left(\frac{\partial w}{\partial y}\right)^2\right] \\ \partial w/\partial z + \frac{1}{2}\left[\left(\frac{\partial u}{\partial z}\right)^2 + \left(\frac{\partial v}{\partial z}\right)^2 + \left(\frac{\partial w}{\partial z}\right)^2\right] \\ \frac{\partial u}{\partial y} + \frac{\partial v}{\partial x} + \frac{\partial u}{\partial x}\frac{\partial u}{\partial y} + \frac{\partial v}{\partial x}\frac{\partial v}{\partial y} + \frac{\partial w}{\partial x}\frac{\partial w}{\partial y} \\ \frac{\partial v}{\partial z} + \frac{\partial w}{\partial y} + \frac{\partial u}{\partial y}\frac{\partial u}{\partial z} + \frac{\partial v}{\partial y}\frac{\partial v}{\partial z} + \frac{\partial w}{\partial y}\frac{\partial w}{\partial z} \\ \frac{\partial u}{\partial z} + \frac{\partial w}{\partial x} + \frac{\partial u}{\partial x}\frac{\partial u}{\partial z} + \frac{\partial v}{\partial x}\frac{\partial v}{\partial z} + \frac{\partial w}{\partial x}\frac{\partial w}{\partial z} \end{Bmatrix} \qquad \text{...(٣.٣)}$$

where u, v, and w are the displacement components in the x, y, and z directions respectively. Equation (٣.٣) reveals the nonlinearity of the strain-displacement relationships. If the displacements are small, the general first order linear strain approximation is obtained by neglecting the quadratic terms. The engineering strains are considered valid for the new strains measured in the original configuration

(Timoshenko and Goodier ١٩٥١). Equation (٣.٣) can be written by using shape functions as:

$$\begin{Bmatrix} \varepsilon_x \\ \varepsilon_y \\ \varepsilon_z \\ \gamma_{xy} \\ \gamma_{yz} \\ \gamma_{zx} \end{Bmatrix} = \sum_{i=1}^{20} \begin{bmatrix} \frac{\partial N_i}{\partial x} + \frac{1}{2}\frac{\partial N_i}{\partial x}\frac{\partial N_i}{\partial x}u_i & \frac{1}{2}\frac{\partial N_i}{\partial x}\frac{\partial N_i}{\partial x}v_i & \frac{1}{2}\frac{\partial N_i}{\partial x}\frac{\partial N_i}{\partial x}w_i \\ \frac{1}{2}\frac{\partial N_i}{\partial y}\frac{\partial N_i}{\partial y}u_i & \frac{\partial N_i}{\partial y} + \frac{1}{2}\frac{\partial N_i}{\partial y}\frac{\partial N_i}{\partial y}v_i & \frac{1}{2}\frac{\partial N_i}{\partial y}\frac{\partial N_i}{\partial y}w_i \\ \frac{1}{2}\frac{\partial N_i}{\partial z}\frac{\partial N_i}{\partial z}u_i & \frac{1}{2}\frac{\partial N_i}{\partial z}\frac{\partial N_i}{\partial z}v_i & \frac{\partial N_i}{\partial z} + \frac{1}{2}\frac{\partial N_i}{\partial z}\frac{\partial N_i}{\partial z}w_i \\ \frac{\partial N_i}{\partial y} + \frac{\partial N_i}{\partial x}\frac{\partial N_i}{\partial y}u_i & \frac{\partial N_i}{\partial x} + \frac{\partial N_i}{\partial x}\frac{\partial N_i}{\partial y}v_i & \frac{\partial N_i}{\partial x}\frac{\partial N_i}{\partial y}w_i \\ \frac{\partial N_i}{\partial y}\frac{\partial N_i}{\partial z}u_i & \frac{\partial N_i}{\partial z} + \frac{\partial N_i}{\partial y}\frac{\partial N_i}{\partial z}v_i & \frac{\partial N_i}{\partial y} + \frac{\partial N_i}{\partial y}\frac{\partial N_i}{\partial z}w_i \\ \frac{\partial N_i}{\partial z} + \frac{\partial N_i}{\partial x}\frac{\partial N_i}{\partial z}u_i & \frac{\partial N_i}{\partial x}\frac{\partial N_i}{\partial z}v_i & \frac{\partial N_i}{\partial x} + \frac{\partial N_i}{\partial x}\frac{\partial N_i}{\partial z}w_i \end{bmatrix} \begin{Bmatrix} u_i \\ v_i \\ w_i \end{Bmatrix} \quad \text{...(٣.٤)}$$

Since the shape functions, N_I, are functions of local coordinates rather than Cartesian coordinates, the Jacobian matrix [J], is needed to relate the derivatives in the two coordinate systems,

$$[J] = \sum_{i=1}^{n} \begin{bmatrix} \frac{\partial N_i}{\partial \xi}x_i & \frac{\partial N_i}{\partial \xi}y_i & \frac{\partial N_i}{\partial \xi}z_i \\ \frac{\partial N_i}{\partial \eta}x_i & \frac{\partial N_i}{\partial \eta}y_i & \frac{\partial N_i}{\partial \eta}z_i \\ \frac{\partial N_i}{\partial \zeta}x_i & \frac{\partial N_i}{\partial \zeta}y_i & \frac{\partial N_i}{\partial \zeta}z_i \end{bmatrix} \quad \text{...(٣.٥)}$$

where n is the number of node per element. Then, the shape function derivatives with respect to x, y, and z can be obtained as:

$$\begin{Bmatrix} \partial N_i/\partial x \\ \partial N_i/\partial y \\ \partial N_i/\partial z \end{Bmatrix} = [J]^{-1} \begin{Bmatrix} \partial N_i/\partial \xi \\ \partial N_i/\partial \eta \\ \partial N_i/\partial \zeta \end{Bmatrix} \quad \text{...(٣.٦)}$$

The vector of stresses is given by:

$$\{\sigma\} = \begin{Bmatrix} \sigma_x \\ \sigma_y \\ \sigma_z \\ \tau_{xy} \\ \tau_{yz} \\ \tau_{zx} \end{Bmatrix} \qquad \text{...(٣.٧)}$$

and the stress – strain relationship is represented as:

$$\{\sigma\} = [D].\{\varepsilon\} \qquad \text{...(٣.٨)}$$

where [D] is the constitutive matrix.

٣.٢.٣ Stiffness Matrix Calculation

In order to establish the governing equations of static equilibrium, which will lead to the derivation of the stiffness matrix, the principle of virtual displacements for a deformable body is used. It simply states that a deformable body is in equilibrium if the total work done by all the external forces plus the total work done by all the internal forces during any kinematically admissible virtual displacement is zero (Dawe ١٩٨٤) or in other words, strain energy is equal to loss of potential work by external forces:

$$\delta W_{int} - \delta W_{ext} = 0$$

...(٣.٩)

The external work can be expressed as the work done in moving the body forces ***b*** and surface traction t_s through the virtual displacement $\{\partial u\}$, as:

$$\delta W_{ext} = \int_V \{\partial u\}^T \{b\}\, dv + \int_S \{\partial u\}^T \{t_S\} ds$$

...(٣.١٠)

where v is the volume of the body and s is that part of the surface of the body where external tractions are prescribed.

The change in the strain energy. or internal work, due to a set of virtual strains, $\{\partial\varepsilon\}$, corresponding to the virtual displacement $\{\partial u\}$ is:

$$\delta W_{int} = \int_V \{\partial\varepsilon\}^T \{\sigma\} dv$$

...(٣.١١)

By substituting equations (٣.٨) into equation (٣.١١) then

$$\delta W_{int} = \int_V \{\partial\varepsilon\}^T [D] \{\varepsilon\} dv$$

... (٣.١٢)

By substituting equations (٣.١٠) and (٣.١٢) into equation (٣.٩), then:

$$\int_V \{\partial\varepsilon\}^T [D]\{\varepsilon\}dv - \int_V \{\partial u\}^T \{b\} dv - \int_S \{\partial u\}^T \{t_S\}ds = 0 \qquad \text{... (٣.١٣)}$$

This expression represents the equation of static equilibrium for a general body.

The basic concept of finite element analysis is to discretize the continuum into arbitrary numbers of small elements connected together at their common nodes. For a finite element, e, of the discrete model, the displacement vector at any point is:

$$\{u\}^e = [N] \{a\}^e \qquad \text{...(٣.١٤)}$$

where [N] is a matrix containing the interpolation functions which relate the displacements $\{u\}^e$ to the nodal displacements $\{a\}^e$.

By differentiation of the displacements, the corresponding strains, $\{\varepsilon\}^e$, are obtained such that:

$$\{\varepsilon\}^e = [A] \{u\}^e \qquad \text{...(٣.١٥)}$$

where [A] is the matrix, which contains the differential operators. Substituting equation (٣.١٤) into equation (٣.١٥) yields:

$$\{\varepsilon\}^e = [A]\ [N]\ \{a\}^e \qquad ...(٣.١٦)$$

or

$$\{\varepsilon\}^e = [B]\ \{a\}^e \qquad ...(٣.١٧)$$

where [B] is the strain-displacement matrix, which represents the values of the strains at any point within the element, due to unit values of nodal displacements. In the discrete model, the equations of equilibrium of the continuum may be written as the sum of integration over the volume and surface area for all the finite elements. Therefore, by making use of equation (٣.١٤) and (٣.١٧), equation (٣.١٣) becomes:

$$\partial\{a\}^T\left\{\sum_n \int_v [B]^T[D][B]\,dv^e\{a\}^e - \sum_n \int_v [N]^T\{R\}^e\,dv^e - \sum_n \int_s [N]^T\{T_s\}^e\,ds^e\right\} = 0 \qquad ...(٣.١٨)$$

Since the relationship must be valid for any set of virtual displacements, and since $\partial\{a\}^T$ is arbitrary or $\partial\{a\}^T$ is not equal to ٠, then equation (٣.١٨) is written in a brief form for one element ***e*** as:

$$\{f\} = [k]\ .\{a\} \qquad ...(٣.١٩)$$

where [k] is the structural stiffness matrix of the assemblage of the elements and given by:

$$[\mathbf{K}] = \sum_{n} \int_{v} [k]^{e}$$

...(٣.٢٠)

and {a} is the corresponding assemblage of nodal displacement vector, and {f} is the assemblage of external nodal force vector of the structure given by:

$$\{f\} = \sum_{n} \int_{v^{e}} [N]^{T} \{b\}^{e}\, dv^{e} + \sum_{n} \int_{s^{e}} [N]^{T} \{T_{S}\}^{e}\, ds^{e}$$

...(٣.٢١)

For an element of volume ***v***, the stiffness matrix is presented implicitly in equation (٣.٢٠) as:

$$[K]^{e} = \int_{v^{e}} [B]^{T}.[D].[B]\, dv^{e}$$

...(٣.٢٢)

For three – dimensional elements, the differential volume dv^{e}, may be written as:

$$dv^{e} = dxdydz$$

...(٣.٢٣)

Equation (٣.٢٣) can be transformed into the natural coordinates as:

$$dv^{e} = |J| d\xi d\eta d\zeta$$

...(٣.٢٤)

where $|J|$ is the determinant of the Jacobian matrix. The limits of integration in the natural coordinates become –١ an +١ and the element stiffness matrix can therefore be written as:

$$[K]^e = \int_{-1}^{+1}\int_{-1}^{+1}\int_{-1}^{+1}[B]^T[D][B]|J|d\xi d\eta d\zeta$$

...(٣.٢٥)

In general it is not possible to evaluate the element stiffness matrix explicitly. Thus, numerical integration has to be used.

٣.٣ Reinforcement Idealization

In developing a finite element model for reinforced concrete members, at least three alternative representations of reinforcement have been used:

١. *Distributed Representation*

In this representation, Fig. (٣.٣a), the steel is assumed to be distributed withen the concrete element with a particular orientation angle θ. The composite concrete-reinforcement constitutive relation is used in this case [ASCE (١٩٨١), Chen (١٩٨٢)]. To derive such a relation, perfect bond is usually assumed between concrete and steel.

٢. *Discrete Representation*

A discrete representation of the reinforcement by using independent one -dimensional elements has been widely used, Fig. (٣.٣b). Axial force members, or bar links, may be used and they are assumed to be pin -connected with two degrees of freedom at the nodal points. Beam elements may also be used, and they are assumed to be capable of resisting axial force, shear, and bending, with three degrees of freedom assigned at each node. In either case, the one – dimensional reinforcement elements are easily superimposed on the multi – dimensional finite element mesh representing the concrete. A significant advantage of the discrete representation in addition to its simplicity is that it can account for possible displacement of the reinforcement with respect to the surrounding concrete. [Cook (١٩٨١), Chen (١٩٨٢)].

٣. *Embedded Representation*

An embedded representation, Fig. (٣.٣c), may be used in connection with higher order isoparametric concrete elements [ASCE (١٩٨١), Al-Mahaidi (١٩٧٩)]. The reinforcement bar is considered to be an axial member built into the isoparametric concrete element such that its displacements are consistent with those of the element. Perfect bond between the steel and the concrete has been assumed in this case. A major advantage of this approach is that the steel bars can be placed in their correct positions without imposing any restrictions on mesh choice and hence the finite element analysis can be carried out with a smaller number of brick elements compared to the discrete representation of reinforcement. Therefore, the embedded representation is adopted in present work.

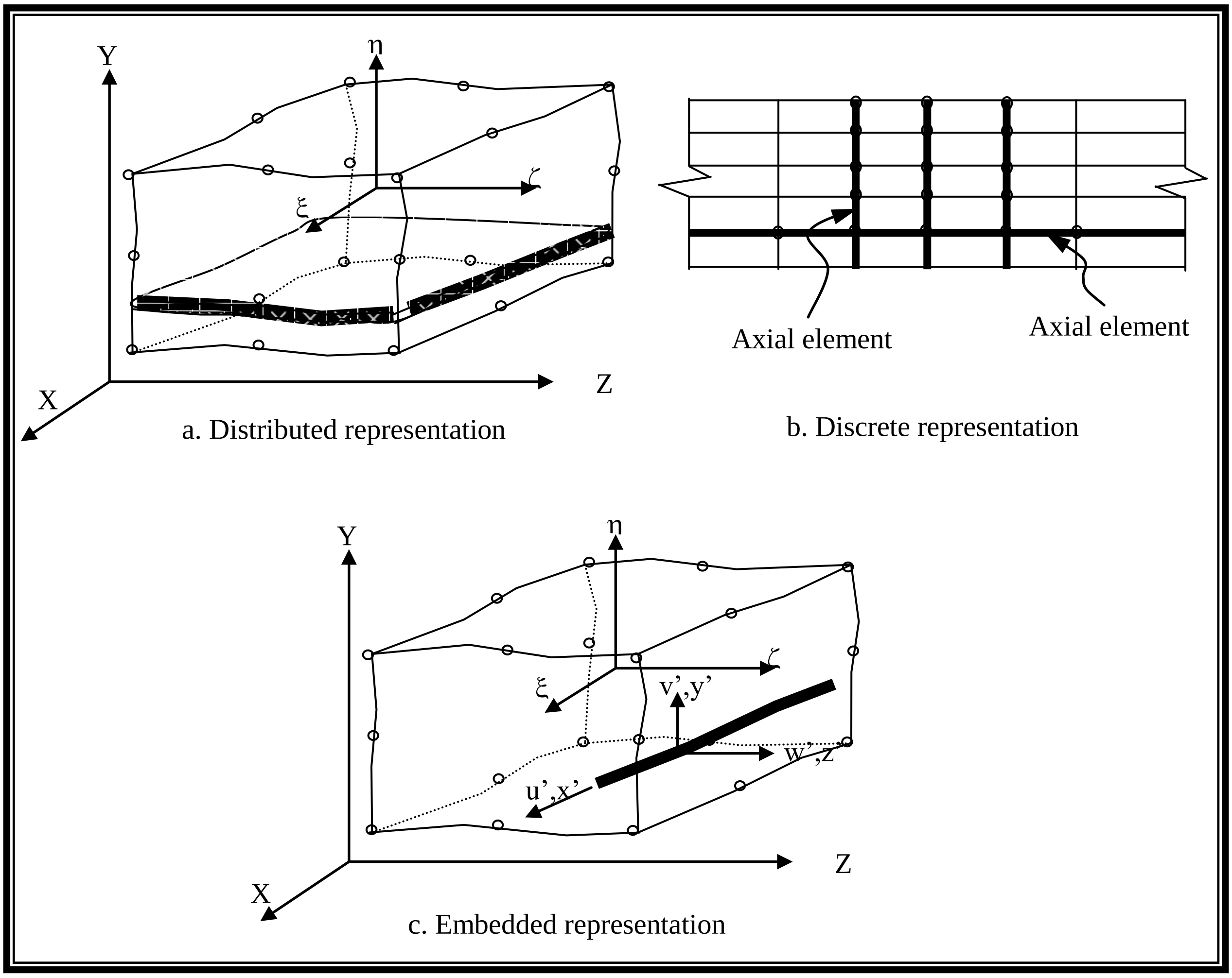

Fig. (٣.٣) Alternative Representations of Steel Reinforcement

For particular types of problems, a combination of representations may be used. As an example, discrete beam elements may be used for main reinforcement in beams while axial bar elements for stirrups. Or a distributed model can be used for the steel throughout the surface of the curved shell and discrete bar or beam elements for special reinforcement along the edge.

A derivation is presented in this section for a bar parallel to the local coordinate axis ξ. A similar derivation can be used for bars paralleled to η and ξ axes [Phillips and Zienkiewicz (١٩٧٦), Mohamed (١٩٨٦)].

For a bar lying inside a hexahedral brick element and parallel to the local coordinate axis ξ, with $\eta = \eta_c$ and $\zeta = \zeta_c$, the displacement representations are:

$$\left.\begin{aligned} u &= \sum_{i=1}^{n} N_i(\xi) u_i \\ v &= \sum_{i=1}^{n} N_i(\xi) v_i \\ w &= \sum_{i=1}^{n} N_i(\xi) w_i \end{aligned}\right\} \quad \text{...(٣. ٢٦)}$$

The strain-displacement relationship can be expressed in the local coordinate system as:

$$\varepsilon' = \sum_{i=1}^{n} \left[\frac{1}{h^2} \begin{bmatrix} c_1 & c_1 & c_3 \\ c_2 & c_4 & c_5 \\ c_3 & c_5 & c_6 \end{bmatrix} \begin{bmatrix} \dfrac{\partial N_i}{\partial x} \\ \dfrac{\partial N_i}{\partial y} \\ \dfrac{\partial N_i}{\partial z} \end{bmatrix} \right] . \begin{bmatrix} u_i \\ v_i \\ w_i \end{bmatrix} \quad \text{...(٣. ٢٧)}$$

where:

$c_1 = (\partial x / \partial \xi)^2,$

$c_2 = (\partial x / \partial \xi)(\partial y / \partial \xi),$

$c_3 = (\partial x / \partial \xi)(\partial z / \partial \xi)$

$c_4 = (\partial y / \partial \xi)^2,$

$c_5 = (\partial y / \partial \xi)(\partial z / \partial \xi),$

$c_6 = (\partial z / \partial \xi)^2$

and

$$h = \sqrt{c_1^2 + c_4^2 + c_6^2}$$

...(٣. ٢٨)

Eq. (٣.٢٩) is expressed in a compact form as:

$\{\varepsilon'\}=[B']\{a\}^e$ ...(٣.٢٩)

where [B′] is the strain-displacement matrix of the bar element. Then the stiffness matrix of an axially loaded bar element may be expressed as:

$[K']^e=\int [B']^T [D'] [B']dv^e$ ...(٣.٣٠)

The constitutive matrix [D′] represents the modulus of elasticity of the steel bar for the case of one-dimensional bar element lying in the direction parallel to the natural coordinate lineξ, and thus the volume differential dv^e can be written as:

$dv^e=As.dx'=As.h.d\xi$ ...(٣.٣١)

where ***As*** is the cross-sectional area of the bar. By substitution of Eq. (٣.٣١) into Eq.(٣.٣٠), the stiffness matrix of the embedded bar can be expressed as:

$$[K']^e = As\int_{-1}^{+1} [B]^T [D'] [B']\}hd\xi$$

...(٣.٣٢)

٣.٤ Numerical Integration

To perform the integration required to set up the element stiffness matrix, suitable scheme of numerical integration has to be made. In finite element work, the Gauss-Legendre quadrature scheme has been found to be accurate and efficient. The integral of the finite element stiffness matrix given in Eq. (٣.٢٥), can be expressed in the form [Robinson (١٩٧٣), Dawe (١٩٨٤)]:

$$I = \int_{-1}^{1}\int_{-1}^{1}\int_{-1}^{1} F(\xi,\eta,\zeta)\,d\xi\,d\eta\,d\zeta$$

...(٣.٣٣)

which may be rewritten numerically as:

$$I = \sum_{i=1}^{ni}\sum_{j=1}^{nj}\sum_{k=1}^{nk} Wi.Wj.Wk\,F(\xi_i,\eta_j,\zeta_k)$$

...(٣.٣٤)

where ***ni, nj, nk*** are the number of Gaussian points in the $\xi_i,\eta_j and \zeta_k$ direction respectively. The function $\boldsymbol{F(\xi_i,\eta_j,\zeta_k)}$ represents the matrix multiplication $(\boldsymbol{[B]^T.[D].[B].det[J]})$ at sampling points ξ_i,η_j,ζ_k.

In a similar manner, the integral of the stiffness matrix of the embedded reinforcement can be written as:

$$I = \sum_{i=1}^{ni} Wi\,F(\xi_i)$$

...(٣.٣٥)

The application of the three-dimensional finite element analysis in connection with the nonlinear behavior of reinforced concrete structures needs a large amount of computation time due to the frequent evaluation of the stiffness matrix. Therefore, it is necessary to choose a suitable integration rule that minimizes the computation time with sufficient accuracy. Several types of integration rules can be used such as the eight (٢x ٢x٢), and the twenty-seven (٣x٣x٣) Gaussian point rules are used to integrate the stiffness matrix of brick elements (Bathe ١٩٩٦). Also, there is the fifteen - point Gauss type integration rule (Irons ١٩٧١).

The integration rules, which exist in this program, are the eight=(٢x٢x٢), ٢٧=(٣x٣x٣) Gauss quadrature and the ١٥ points type integration rule. The weights and abscissa of the sampling points are listed in Tab. (٣.٤) .The relative distribution of the Gaussian points over the element is given in Fig. (٣.٤).

In the present study, all the above numerical integration rules are used.

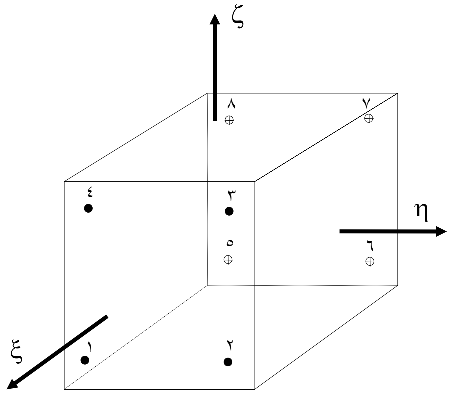

(a) ٨- point integration rule

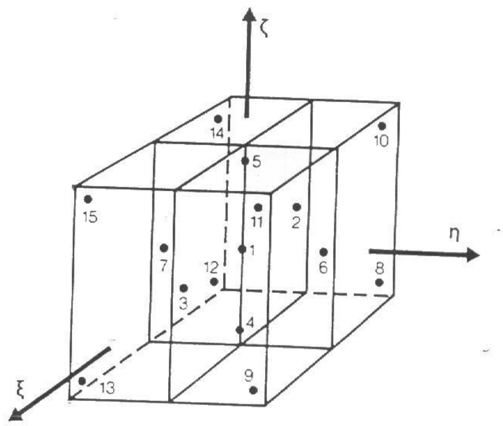

(b) ١٥- point integration rule

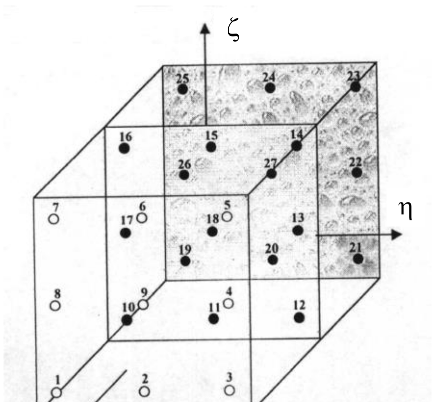

Table (٣.٤) Weights and Abscissa of Sampling Points in ٨, ١٥ a and ٢٧ Points Integration Rules.

Integration rule	Sampling point Number	ξ	η	ζ	Weight
٨-Point Rule	١ - ٨	+٠.٥٧٧٣٤	+٠.٥٧٧٣٤	+٠.٥٧٧٣٤	١.٠
١٥a-point Rule	١	٠.٠	٠.٠	٠.٠	١.٥٦٤٤
	٢ , ٣	±١.٠	٠.٠	٠.٠	٠.٣٥٥٥٦
	٤ , ٥	٠.٠	٠.٠	±١.٠	٠.٣٥٥٥٦
	٦ , ٧	٠.٠	±١.٠	٠.٠	٠.٣٥٥٥٦
	٨ - ١٥	±٠.٦٧٤١٠	±٠.٦٧٤١٠	±٠.٦٧٤١٠	٠.٥٣٧٧٨
٢٧-Point Rule	١, ٣, ٥ ,٧, ١٩, ٢١, ٢٣, ٢٥	±٠.٧٧٤٦	±٠.٧٧٤٦	±٠.٧٧٤٦	٠.١٧١٤٦٨
	٢, ٤, ٦, ٨, ١٠, ١٢, ١٤, ١٦, ٢٠, ٢٢, ٢٤, ٢٦	±٠.٧٧٤٦	±٠.٧٧٤٦	±٠.٧٧٤٦	٠.٢٧٤٣٤٨
	٩, ١١, ١٣, ١٥, ١٧, ٢٧	±٠.٧٧٤٦	±٠.٧٧٤٦	±٠.٧٧٤٦	٠.٤٣٨٩٥٧
	١٨	٠.٠	٠.٠	٠.٠	٠.٧٠٢٣٣٢

٣.٥ Nonlinear Solution Techniques

The solution of finite element equations for linear problems can be accomplished in a direct manner without major difficulties. However, this is no longer the case for nonlinear problems where certain sophisticated solution strategies must be employed. In the analysis of reinforced concrete structures, the material nonlinear behavior, including sudden changes in the element stiffness due to cracking and crushing of concrete and yielding of reinforcement, represents the main source of nonlinearity. The influence of geometry changes on the behavior is also significant in many cases. An analysis based on large deformations must be considered for those cases. An incremental finite element formulation with corrective iteration cycles is usually used for nonlinear finite element analysis to trace out the entire structural response of reinforced concrete structures and to guarantee the convergence towards the correct solution path.

٣.٥.١ Solution Techniques for Nonlinear Equations

Applying the finite element method for any problem leads in general to a set of algebraic equations in the following form:

$$[K]\{a\}=\{f\} \qquad \text{...(٣.٣٦)}$$

where,

{a} is the unknown nodal displacement vector.

{f} is the nodal applied force vector.

[K] is the stiffness matrix $\left(\int_V [B]^T[D][B]dV\right)$

The solution for these equations for linear elastic structural problems can be obtained directly. In nonlinear problems, a direct solution is no longer possible since the stiffness matrix [K] depends on the displacement level ([K]=[K]({a})), and therefore, it cannot be exactly calculated before the determination of the unknown nodal displacements {a}. For the solution of a nonlinear structural problem, the state of equilibrium of the structural system corresponding to the applied load must be found. These equilibrium equations can be derived by applying the equilibrium to the structural system. In finite element terms, the equilibrium equations can be expressed as:

$$\{r\}=\{p\}-\{f\} \qquad \text{...(٣.٣٧)}$$

where {r} is the out-of-balance force vector and {p} represents the vector of the nodal forces equivalent to the internal stress level, which is given by:

$$\{p\}=\int_V [B]^T\{\sigma\}\ dV \qquad \text{...(٣.٣٨)}$$

The equivalent internal forces also depend on the displacement level ({p}={p}({a})) and have to be approximated in successive steps until equation (٣.٣٧) approaches zero.

The techniques used in solving the nonlinear equations are (Cook ١٩٨١):

١. Linear-incremental technique.
٢. Iterative technique.
٣. Incremental – iterative technique.

3.5.1.1 Linear – Incremental Technique

In this method, Fig. (٣.٥), the nonlinear behavior is determined by solving a sequence of linear problems. The load is applied as a sequence of sufficiently small increments, so that during each load increment, the structure is assumed to respond linearly. The basic disadvantage of this method is that a real estimate of the solution accuracy is not possible, since equilibrium is not satisfied at any given load level. So, for stability requirements, it is necessary to use small load increments, which in turn will increase the computation cost if compared with the other techniques.

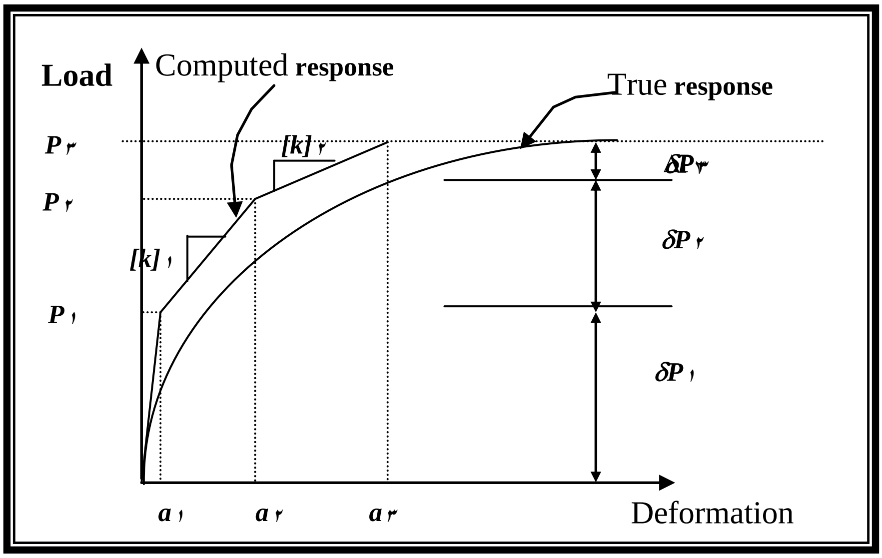

Fig. (٣.٥) Linear-Incremental Method

3.5.1.2 Iterative Technique

The iterative procedure is a sequence of calculations in which the structure is fully loaded in one step to get an initial approximate solution. Then, this solution is improved step – by – step by using an iteration process until equilibrium is satisfied within a prescribed tolerance.

After each iteration, the portion of the total loading that is not balanced is calculated and used in the iterative process as an additional load to compute an approximate additional increment of the total displacements. This process is repeated until equilibrium is approximated to some acceptable degree. These techniques fail to reach the required convergence for structures with high nonlinearity. There are several types of iteration procedure, some of them are:

- Conventional Newton – Raphson method.

- Modified Newton – Raphson method.
- Combined (conventional and modified) Newton – Raphson method.

3.5.1.3 Incremental – Iterative Technique

In this type of technique, Fig. (٣. ٦), the load is applied as a series of increments, and at each increment, iterative solution is carried out to find the truest response of the structure. The conventional, modified and combined Newton – Raphson methods may also be used in the iteration process within each step. These methods are briefly discussed in the following sections.

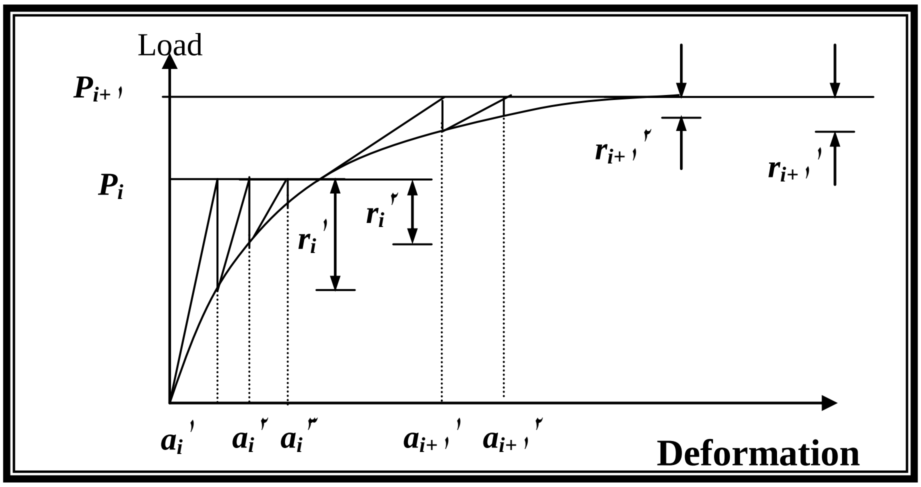

Fig. (٣. ٦) Incremental - Iterative Technique

3.5.1.3.1 Conventional Newton – Raphson Method

The conventional Newton – Raphson method, Fig. (٣. ٧), is one of the earliest known methods used in solving nonlinear problems. For simplicity, a single degree of freedom system is considered with a load level $\{P\}_0$, with the assumption that the corresponding deformed configuration of the system which may be denoted symbolically by $\{a\}_0$ is known. Then, to determine a new configuration, $\{a\}_1$, corresponding to a load level $\{p\}_1$ where:

$$\{P\}_1 = \{P\}_0 + \{\delta P\}_1$$

...(٣. ٣٩)

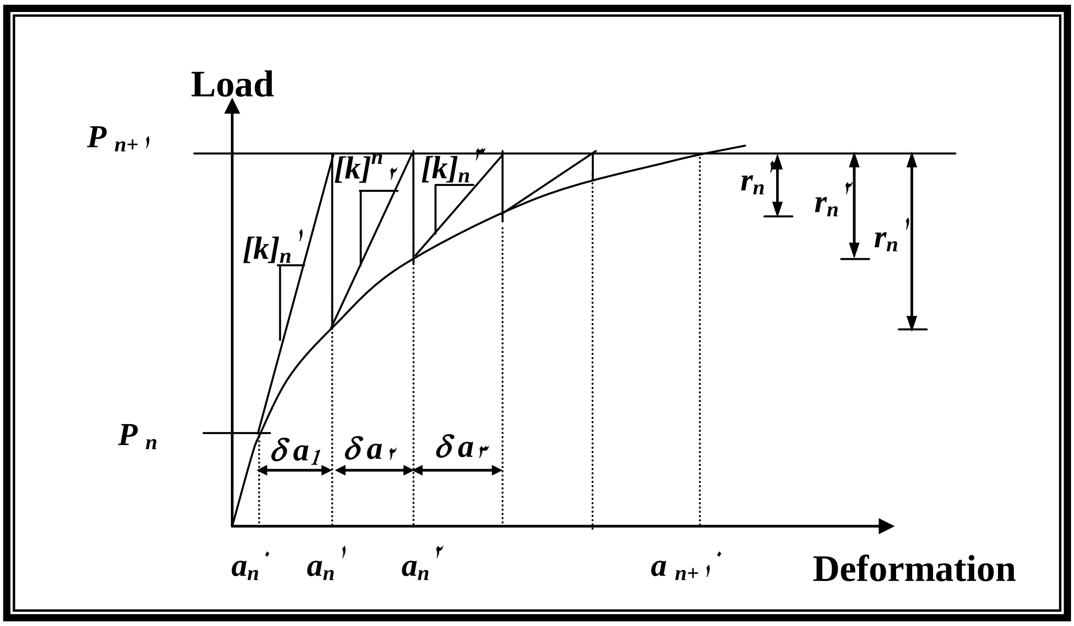

Fig. (٣. ٧) Conventional Newton – Raphson Method

and $\{\delta P\}_1$ is the additional applied load is obtained by using a linearized analysis, where the change in configuration $\{\delta a\}_1$ is first computed from:

$$\{\delta \mathrm{P}\}_1 = [\mathrm{k}]_0 \{\delta a\}_1$$

...(٣. ٤٠)

in which the tangent stiffness matrix $[k]_0$ is evaluated at the beginning of the load interval, i.e. the load level $\{P\}_0$. The term $\{a\}_1 = \{a\}_0 + \{\delta a\}_1$ represents an approximate configuration which is then corrected by updating new tangent stiffness matrix from the approximate configuration $\{a\}_1$. The internal forces $\{\mathrm{f}\}_1$ corresponding to this configuration can be determined as:

$$\{\mathrm{f}\}_1 = [\mathrm{k}]_1 \{\mathrm{a}\}_1$$

...(٣.٤١)

Generally for any level of iteration (j):

$$\{a\}_j = \{a\}_{j-1} + \sum_{m=1}^{n} \{\delta a\}_m$$

...(٣.٤٢)

where:

$\{a\}_j$ is the vector of displacement after the iteration. Then, the out-of-balance force vector $\{r\}_j$ can be obtained from:

$$\{r\}_j = \{P\}_f - \{f\}_j$$

...(٣.٤٣)

The unbalanced joint forces are then treated as load increments and the correction vector $\{\delta a\}_{j+1}$ is then obtained from the incremental relationship:

$$[k]_j \{\delta a\}_{j+1} = \{r\}_j$$

...(٣.٤٤)

A new approximate configuration is then computed by making use of Eq. (٣.٤٤). The process continues until the latest correction vector is sufficiently small.

The conventional Newton – Raphson method requires that the tangent stiffness matrix is to be updated and a new system of equations is solved for each iteration. This is expensive if the problem to be solved is too large. Accordingly various modifications have been proposed.

3.5.1.3.2 Modified Newton – Raphson Method

In this method, Fig. (٣. ٨), the stiffness matrix is updated only once for each increment of loading. As compared with the conventional Newton – Raphson method, the modified Newton – Raphson method is more economical. However, this method requires more steps for convergence, but each step is done quickly by avoiding time-consuming repetitions of forming the tangent stiffness matrix.

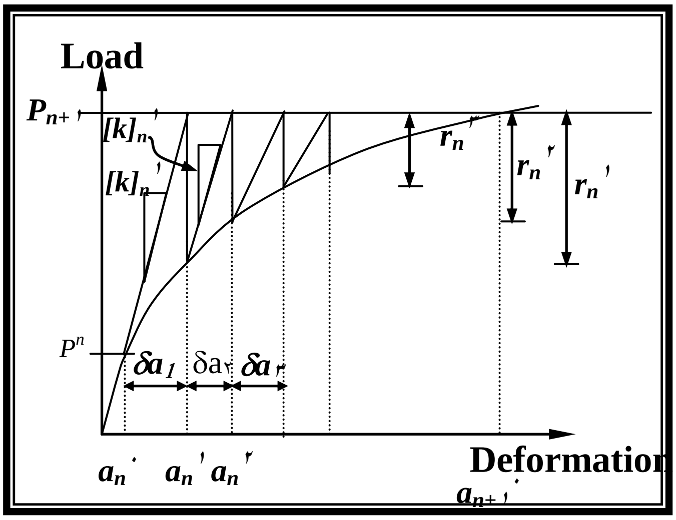

Fig. (٣. ٨) Modified Newton – Raphson Method

3.5.1.3.3 Combined Newton - Raphson Method

This method, Fig. (٣.٩), is a modification of the conventional Newton – Raphson method. It involves updating the stiffness matrix after remaining constant for a certain number of iterations. The stiffness matrix can be recalculated at:

- The beginning of first iteration of each increment.
- Beginning of second iteration.
- First, eleventh, twenty first, … stiffness matrices over each load increment.
- Second, twelfth, twenty second, … stiffness matrices over each load increment.

The disadvantage of this method is represented in the fact that the convergence is slower than the conventional Newton – Raphson method and requires a great number of iterations to achieve the solution within each load increment.

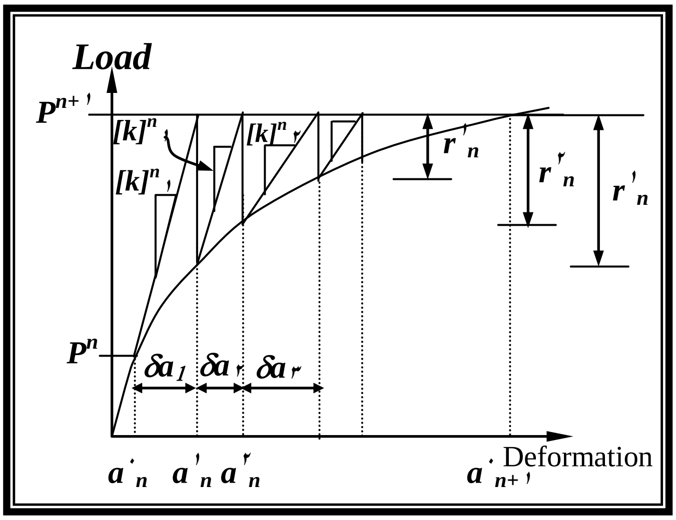

Fig. (٣. ٩) Combined Newton – Raphson Method

٣ . ٥ . ٢ Convergence Criterion

A termination criterion for the iterative process should be used to stop iteration when a sufficient accuracy is achieved, i.e, when no further iterations are necessary. The different useful criteria are the displacement, the force and the work done criteria. Only the force criterion is adopted in the present study. This criterion depends on comparing the internal force vector $\{P\}$ and the applied load vector $\{f\}$. In other words, seeking a vector called “unbalanced force vector” to be small within a prescribed tolerance. The convergence is assumed to occur when the inequality:

$$\left[\frac{\sum_{i=1}^{n}\left(\{f\}_i-\{P\}_i\right)^2}{\sum\left(\{f\}i\right)^2}\right]^{0.5} \le \text{tol.}$$

...(٣.٤٥)

is satisfied.

٣.٦ Nonlinear Geometric Analysis

Consideration of geometric nonlinearity plays an important role in the analysis of thin reinforced concrete slabs, plates, and shells (Bergan and Holand ١٩٧٩). In general, it is not known in advance in what category the real structure can be classified and where the geometrical nonlinear analysis is needed to avoid underestimating or overestimating the failure load.

٣.٦.١ Geometric Nonlinear Formulations for Hexahedral Brick Element

The strain components in equation (٣.٣) can be separated into a linear $\{\varepsilon_o\}$ and a nonlinear $\{\varepsilon_{nl}\}$ part, which can be written as:

$$\{\varepsilon\} = \{\varepsilon_o\} + \{\varepsilon_{nl}\} \qquad \text{...(٣.٤٦)}$$

where,

$$\{\varepsilon_o\} = \begin{bmatrix} \dfrac{\partial u}{\partial x} \\ \dfrac{\partial v}{\partial y} \\ \dfrac{\partial w}{\partial z} \\ \dfrac{\partial u}{\partial y} + \dfrac{\partial v}{\partial x} \\ \dfrac{\partial v}{\partial z} + \dfrac{\partial w}{\partial y} \\ \dfrac{\partial w}{\partial x} + \dfrac{\partial u}{\partial z} \end{bmatrix}, \quad \{\varepsilon_{nl}\} = \begin{bmatrix} \dfrac{1}{2}\left[\left(\dfrac{\partial u}{\partial x}\right)^2 + \left(\dfrac{\partial v}{\partial x}\right)^2 + \left(\dfrac{\partial w}{\partial x}\right)^2\right] \\ \dfrac{1}{2}\left[\left(\dfrac{\partial u}{\partial y}\right)^2 + \left(\dfrac{\partial v}{\partial y}\right)^2 + \left(\dfrac{\partial w}{\partial y}\right)^2\right] \\ \dfrac{1}{2}\left[\left(\dfrac{\partial u}{\partial z}\right)^2 + \left(\dfrac{\partial v}{\partial z}\right)^2 + \left(\dfrac{\partial w}{\partial z}\right)^2\right] \\ \dfrac{\partial u}{\partial x}\dfrac{\partial u}{\partial y} + \dfrac{\partial v}{\partial x}\dfrac{\partial v}{\partial y} + \dfrac{\partial w}{\partial x}\dfrac{\partial w}{\partial y} \\ \dfrac{\partial u}{\partial y}\dfrac{\partial u}{\partial z} + \dfrac{\partial v}{\partial y}\dfrac{\partial v}{\partial z} + \dfrac{\partial w}{\partial y}\dfrac{\partial w}{\partial z} \\ \dfrac{\partial u}{\partial x}\dfrac{\partial u}{\partial z} + \dfrac{\partial v}{\partial x}\dfrac{\partial v}{\partial z} + \dfrac{\partial w}{\partial x}\dfrac{\partial w}{\partial z} \end{bmatrix} \qquad \text{...(٣.٤٧)}$$

and,

$$d\{\varepsilon\} = d\{\varepsilon_o\} + d\{\varepsilon_{nl}\} \qquad \text{...(٣.٤٨)}$$

٣.٦.١.١ Strain-Displacement Matrix [B]

The strain-displacement matrix [B] may be separated into two parts,

$$[B] = [B_o] + [B_{nl}] \qquad \text{...(٣.٤٩)}$$

where, $[B_o]$ is the linear part, and $[B_{nl}]$ is the nonlinear part

The strain-displacement matrix $[B_o]$ is related to the linear components of the strain vector $\{\varepsilon_o\}$, while, the large strain-displacement matrix $[B_{nl}]$ is related to the nonlinear components of the strain vector, $\{\varepsilon_{nl}\}$, and can be defined for use in the nonlinear process. In modeling the reinforced concrete, the total strain has been used and the total strain-displacement relationship should be defined. For the hexahedral brick elements, the nonlinear components of the strain vector can be expressed by:

$$\{\varepsilon_{nl}\} = \frac{1}{2}\begin{bmatrix} \frac{\partial u}{\partial x} & 0 & 0 & \frac{\partial v}{\partial x} & 0 & 0 & \frac{\partial w}{\partial x} & 0 & 0 \\ 0 & \frac{\partial u}{\partial y} & 0 & 0 & \frac{\partial v}{\partial y} & 0 & 0 & \frac{\partial w}{\partial y} & 0 \\ 0 & 0 & \frac{\partial u}{\partial z} & 0 & 0 & \frac{\partial v}{\partial z} & 0 & 0 & \frac{\partial w}{\partial z} \\ \frac{\partial u}{\partial y} & \frac{\partial u}{\partial x} & 0 & \frac{\partial v}{\partial y} & \frac{\partial v}{\partial x} & 0 & \frac{\partial w}{\partial y} & \frac{\partial w}{\partial x} & 0 \\ 0 & \frac{\partial u}{\partial z} & \frac{\partial u}{\partial y} & 0 & \frac{\partial v}{\partial z} & \frac{\partial v}{\partial y} & 0 & \frac{\partial w}{\partial z} & \frac{\partial w}{\partial y} \\ \frac{\partial u}{\partial z} & 0 & \frac{\partial u}{\partial x} & \frac{\partial v}{\partial z} & 0 & \frac{\partial v}{\partial x} & \frac{\partial w}{\partial z} & 0 & \frac{\partial w}{\partial x} \end{bmatrix} \begin{Bmatrix} \partial u/\partial x \\ \partial u/\partial y \\ \partial u/\partial z \\ \partial v/\partial x \\ \partial v/\partial y \\ \partial v/\partial z \\ \partial w/\partial x \\ \partial w/\partial y \\ \partial w/\partial z \end{Bmatrix} \qquad \text{...(٣.٥٠)}$$

The nonlinear contribution to the strain vector can be written in a compact form as:

$$\{\varepsilon_{nl}\} = \frac{1}{2}[A]\{R\}$$

...(٣.٥١)

The derivatives of u, v and w can be calculated by summation of the contribution of each nodal variable, and vector {R} can be written as:

$$\{R\}=\begin{bmatrix} \sum \partial N_i/\partial x & 0 & 0 \\ \sum \partial N_i/\partial y & 0 & 0 \\ \sum \partial N_i/\partial z & 0 & 0 \\ 0 & \sum \partial N_i/\partial x & 0 \\ 0 & \sum \partial N_i/\partial y & 0 \\ 0 & \sum \partial N_i/\partial z & 0 \\ 0 & 0 & \sum \partial N_i/\partial x \\ 0 & 0 & \sum \partial N_i/\partial y \\ 0 & 0 & \sum \partial N_i/\partial z \end{bmatrix} \begin{Bmatrix} u_i \\ v_i \\ w_i \end{Bmatrix} \qquad \text{...(٣.٥٢)}$$

Equation (٣.٥٢) can be written in the following form as:

$$\{R\}=[G]\ \{a\} \qquad \text{...(٣.٥٣)}$$

By taking the variation of equation (٣.٥١) the following expression is obtained:

$$d\{\varepsilon_{nl}\}=\frac{1}{2}d[A]\{R\}+\frac{1}{2}[A]\ d\{R\}=[A]\ d\{R\}=[A]\ [G]\{a\} \qquad \text{...(٣.٥٤)}$$

Then from the definition of the strain matrix, the following expression can be obtained:

$$[B_{nl}]=[A]\ [G]$$

...(٣.٥٥)

In the present study, the incremental strain-displacement matrix [B] is evaluated by summing the matrix $[B_o]$ to the current value of matrix $[B_{nl}]$. In the modified finite element program developed in the present study, the matrices $[B_o]$ and [G] are initially calculated and stored for linear elastic conditions.

٣.٦.١.٢ Tangential Stiffness Matrix [K]

The tangential stiffness matrix [K] for the current configuration can be derived from the variation of equation (٣.٣٨) with respect to a displacement variation {a}.

$$d\{p\} = \int_V [B^T] d\{\sigma\} dV + \int_V d[B]^T \{\sigma\} dV = [K] \; d\{a\} \qquad \text{...(٣.٥٦)}$$

where,

$$d\{\sigma\} = [D] \; d\{\varepsilon\} = [D] \; [B] \; d\{a\} \qquad \text{...(٣.٥٧)}$$

and,

$$d[B]^T = d[B_{nl}]^T$$

...(٣.٥٨)

The initial stress or geometric stiffness matrix, $[K]_\sigma$, for the definition of the second term of equation (٣.٥٦) is given by:

$$[K]_\sigma d\{a\} = \int_V d[B]^T \{\sigma\} dV = \int_V d[B_{nl}]^T \{\sigma\} dV \qquad \text{...(٣.٥٩)}$$

then the tangential stiffness matrix can be written as:

$$[K] = [\overline{K}] + [K]_\sigma \qquad \text{...(٣.٦٠)}$$

where, $[\overline{K}]$ is the stiffness matrix of concrete element, which was calculated in section (٣.٢.٣). The geometric stiffness matrix $[K]_\sigma$ must be defined explicitly in order to determine the tangential stiffness matrix [K]. Substitution of equation (٣.٥٥) into equation (٣.٥٩) yields:

$$[K]_\sigma d\{a\} = \int_V [G]^T d[A]^T \{\sigma\} dV$$

...(٣.٦١)

where $d[A]^T \{\sigma\}$ can be written in the form as:

$$d[A]^T\{\sigma\} = d\begin{bmatrix} \partial u/\partial x & 0 & 0 & \partial u/\partial y & 0 & \partial u/\partial z \\ 0 & \partial u/\partial y & 0 & \partial u/\partial x & \partial u/\partial z & 0 \\ 0 & 0 & \partial u/\partial z & 0 & \partial u/\partial y & \partial u/\partial x \\ \partial v/\partial x & 0 & 0 & \partial v/\partial y & 0 & \partial v/\partial z \\ 0 & \partial v/\partial y & 0 & \partial v/\partial x & \partial v/\partial z & 0 \\ 0 & 0 & \partial v/\partial z & 0 & \partial v/\partial y & \partial v/\partial x \\ \partial w/\partial x & 0 & 0 & \partial w/\partial y & 0 & \partial w/\partial z \\ 0 & \partial w/\partial y & 0 & \partial w/\partial x & \partial w/\partial z & 0 \\ 0 & 0 & \partial w/\partial z & 0 & \partial w/\partial y & \partial w/\partial x \end{bmatrix} \begin{Bmatrix} \sigma_x \\ \sigma_y \\ \sigma_z \\ \tau_{xy} \\ \tau_{yz} \\ \tau_{xz} \end{Bmatrix} \quad \text{...(٣.٦٢)}$$

which can be written as:

$$d[A]^T\{\sigma\} = \begin{bmatrix} \sigma_x & \tau_{xy} & \tau_{xz} & 0 & 0 & 0 & 0 & 0 & 0 \\ \tau_{xy} & \sigma_y & \tau_{yz} & 0 & 0 & 0 & 0 & 0 & 0 \\ \tau_{xz} & \tau_{yz} & \sigma_z & 0 & 0 & 0 & 0 & 0 & 0 \\ 0 & 0 & 0 & \sigma_x & \tau_{xy} & \tau_{xz} & 0 & 0 & 0 \\ 0 & 0 & 0 & \tau_{xy} & \sigma_y & \tau_{yz} & 0 & 0 & 0 \\ 0 & 0 & 0 & \tau_{xz} & \tau_{yz} & \sigma_z & 0 & 0 & 0 \\ 0 & 0 & 0 & 0 & 0 & 0 & \sigma_x & \tau_{xy} & \tau_{xz} \\ 0 & 0 & 0 & 0 & 0 & 0 & \tau_{xy} & \sigma_y & \tau_{yz} \\ 0 & 0 & 0 & 0 & 0 & 0 & \tau_{xz} & \tau_{yz} & \sigma_z \end{bmatrix} d\begin{Bmatrix} \partial u/\partial x \\ \partial u/\partial y \\ \partial u/\partial z \\ \partial v/\partial x \\ \partial v/\partial y \\ \partial v/\partial z \\ \partial w/\partial x \\ \partial w/\partial y \\ \partial w/\partial z \end{Bmatrix} \quad \text{...(٣.٦٣)}$$

The term $d[A]^T\{\sigma\}$ can be written, with the definition of [G] from equation (٣.٥٣) as:

$$d[A]^T\{\sigma\} = \begin{bmatrix} \sigma_x & \tau_{xy} & \tau_{xz} & 0 & 0 & 0 & 0 & 0 & 0 \\ \tau_{xy} & \sigma_y & \tau_{yz} & 0 & 0 & 0 & 0 & 0 & 0 \\ \tau_{xz} & \tau_{yz} & \sigma_z & 0 & 0 & 0 & 0 & 0 & 0 \\ 0 & 0 & 0 & \sigma_x & \tau_{xy} & \tau_{xz} & 0 & 0 & 0 \\ 0 & 0 & 0 & \tau_{xy} & \sigma_y & \tau_{yz} & 0 & 0 & 0 \\ 0 & 0 & 0 & \tau_{xz} & \tau_{yz} & \sigma_z & 0 & 0 & 0 \\ 0 & 0 & 0 & 0 & 0 & 0 & \sigma_x & \tau_{xy} & \tau_{xz} \\ 0 & 0 & 0 & 0 & 0 & 0 & \tau_{xy} & \sigma_y & \tau_{yz} \\ 0 & 0 & 0 & 0 & 0 & 0 & \tau_{xz} & \tau_{yz} & \sigma_z \end{bmatrix} [G] \; d\{a\} \qquad \text{...(٣.٦٤)}$$

By substituting equation (٣.٦٤) into equation (٣.٦١), the geometric stiffness matrix can be written as:

$$[K]_\sigma = \int_V [G]^T \{\sigma\} [G] \; dV$$

...(٣.٦٥)

٣.٦.٢ Geometric Nonlinear Formulations for Embedded Reinforcement Element

Since the bar is capable of transmitting axial force only, one component of strain contributes to the strain energy, which is defined locally as(Mohammed ٢٠٠١):

$$\varepsilon' = \frac{\partial u'}{\partial x'} \qquad \text{...(٣.٦٦)}$$

If general strain-displacement equations are considered to cover the geometrical nonlinear behavior of the structure, then the strain component of the bar will be:

$$\varepsilon' = \frac{\partial u'}{\partial x'} + \frac{1}{2}\left((\frac{\partial u'}{\partial x'})^2 + (\frac{\partial v'}{\partial x'})^2 + (\frac{\partial w'}{\partial x'})^2 \right) \qquad \text{...(٣.٦٧)}$$

The strain component in equation (٣.٦٧) can be separated into a linear ε'_o and a nonlinear ε'_{nl} part, which can be written as,

$$\varepsilon' = \varepsilon'_o + \varepsilon'_{nl} \qquad \text{...(٣.٦٨)}$$

where,

$$\varepsilon'_o = \frac{\partial u'}{\partial x'} \quad , \quad \varepsilon'_{nl} = \frac{1}{2}\left((\frac{\partial u'}{\partial x'})^2 + (\frac{\partial v'}{\partial x'})^2 + (\frac{\partial w'}{\partial x'})^2 \right) \qquad \text{...(٣.٦٩)}$$

and,

$$d\varepsilon' = d\varepsilon'_o + d\varepsilon'_{nl} \qquad \text{...(٣.٧٠)}$$

٣.٦.٢.١ Strain–Displacement Matrix $\{B'\}$

The strain–displacement vector $\{B'\}$ may be separated into two parts,

$$\{B'\} = \{B'_o\} + \{B'_{nl}\} \qquad \text{...(٣.٧١)}$$

where,

$\{B'_o\}$ is the linear part.

$\{B'_{nl}\}$ is the nonlinear part.

The nonlinear part of the strain component of the bar element can be expressed by:

$$\varepsilon'_{nl} = \frac{1}{2}\left\{ \frac{\partial u'}{\partial x'} \quad \frac{\partial v'}{\partial x'} \quad \frac{\partial w'}{\partial x'} \right\} \begin{Bmatrix} \frac{\partial u'}{\partial x'} \\ \frac{\partial v'}{\partial x'} \\ \frac{\partial w'}{\partial x'} \end{Bmatrix} \qquad \text{...(٣.٧٢)}$$

The nonlinear contribution to the strain component can be written in a compact form as:

$$\varepsilon'_{nl} = \frac{1}{2}\{A\}\{R\} \qquad \text{...(٣.٧٣)}$$

The derivatives of u', v' and w' can be calculated by summation of the contribution of each nodal variable, and the vector $\{R\}$ can be written as:

$$\{R\}=\frac{1}{h^2}\begin{bmatrix} c_1d_1+c_2d_2+c_3d_3 & c_2d_2+c_4d_2+c_5d_3 & c_3d_1+c_5d_2+c_6d_3 \\ c_2d_1+c_4d_2+c_5d_3 & c_1d_1+c_2d_2+c_3d_3 & c_2d_1+c_4d_2+c_5d_3 \\ c_1d_1+c_2d_2+c_3d_3 & c_3d_1+c_5d_2+c_6d_3 & c_3d_1+c_5d_2+c_6d_3 \end{bmatrix}\begin{Bmatrix} u_i \\ v_i \\ w_i \end{Bmatrix} \qquad \text{...(٣.٧٤)}$$

where $c_1, c_2, ...c_6$ are defined in section (٣.٣)

$$\left.\begin{aligned} d_1 &= \frac{\partial N_i}{\partial x} \\ d_2 &= \frac{\partial N_i}{\partial y} \\ d_3 &= \frac{\partial N_i}{\partial z} \end{aligned}\right\} \qquad \text{...(٣.٧٥)}$$

and,

$$h^2 = \left(\frac{\partial x}{\partial \xi}\right)^2 + \left(\frac{\partial y}{\partial \xi}\right)^2 + \left(\frac{\partial z}{\partial \xi}\right)^2 \qquad \text{...(٣.٧٦)}$$

Equation (٣.٧٤) can be written as:

$$\{R\}=[G]\{a\} \qquad \text{...(٣.٧٧)}$$

By taking the variation of equation (٣.٧٣), the following expression is obtained:

$$d\varepsilon'_{nl} = \frac{1}{2}d\{A\}\{R\}+\frac{1}{2}\{A\}d\{R\} = \{A\}d\{R\} = \{A\}[G]\{a\} \qquad \text{...(٣.٧٨)}$$

Then, from the definition of the strain vector,

$$\{B'_{nl}\} = \{A\}\ [G] \qquad \text{...(٣.٧٩)}$$

٣.٦.٢.٢ Tangential Stiffness Matrix *[K']*

The tangential stiffness matrix for the bar element can be written as,

$$[K'] = [\overline{K}'] + [K']_\sigma \qquad \text{...(٣.٨٠)}$$

where,

$[\overline{K}']$ is the main stiffness matrix for the bar element calculated in section (٣.٣), and $[K']_\sigma$ is the geometric stiffness matrix for the bar element.

Following the same formulations for the brick element in section (٣.٦.١), the geometric stiffness matrix for bar element $[K']_\sigma$ can be written as:

$$[K']_\sigma d\{a\} = \int_V [G] d\{A\}^T \{\sigma\} dV \qquad \text{...(٣.٨١)}$$

where $d\{A\}^T \{\sigma\}$ can take the following form,

$$d\{A\}^T \{\sigma\} = d\begin{Bmatrix} \dfrac{\partial u'}{\partial x'} \\ \dfrac{\partial v'}{\partial x'} \\ \dfrac{\partial w'}{\partial x'} \end{Bmatrix} \{\sigma_x\} \qquad \text{...(٣.٨٢)}$$

which can be written as:

$$d\{A\}^T \{\sigma\} = \begin{bmatrix} \sigma_x & 0 & 0 \\ 0 & 0 & 0 \\ 0 & 0 & 0 \end{bmatrix} d\begin{Bmatrix} \dfrac{\partial u'}{\partial x'} \\ \dfrac{\partial v'}{\partial x'} \\ \dfrac{\partial w'}{\partial x'} \end{Bmatrix} \qquad \text{...(٣.٨٣)}$$

The term $d\{A\}^T\{\sigma\}$ can be written, with the definition of [G] from equation (٣.٧٧),

$$d\{A\}^T\{\sigma\}=\begin{bmatrix}\sigma_x & 0 & 0\\ 0 & 0 & 0\\ 0 & 0 & 0\end{bmatrix}[G]\ \ d\{a\} \qquad \text{…(٣.٨٤)}$$

By substituting equation (٣.٨٤) into equation (٣.٨١), the geometric stiffness matrix for the bar element can be written as:

$$[K']_{\sigma}=\int_V [G]^T\{\sigma\}\ [G]\ \ dV \qquad \text{…(٣.٨٥)}$$

٣ . ٧ Uniaxial and Multi-Axial Behavior of Concrete

A typical stress-strain relationship for concrete in compression is shown in Fig. (٣.١٠). It can be seen that the stress-strain curve has a nearly elastic behavior up to about ٣٠ percent of its maximum compressive strength ***(f′c)***. For stress above this point, the curve shows a gradual increase in curvature up to about ***(٠.٧٥ f′c - ٠.٩٠ f′c)***, beyond which it bends more sharply and approaches the peak point at ***(f′c)***. Beyond this point, the stress-strain curve has a descending part until crushing failure occurs at some ultimate strain ε_u (Chen ١٩٨٢).

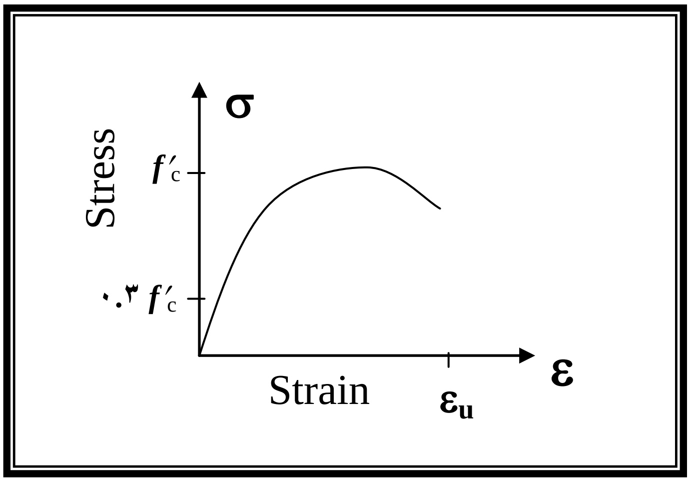

Fig.(٣.١٠) Typical Uniaxial Stress –Strain Curve for Concrete in Compression

Poisson ratio ***(ν)***, which is defined as the ratio of lateral tensile strain to the principal longitudinal compressive strain has been observed in experiments to be constant up to a stress level of ***(٨٠٪)*** of f′c and ranges between ٠.١٥ and ٠.٢٢ (Chen ١٩٨٢).

Under tensile stresses, the shape of the stress-strain curve of concrete shows many similarities to the uniaxial compression curves. There are, however, some differences exist, that the uniaxial tension state of stress tends to hold the crack much less frequently than the compressive state of stress. Therefore, and it can be expected that the interval of stable crack propagation is relatively short. It has been found that the ratio between the uniaxial tensile and compressive strength may vary considerably but usually ranges from ٠.٠٥ to ٠.١. The modulus of elasticity under uniaxial tension is somewhat higher and Poisson ratio somewhat lower than in compression (Mehta ١٩٨٦).

The behavior of concrete under multi-axial stress condition is very complex if compared with that under uniaxial stress condition and has not yet been assessed experimentally in a complete manner. Various material models with considerable simplifying assumptions have been proposed in literature. A typical biaxial strength envelope is shown in Fig. (٣.١١) (Chen and Saleeb ١٩٨٢). It was seen that the maximum compressive strength increases for biaxial compression state. A maximum strength increase of approximately ٢٥ percent is achieved at a stress ratio of ($\sigma_2/\sigma_1 = 0.5$), and this is reduced to about ١٦ percent at an equal biaxial compressive state $(\sigma_2/\sigma_1 = 1)$. Under biaxial compression – tension state of stress, the compressive strength decreases almost linearly as the applied tensile stress is increased (Chen ١٩٨٢).

Under biaxial or triaxial tension, the strength is almost the same as that of uni-axial tensile strength. When subjected to triaxial compressive stresses, concrete exhibits strength which increases with increasing the confining pressure (Mehta ١٩٨٦).

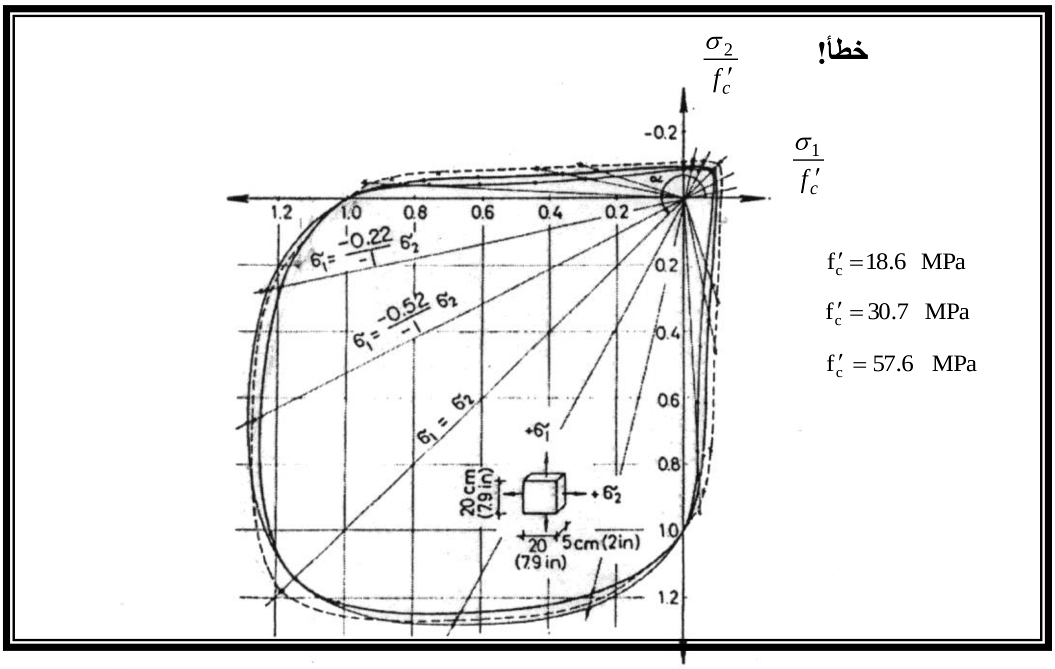

Fig. (٣.١١) Failure Envelope of Concrete in Biaxial Stress Space (Chen and Saleeb ١٩٨٢).

Experiments indicate that concrete in triaxial stresses has a fairly consistent failure surface which is a function of the three principal stresses, Fig. (٣.١٢). This failure surface can be represented by three-stress invariants. These invariants are the first invariant of the stress tensor ***(I)***, and the second and the third invariant of the stress deviatoric tensor ***(J ٢)*** and ***(J ٣)*** (Chen ١٩٨٢).

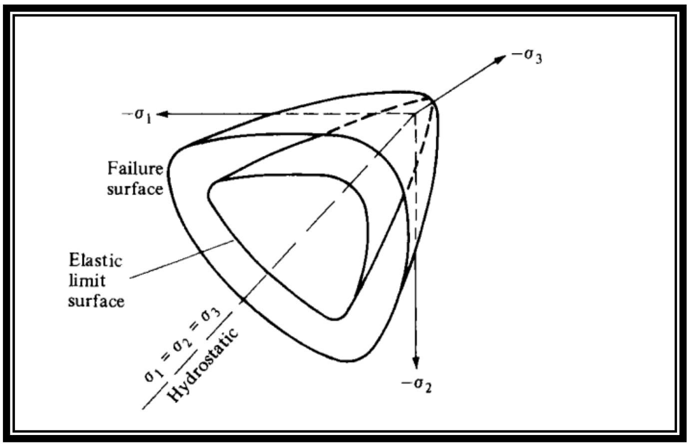

Fig.(٣.١٢) Triaxial Strength Envelope of Concrete (Chen ١٩٨٢)

٣.٨ Numerical Modeling of Concrete Properties

Concrete is a heterogeneous material. So, it has a nonlinear behavior under loading. This nonlinearity in reinforced concrete structures may be caused due to inelastic response of concrete in compression, cracking of concrete in tension and interactive effects between concrete and reinforcement.

Despite the complex behavior, it is required to model these properties to include the different sources of nonlinearity in the finite element analysis. Therefore, the following aspects of behavior must be included in the numerical modeling of concrete: [AL-Shaarbaf (١٩٩٠), Bathe and Ramaswamy (١٩٧٩)]

- Stress-strain model to represent the behavior of concrete prior to failure.
- A failure criterion to simulate the cracking and crushing of concrete.
- A model for crack representation.
- Modeling of the post-cracking stress-strain relationship.
- Modeling of the reduction in compressive strength due to orthogonal cracking.

٣.٨.١ Stress-Strain Models

Several approaches for describing the complicated stress-strain relationship of concrete under various stress-strain state have been usually used. These approaches can be divided generally into:

- Elasticity based models.
- Plasticity based models.

Elasticity based models may be linear or nonlinear elastic models. In the former, the stress-strain relation for uncracked and cracked concrete is developed depending on the theory of linear elasticity. These models are adequate when the failure condition is the tensile cracking of concrete. However, these models fail to identify the inelastic deformation. This disadvantage becomes obvious when the material experiences unloading. This can be improved by introducing nonlinear elastic models.

Nonlinear elastic models are based on two approaches, the total and the incremental stress-strain formulation. With the total stress-strain model, the current state of stress is assumed to be uniquely expressed as a function of the current state of strain. This type of model is reversible and path independent, which is generally not true for concrete. Also, it suffers from inability to predict the inelastic deformation. For the incremental formulation, the state of stress is dependent on the current state of strain and on the stress path followed to reach such a state (this type of formulation is incrementally reversible and path dependent). This formulation gives a good representation for concrete behavior as compared with the total stress formulation.

Plasticity based models have been used extensively in recent years for concrete modeling in compression. It is known that under triaxial compression, concrete can flow as a ductile material on the yield surface before reaching the crushing strain.

To account for property, various plasticity models have been introduced. In these models, concrete may be defined as an elastic – perfect plastic material or as a strain hardening material. The prediction of the overall behavior by using the plasticity based models gives a good agreement with experimental results. So, this type of modeling is adopted in the present work.

٣ . ٩ Modeling of Concrete Fracture

Generally, concrete fracture may be either a compression fracture (i.e. crushing of concrete) or a tension fracture (i.e. cracking of concrete).

The crushing failure occurs when the material can resist no further compressive loading while the tension failure of concrete is characterized by a gradual growth of cracks which join together and eventually disconnect larger parts of the structure. It is a usual assumption that formation of cracks is a brittle process and that the strength in the tension-loading direction abruptly goes to zero after such cracks have formed, Fig. (٣.١٣a). But when reinforcement bars bridge the concrete cracks, the strength mechanism becomes more complex and the carrying strength of concrete between cracks can be safely exploited [Chen (١٩٨٢)].

3.9.1 Cracking Models

In general, the models, which have been developed to represent cracking in connection with the finite element analysis of reinforced concrete members, are composed of three basic components, (١)a criterion for crack initiation, (٢)a method of crack representation and (٣)a method for cracking propagation.

Two fracture criteria are commonly used, the maximum principal stress criterion and the maximum principal strain criterion. When a principal stress or strain exceeds its limiting value a crack is assumed to occur in a plane normal to the direction of the offending principal stress or strain, Fig. (٣.١٣b).

In finite element analysis of concrete structures, two approaches have been employed for crack modeling, these are the smeared cracking and the discrete cracking models. The particular cracking model to be selected depends upon the purpose of the analysis. If overall load-deflection behavior is desired, without regard to completely realistic crack patterns and local stresses, the smeared crack model is probably the best choice, while if detailed local behavior is of interest, adoption of the discrete cracking model is useful. The two approaches will be discussed in the following sections.

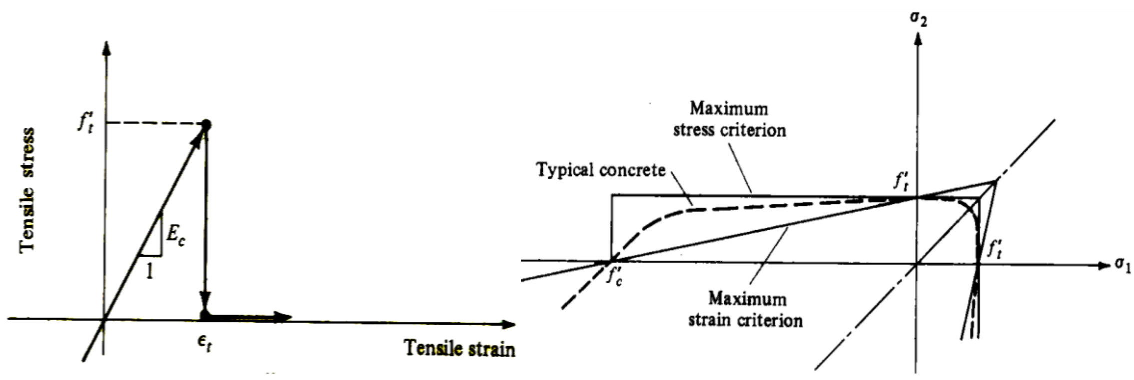

***a*- Biaxial-fracture criteria in tensile zones** ***b*- Tensile stress- strain- fracture relations**

Fig. (٣.١٣) Cracking of Concrete (Chen ١٩٨٢)

3.9.1.1 Smeared Cracking Model

Reshid in١٩٦٨ firstly introduced this model (Schnobrich ١٩٧٧). In this approach, the cracked concrete is assumed to remain a continuum, i.e., the cracks are smeared out in a continuos fashion. It is assumed that the concrete becomes orthotropic or transversely isotropic after the first cracking has occurred, one of the material axis being oriented along the direction of cracking. In the smeared cracking model, a crack is not discrete but implies an infinite number of parallel fissures across that part of the finite element, Fig.(٣.١٤) [Bathe and Ramaswamy (١٩٧٩), Chen (١٩٨٢)].

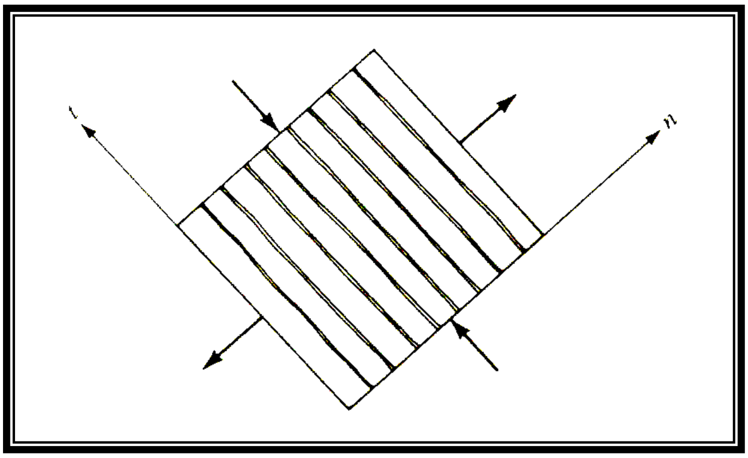

Fig.(٣.١٤) Smeared Crack Model (Hu and Schnobrich

Two different models are used for defining the crack direction. The first is the fixed orthogonal crack. In this approach, the direction of the crack is fixed normally to the direction of the first principal tensile stress that exceeds the cracking stress. By fixing the direction of the cracks, the subsequent rotation of the principal stress is ignored. The second model is the rotating or swinging crack model. In this approach, the crack direction is assumed to be normal to the principal tensile strain direction when the tensile strain reaches a specified limiting value. With further loading and changing of the principal strain direction, the crack is assumed to rotate and the orthotropic material axes are set in the new crack direction.

3.9.1.2 Discrete Cracking Model

As shown in Fig. (٣.١٥), this model represents the individual cracks as actual discontinuities in the finite element mesh. This model was firstly used by Ngo and Scordelis in ١٩٦٧ to analyze simply supported reinforced concrete beams. Cracking is initiated when failure criterion at a certain node is achieved and crack discontinuity is represented by physically splitting that node. An obvious restriction of such model is that the cracks must be formed along the element boundaries. This makes crack patterns mostly dependent on the local mesh refinement. These difficulties have resulted in a very limited acceptance of this model in general structural applications. In the present study, the smeared fixed-crack model has been adopted.

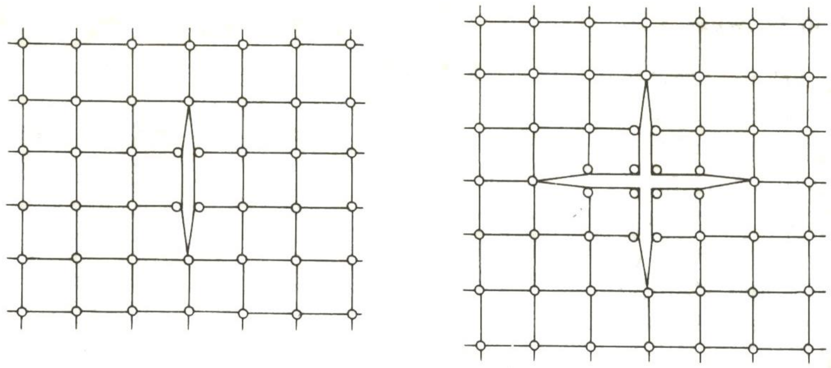

(a)One -Direction Cracking **(b)Two- Direction Cracking**

Fig.(٣.١٥) Discrete Crack Model

3.9.2 Post-Cracking Model

In plain and reinforced concrete structures, cracking is not a perfectly brittle phenomenon and experimental evidence shows that the tensile stresses normal to a cracking plane are gradually released as the crack width increases. This type of response is usually modeled in the finite element analysis by using either the tension stiffening or the strain softening concepts. For reinforced concrete structures where the behavior is characterized by the formation of closely spaced cracks, the first concept seems to be more suitable than the latter. The latter is found to be useful for analyzing plain concrete structures where the behavior is governed by the formation of a single microcrack or a few dominants cracks (Chen ١٩٨٢).

In the case where reinforcement exists, the nature of the stress release is further complicated by the restraining effect of the reinforcing steel. After cracking, the concrete stresses at the crack drop to zero and the steel carries the full load. The concrete between cracks, however, still carries some tensile stresses. This tensile stress drops as the load increases and the drop is associated primarily with bond deterioration between steel and concrete. This ability of concrete to share the tensile load with the reinforcement is termed as ***tension stiffening*** phenomenon.

The tension stiffening effect of concrete has been studied in finite element analysis by using two procedures. First, the tension portion of the concrete stress-strain curve has been given a descending branch. The form of tension–stiffening effect was first introduced by Scanlon. Descending branches of many different shapes have been employed, Linear, bilinear and curved shapes. The second is to increase the steel stiffness. The additional stress in the steel represents the total tensile force carried by both the steel and the concrete between the cracks (Chen ١٩٨٢).

3.9.3 Shear Transfer across The Cracks

Several mechanisms exist by which shear is transferred across reinforced concrete sections. Among these mechanisms are the shear stiffness of uncracked portion of concrete, aggregate interlock in the crack surface (or interface shear transfer), dowel in the reinforcement bars action and the combined effect of tension in reinforcement and arching action.

For the shear transfer across the cracked concrete planes crossed by reinforcement, the two major mechanisms are the dowel action and the aggregate interlock. Shear transfer by these two mechanisms is accompanied by slippage or relative movement of crack faces. In the dowel action, shear forces are partially resisted by the stiffness of reinforcing bars because slippage imposes bearing forces of opposite direction on the bars. The aggregate interlock mechanism is of frictional nature. Slippage causes the irregular faces of the crack to separate slightly. Tensile stresses created in the steel bars by the separation of crack faces in turn develop same shear resistance (AL-Shaarbaf ١٩٩٠).

٣.١٠ Concrete Model Adopted in The Analysis

In this study, a plasticity-based model is adopted for the nonlinear analysis of three-dimensional reinforced concrete structures under static loads. In compression, the behavior of concrete is simulated by an elastic-plastic work hardening model followed by a perfectly plastic response, which is terminated at the onset of crushing. The plasticity model in compression state of stress has the following characteristics: (AL-Shaarbaf ١٩٩٠).

- yield criterion
- hardening rule
- flow rule
- crushing condition

In tension, linear elastic behavior prior to cracking is assumed. A smeared crack model with fixed orthogonal cracks is adopted to represent the fractured concrete. The model will be described in terms of the following:

- cracking criterion
- post-cracking formulation
- shear retention model

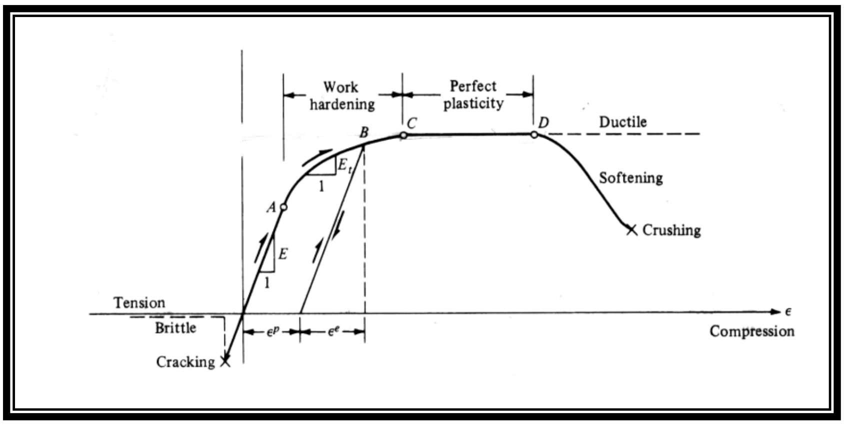

3.10.1 Modeling of Concrete in Compression

3.10.1.1 The Yield Criterion

Under a triaxial state of stress, the yield criterion for concrete is generally assumed to be dependent on three stress invariants. However, a yield criterion dependent on two stress invariants only has been proved to be adequate for most practical situations. The yield criterion incorporated in the present model is of such type and it has been successfully used in research. It can be expressed as (Hinton and Owen ١٩٨٤)

$$f(\sigma) = f(I_1, J_2) = (\alpha I_1 + 3\beta J_2)^{1/2} = \sigma_o \quad \text{...(٣.٨٦)}$$

where (α) and (β) are material parameters, ($I_١$) is the first stress invariant given by:

$$I_1 = \sigma_x + \sigma_y + \sigma_z \quad \text{...(٣.٨٧)}$$

$J_٢$ is the second deviatoric stress invariant given by:

$$J_2 = \frac{1}{3}\{(\sigma_x^2 + \sigma_y^2 + \sigma_z^2) - (\sigma_x\sigma_y + \sigma_y\sigma_z + \sigma_z\sigma_x)\} + \tau_{xy}^2 + \tau_{yz}^2 + \tau_{xz}^2 \quad \text{(٣.٨٨)}$$

and $\sigma o \geq 0$ is the equivalent effective stress at the onset of plastic deformation, this σ_o can be determined from the uniaxial compression test as:

$$\sigma_o = Cp \, . \, f'c \qquad \ldots(٣.٨٩)$$

where $0 \leq Cp \leq 1.0$ is the plasticity coefficient, which is used to mark the initiation of the plastic deformation.

The parameters (α) and (β) are determined by using the uniaxial and biaxial compression tests. Then for a uniaxial compression state, the yield stress is given by:

$$\sigma_x = -\sigma_o \qquad \ldots(٣.٩٠)$$

and for the equal biaxial compression state, the yield stress is given by:

$$\sigma_x = \sigma_y = -\gamma\sigma_o \qquad \ldots(٣.٩١)$$

If the results obtained by Kupfer and Gerstle (١٩٧٣) for the failure envelope is employed for initial yield, the value of the constant (γ) is equal to (١.١٦). From Eq.(٣.٨٦) through Eq.(٣.٩١), the material constants can be found to be:

$$\alpha = 0.35468\sigma_o \quad \text{and} \quad \beta = 1.35468 \qquad \ldots(٣.٩٢)$$

writing $C = \dfrac{\alpha}{(2\,\sigma o)} = 0.17734$

Therefore, Eq. (٣.٨٦) can be written as:

$$f(\sigma) = (2\,C\,\sigma_o \;I_1 + 3\beta J_2)^{1/2} = \sigma_o \qquad \ldots(٣.٩٣)$$

This can be solved for σ_o as:

$$f(\sigma) = C.I_1 + \{(C.I_1)^2 + 3\beta J_2\}^{1/2} = \sigma_o \qquad \ldots(٣.٩٤)$$

3.10.1.2 Hardening Rule

The concept of plastic flow in work hardening materials extends to the notion of perfectly plastic solids for which the yield or failure surface remains fixed in stress space. The hardening rule defines the motion of the subsequent loading surfaces during plastic loading. A number of hardening rules has been proposed to describe the growth of subsequent loading surface for work-hardening materials. Some of these rules are; isotropic hardening, kinematic hardening and mixed hardening. The isotropic model applies mainly to proportional loading. For cyclic and reversed types of loading, kinematic hardening rule is more appropriate. Combinations of isotropic and kinematic hardening are called mixed hardening rules (Chen ١٩٨٢).

An isotropic hardening rule is used in the present study. Therefore, from Eq. (٣.٩٤), the subsequent loading surface may be expressed as: (AL-Shaarbaf ١٩٩٠).

$$f(\sigma) = C.I_1 + \{(C - I_1)^2 + 3\beta J_2\}^{1/2} = \bar{\sigma} \qquad ...(٣.٩٥)$$

where $\bar{\sigma}$ represents the stress level at which further plastic deformation will occur and this is termed as the effective stress or equivalent uniaxial stress.

The incremental theory of plasticity implies a relationship between the effective stress and the effective plastic strain. The effective plastic strain increment $\delta\varepsilon_p$ that results from an incremental plastic work dw_p, may be determined by using the work-hardening hypothesis as:

$$d\varepsilon_p = \frac{dw_p}{\bar{\sigma}} = \frac{\{\sigma\}d\{\varepsilon_p\}}{\bar{\sigma}} \qquad ...(٣.٩٦)$$

where $d\varepsilon_p$ represents the effective accumulated plastic strain increment, along the strain path.

The effective plastic strain can be written as:

$$\varepsilon_p = \int d\varepsilon_p \qquad ...(٣.٩٧)$$

In the present model, a parabolic stress-strain curve is used for the equivalent uniaxial stress-strain relationship beyond the limit of elasticity, $(C_p f'c)$. This relationship represents the work-hardening stage of behavior. When the peak compressive stress is reached, a perfectly plastic response is assumed to occur. Fig. (٣.١٧) shows the equivalent uniaxial stress-strain curve in the various stages of behavior. These are given by:

(a) During the elastic stage, when $\bar{\sigma} \le C_p . f'c$

$$\bar{\sigma} = E . \varepsilon_c \qquad ...(٣.٩٨)$$

(b) After the initial yielding and up to the ultimate concrete compressive strength, when:- $C_p \; f'c \; \le \bar{\sigma} \le f'c$

$$\bar{\sigma} = C_p \; f'c + E \left[\varepsilon_c - \frac{C_p . f'c}{E} \right] - \left[\frac{E}{2\varepsilon_o} \right] \left[\varepsilon_c - \frac{C_p f'c}{E} \right]^2 \qquad ...(٣.٩٩)$$

c) for $\varepsilon_c \ge (2 - C_p) f'c / E$

$$\bar{\sigma} = f'c \qquad ...(٣.١٠٠)$$

where $\boldsymbol{\varepsilon_o}^{-}$ represents the total strain corresponding to the parabolic part of the curve that can be calculated from:

$$\bar{\varepsilon}_O = \frac{2(1\text{-}C_p)}{E} f'c \qquad ...(٣.١٠١)$$

A value of ٠.٣ is assumed for the plasticity coefficient ***(Cp)*** in the present study and hence plastic yielding begins at a stress level equal to ***(٠.٣f′c)***(Chen ١٩٨٢).

The total effective strain ε_c is composed of two parts, elastic and plastic components:

$$\varepsilon_c = \varepsilon_e + \varepsilon_p \qquad ...(٣.١٠٢)$$

The elastic strain ε_p is given by:

$$\varepsilon_e = \frac{\bar{\sigma}}{E} \qquad \text{...(٣.١٠٣)}$$

By substituting Eq. (٣.١٠٢) and Eq. (٣.١٠٣) into Eq. (٣.٩٩), the effective stress- plastic strain relation can be expressed as:

$$\bar{\sigma} = C_p\ f'c - E\ C_p + (\ 2E^2 . \bar{\varepsilon}_o \varepsilon_p)^{1/2} \qquad \text{...(٣.١٠٤)}$$

Differentiation of Eq. (٣.١٠٤) with respect to the plastic strain leads to the slope of the tangent of the effective stress-plastic strain curve, which represents the hardening coefficient, H, that is needed in the formulation of the incremental stress-strain relation:

$$H' = \frac{d\,\bar{\sigma}}{d\varepsilon_p} = E\left(\sqrt{\frac{\varepsilon_0}{2\varepsilon_p}} - 1\right) \qquad \text{...(٣.١٠٥)}$$

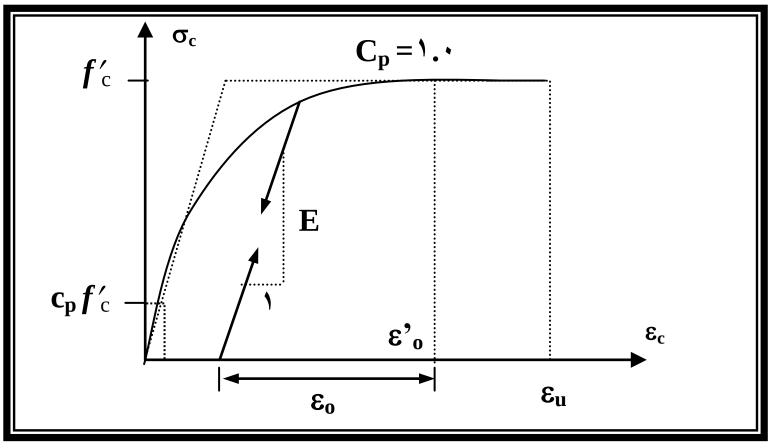

Fig.(٣.١٧) Uniaxial Stress-Strain Curve for Concrete (AL-Shaarbaf ١٩٩٠)

3.10.1.3 Flow Rule

In plasticity theory, a flow rule must be defined so that the plastic strain increment can be determined for a given stress increment. The associated flow rule has been widely used for concrete models mainly because of its simplicity. This approach is adopted in the current model. The plastic strain increment is expressed as:

$$d(\varepsilon_p) = d\lambda \ \frac{\partial f(\sigma)}{\partial \sigma} \qquad \text{...(٣.١٠٦)}$$

The normal to the current loading surface $\frac{\partial f(\sigma)}{\partial \sigma}$ is termed as the flow vector The yield function derivatives with respect to the stress components define the flow vector **{a}** as:

$$\{a\} = \left[\frac{\partial f}{\partial \sigma_x}, \frac{\partial f}{\partial \sigma_y}, \frac{\partial f}{\partial \sigma_z}, \frac{\partial f}{\partial \tau_{xy}}, \frac{\partial f}{\partial \tau_{yz}}, \frac{\partial f}{\partial \tau_{zx}} \right]^T \qquad \text{...(٣.١٠٧)}$$

where,

$$\left.\begin{aligned}
a_{١} &= \frac{\partial f}{\partial \sigma_x} = c + \left[2\left(c^2 + \beta\right)\sigma_x + \left(2c^2 - \beta\right)\left(\sigma_y - \sigma_z\right)\right] / Q \\
a_{٢} &= \frac{\partial f}{\partial \sigma_y} = c + \left[2\left(c^2 + \beta\right)\sigma_y + \left(2c^2 - \beta\right)\left(\sigma_x - \sigma_z\right)\right] / Q \\
a_{٣} &= \frac{\partial f}{\partial \sigma_z} = c + \left[2\left(c^2 + \beta\right)\sigma_z + \left(2c^2 - \beta\right)\left(\sigma_x - \sigma_z\right)\right] / Q
\end{aligned}\right\}$$

...(٣.١٠٨)

$$a_٤ = \frac{\partial f}{\partial \sigma_x} = 6.\beta.\tau_{xy}/Q$$

$$a_٥ = \frac{\partial f}{\partial \sigma_y} = 6.\beta.\tau_{yz}/Q$$

$$a_٦ = \frac{\partial f}{\partial \sigma_z} = 6.\beta.\tau_{zx}/Q$$

where c and β, are the material constants, and Q is given by:

$$Q = 2\begin{bmatrix}\left(c^2+\beta\right)\left(\sigma_x^2+\sigma_y^2+\sigma_z^2\right)+\left(2c^2-\beta\right)\left(\sigma_x\sigma_y+\sigma_y\sigma_z+\sigma_z\sigma_x\right)\\ .3\beta\left(\tau_{xy}^2+\tau_{yz}^2+\tau_{zx}^2\right)\end{bmatrix}^{1/2} \quad ...(٣.١٠٩)$$

3.10.1.4 The Incremental Stress-Strain Relationship

During the plastic loading, both of the initial yield and the subsequent stress states must satisfy the yield condition. $\boldsymbol{F\left(\sigma, K\right)=0}$. The yield function defined in Eq. (٣.٩٤), can be rewritten as,

$$F\left(\sigma, K\right)=f\left(\sigma\right)+K\left(k\right)=0 \quad ...(٣.١١٠)$$

where k, is the hardening parameter, which governs the expansion of the yield surface. By differentiating Eq. (٣.١١٠), then

$$dF=\frac{\partial F}{\partial \sigma}d\sigma+\frac{\partial F}{\partial K}dK=0 \quad ...(٣.١١١)$$

or

$$a^T d\sigma - A\,d\lambda = 0 \quad ...(٣.١١٢)$$

where

$$A = -\frac{1}{d\lambda}\frac{\partial F}{\partial k}dk \qquad \text{...(٣.١١٣)}$$

The total incremental strain vector can be rewritten as:

$$d\{\varepsilon)\} = d\{\varepsilon^{e}\} + d\lambda\frac{\partial F}{\partial \sigma} \qquad \text{...(٣.١١٤)}$$

The elastic strain increment is related to the stress increment by the elastic constitutive relation which is given in:

$$d\{\sigma\} = [D]d\{\varepsilon_e\} \qquad \text{...(٣.١١٥)}$$

where [D] is the elastic constitutive matrix given by

$$[D] = \frac{E}{(1+\nu)(1-2\nu)}\begin{bmatrix} 1-\nu & \nu & \nu & 0 & 0 & 0 \\ \nu & 1-\nu & \nu & 0 & 0 & 0 \\ \nu & \nu & 1-\nu & 0 & 0 & 0 \\ 0 & 0 & 0 & (1-2\nu)/2 & 0 & 0 \\ 0 & 0 & 0 & 0 & (1-2\nu)/2 & 0 \\ 0 & 0 & 0 & 0 & 0 & (1-2\nu)/2 \end{bmatrix} \qquad \text{...(٣.١١٦)}$$

Substitution of Eq. (٣.١١٥) into Eq. (٣.١١٤) yields

$$d\varepsilon = [D]^{-1}d\sigma + d\lambda\{a\} \qquad \text{...(٣.١١٧)}$$

Pre-multiplying both sides of Eq. (٣.١١٧) by $\{\mathbf{a}\}^{T}[\mathbf{D}]$ and eliminating $a^{T}.d\sigma$ by making use of Eq. (٣.١١٢), the following expression for the plastic multiplier $\mathbf{d\lambda}$ is obtained,

$$d\lambda = \left[\frac{\{a\}^T [D]}{H' + \{a\}^T [D]\{a\}} \right] d\{\varepsilon\} \qquad ...(٣.١١٨)$$

By substituting Eq. (٣.١١٨), into Eq. (٣.١١٤), and pre multiplying both sides by [D], the complete elastic incremental stress-strain relationship can be expressed as:

$$d\{\sigma\} = \left[[D] - \frac{[D]\{a\}\{a\}^T [D]}{H' + \{a\}^T [D]\{a\}} \right] d\{\varepsilon\} \qquad ...(٣.١١٩)$$

where the second term in the brackets represents the stiffness degradation due to the plastic deformation.

3.10.1.5 Crushing Condition

Crushing indicates the complete rupture and disintegration of the material under compressive stress state. After crushing, the current stresses drop rapidly to zero and the concrete is assumed to lose its resistance completely against further deformation. In the adopted model, concrete is considered to crush when the strain reaches a specified ultimate value. Hence, rewriting the yield condition from Eq. (٣.٩٤) in terms of the peak strain, the following crushing criterion is obtained (Chen ١٩٨٢):

$$C\ \bar{I}_1 + \sqrt{\left(C\bar{I}_1\right)^2 + \beta\bar{J}_2} = \varepsilon_{cu} \qquad ...(٣.١٢٠)$$

where $\bar{I}_1$: is the first strain invariant

$\bar{J}_2$: is the second deviatoric strain

ε_{cu} :is the ultimate concrete strain that can be extrapolated from the uniaxial compression test.

3.10.2 Modeling of Concrete in Tension

3.10.2.1 Cracking Criterion

The maximum tensile stress criterion is used in this research work to monitor cracking. For a previously uncracked sampling point, if the principal stress σ_1 exceeds the limiting value of tensile stress, a crack is assumed to form. The limiting tensile stress required to define the onset of cracking can be calculated for states of triaxial tensile stress and for combination of tension and compression principal stresses as follows (Bathe and Ramaswamy ١٩٧٩):

a) For triaxial tension zone $(\sigma_1 \geq \sigma_2 \geq \sigma_3 \geq 0)$

$$\sigma_i = \sigma_{cu} = f_t \qquad i = 1,2,3$$

...(٣.١٢١)

b) For the tension-tension-compression zone $(\sigma_1 \geq \sigma_2 \geq 0, \sigma_3 \leq 0)$

$$\sigma_i = \sigma_{cr} = f_t \left[1 + \frac{0.75\,\sigma_3}{f'_c}\right] \qquad i = 1,2$$

...(٣.١٢٢)

c) For the tension-compression-compression zone $(\sigma_1 \rangle\, 0, \sigma_3 \leq \sigma_2 \leq 0)$

$$\sigma_1 = \sigma_{cr} = f_t \left[1 + \frac{0.75\sigma_2}{f'_c}\right]\left[1 + \frac{0.75\sigma_3}{f'_c}\right]$$

...(٣.١٢٣)

where σ_{cr} is the cracking stress and both f_t and f'_c are given positive values Eq. (٣.١٢٢) incorporates the fact that compression in one direction favors cracking in the others and thus reduces the tensile capacity of the material.

When the major principal stress σ_1 violates the cracking criterion, planes of failure develop perpendicular to its direction. Concrete behavior is no longer isotropic, it becomes orthotropic with the direction of orthotropy coinciding with the direction of σ_1. Therefore, the normal and shear stresses across the plane of failure and the corresponding normal and shear stiffness are reduced, and the concrete is assumed to be transversely isotropic with axes of isotropy being perpendicular to the direction of σ_1. Thus, the incremental stress-strain relationship in the local axes can be expressed as:

$$\begin{Bmatrix} \Delta\sigma_1 \\ \Delta\sigma_2 \\ \Delta\sigma_3 \\ \Delta\tau_{12} \\ \Delta\tau_{23} \\ \Delta\tau_{31} \end{Bmatrix} = \begin{bmatrix} E_1 & 0 & 0 & 0 & 0 & 0 \\ 0 & E/\left(1-\nu^2\right) & \nu E/\left(1-\nu^2\right) & 0 & 0 & 0 \\ 0 & \nu E/\left(1-\nu^2\right) & E/\left(1-\nu^2\right) & 0 & 0 & 0 \\ 0 & 0 & 0 & \beta_1 G & 0 & 0 \\ 0 & 0 & 0 & 0 & G & 0 \\ 0 & 0 & 0 & 0 & 0 & \beta_1 G \end{bmatrix} \begin{Bmatrix} \Delta\varepsilon_1 \\ \Delta\varepsilon_2 \\ \Delta\varepsilon_3 \\ \Delta\gamma_{12} \\ \Delta\gamma_{23} \\ \Delta\gamma_{31} \end{Bmatrix}$$

...(٣.١٢٤)

or in a condensed from:

$$\{\Delta\sigma\} = \lfloor D_{cr} \rfloor \{\Delta\varepsilon\}$$

...(٣.١٢٥)

where E_1 is the reduced modulus of elasticity in the direction of σ_1, $\beta_1 G$ is the reduced shear modulus across the failure plane.

[D_{cr}] is the material stiffness in the local axes. The stress increments in the global axes (***x***, ***y***, ***z***) may be obtained by using the coordinate transformation matrix such that:

$$\{\Delta\sigma\} = [T]^T [D_{cr}][T]\{\Delta\varepsilon\} \qquad \ldots (٣.١٢٦)$$

where ***[T]*** is the transformation matrix expressed in terms of the direction cosines as:

$$[T] = \begin{bmatrix} i_1^2 & m_1^2 & n_1^2 & i_1m_1 & m_1n_1 & n_1i_1 \\ i_2^2 & m_2^2 & n_2^2 & i_2m_2 & m_2n_2 & n_2i_2 \\ i_3^2 & m_3^2 & n_3^2 & i_3m_3 & m_1n_1 & n_1i_1 \\ 2i_1i_2 & 2m_1m_2 & 2n_1n_2 & i_1m_2 + i_2m_1 & n_2m_1 + n_1m_2 & i_2n_1 + i_1n_2 \\ 2i_2i_3 & 2m_2m_3 & 2n_2n_3 & i_2m_3 + i_3m_2 & n_3m_2 + n_2m_3 & i_3n_2 + i_2n_3 \\ 2i_3i_1 & 2m_3m_1 & 2n_3n_1 & i_3m_1 + i_1m_3 & n_1m_3 + n_3m_1 & i_1n_3 + i_3n_1 \end{bmatrix} \qquad (٣.١٢٧$$

where **i**$_i$, **m**$_i$ and **n**$_i$ represent the direction cosines of the local coordinate axes with (x, y and z) direction respectively.

For the tension – tension – compression and the triaxial tension states of stress, the cracking criterion may be violated by the major principal stress σ_1, and the second principal stress σ_2, simultaneously. Thus, two sets of orthogonal cracked planes may develop and the constitutive matrix in the local material axes become diagonal:

$$[D]_{cr} = \begin{bmatrix} E_1 & 0 & 0 & 0 & 0 & 0 \\ 0 & E_2 & 0 & 0 & 0 & 0 \\ 0 & 0 & E_3 & 0 & 0 & 0 \\ 0 & 0 & 0 & \beta_1 G & 0 & 0 \\ 0 & 0 & 0 & 0 & \beta_2 G & 0 \\ 0 & 0 & 0 & 0 & 0 & \beta_1 G \end{bmatrix} \qquad \ldots (٣.١٢٨)$$

In the current model, a maximum of three sets of cracking is allowed to form at each sampling point.

٣.١٠.٢.٢ Post-Cracking Models

٣.١٠.٢.٢.١ Tension- Stiffening Model

The tensile stresses normal to the cracked planes are gradually released, and represented by an average stress-strain curve. In the present study such a relationship may be obtained by using the tension-stiffening model. This is specified by a linear descending stress-strain curve similar to that shown in Fig. (٣.١٨) and this is given by: [Scanlon (١٩٧١), Bathe and Ramsawamy (١٩٧٩)]

a) for $\varepsilon_{cr} \le \varepsilon_n \le \alpha_1 \varepsilon_{cr}$

$$\sigma_n = \alpha_2 \, \sigma_{cr} \left[\frac{\alpha_1 - \dfrac{\varepsilon_n}{\varepsilon_{cr}}}{\alpha_1 - 1.0} \right]$$

...(٣.١٢٩)

b) for $\varepsilon_n \rangle \alpha_1 \varepsilon_{cr}$

$$\sigma_n = 0.0$$

...(٣.١٣

where σ_n and ε_n are the stress and strain normal to the cracked plane, ε_{cr} is the cracking strain associated with the cracking stress σ_{cr} and $\alpha_١$, and $\alpha_٢$ are the tension-stiffening parameters. $\alpha_١$ represents the rate of stress release as the crack widens, while $\alpha_٢$ represents the sudden loss of stress at instant of cracking.

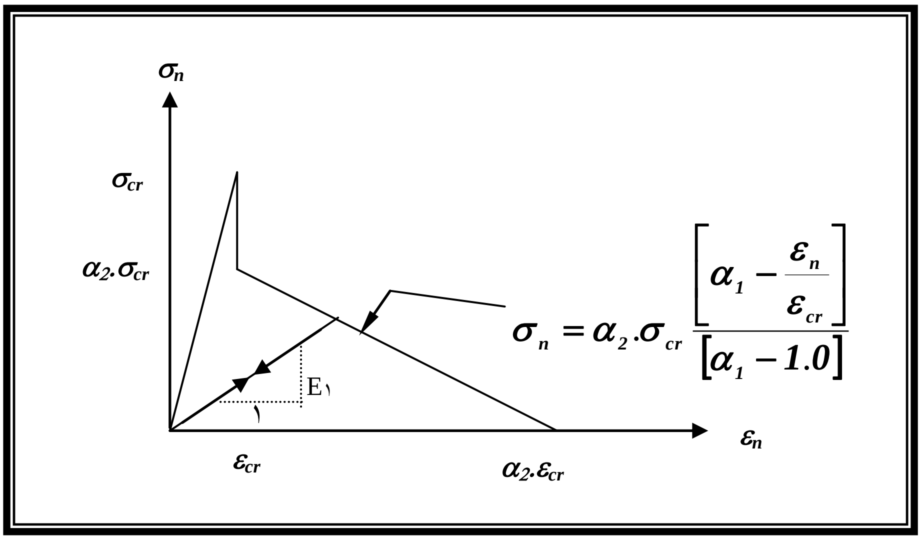

Fig.(۳.۱۷) Post Cracking Model for Concrete

3.10.2.2.2 Shear Retention Model

At a cracked sampling point, the shear stiffness across the cracked plane becomes progressively smaller as the crack widens. A reduced shear modulus βG, has been used across the cracked plane. The value of β depends on the stage of loading and it is given by:

a) For $\varepsilon_n \le \varepsilon_{cr}$

$$\beta = 1$$

...(۳.۱۳۱)

b) For $\varepsilon_{cr} \le \varepsilon_n \le \gamma_1 \varepsilon_{cr}$

$$\beta = \frac{\gamma_2 - \gamma_3}{\gamma_1 - 1}\left[\gamma_1 - \frac{\varepsilon_n}{\varepsilon_{cr}}\right] + \gamma_{cr}$$

...(۳.۱۳۲)

c) For $\varepsilon_n \rangle \gamma_1 \varepsilon_{cr}$

$$\beta = \gamma_3 \qquad ...(٣.١٣٣)$$

Fig. (٣.١٨) shows schematically the value of ***(β)*** for different stages. $\gamma_١$, $\gamma_٢$, $\gamma_٣$ are shear retention parameters. $\gamma_١$ represents the rate of decay of shear stiffness as the crack widens, $\gamma_٢$ is the sudden loss in shear stiffness at the instant of cracking $\gamma_٣$ is the residual shear stiffness due to the dowel action.

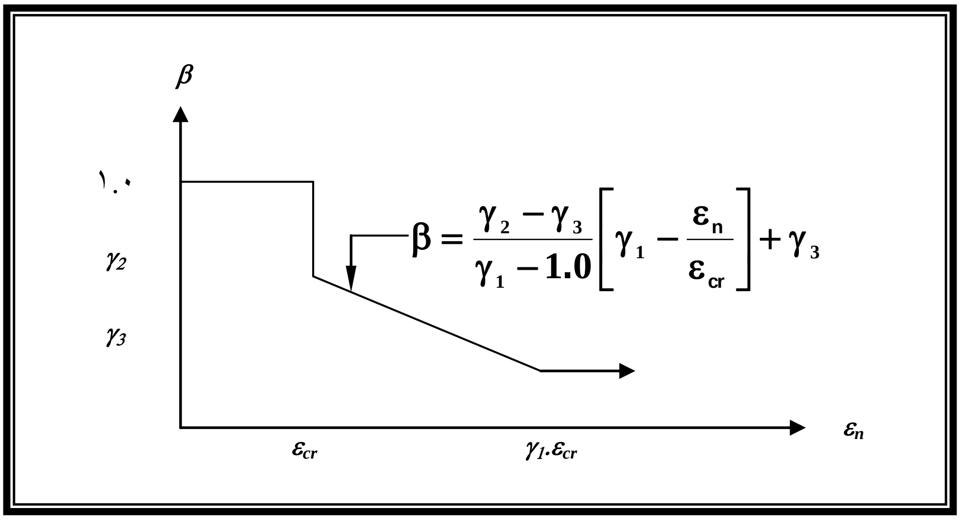

Fig (٣.١٨) Shear Retention for Concrete

3.10.2.3 Modeling The Compressive Strength Reduction Due to Orthogonal Cracks

In a reinforced concrete member, a significant degradation in compressive strength can result due to presence of transverse tensile strain after cracking (Cervenka ١٩٨٥). In plasticity based model, the effect of these tensile strains on the yield criterion and the evolution of the subsequent loading surface can be simulated by scaling the equivalent uniaxial stress-strain relationships given by Eqs. (٣.٩٨) and (٣.١٠٠), according to the current value of the compressive strength reduction factor.

The model used here is due to Cervenka and this depends on the reduction factor $(\lambda)$to reduce both the peak stress and the corresponding strain, Fig. (٣.٢٠). From Eqs. (٣.٩٨-٣.١٠٠), the modified stress-strain relationship may be written: (Cervenka ١٩٨٥).

a) for $\bar{\sigma} \le Cp\,.\,f'c$

$$\bar{\sigma} = E\,\varepsilon_c$$

...(٣.١٣٤)

b) for $\lambda\ Cp\ f'c \le \bar{\sigma} \le \lambda\, f'c$

$$\bar{\sigma} = \lambda\, Cp\, f'c + E\left[\varepsilon_e - \frac{\lambda\, Cp\ f'c}{E}\right] - \frac{E}{2\,\varepsilon_0}\left[\frac{\lambda\ Cp\ f'c}{E}\right]$$

...(٣.١٣٥)

c) for $\varepsilon_c \ge (2 - Cp)\lambda\, f'c / E$

$$\bar{\sigma} \le \lambda\ f'c$$

...(٣.١٣٦)

where

$$\varepsilon'_o = 2(1 - Cp)\lambda\,.\,f'c / E$$

...(٣.١٣٧)

The effective stress-plastic strain relation can be modified as:

$$\bar{\sigma} = \lambda\, c_p\ f'cE.\varepsilon_p + \left(2\,E^2\ \lambda.\varepsilon_o\ \ \varepsilon_p\right)^{1/2}$$

...(٣.١٣٨)

and the hardening parameter can be expressed as:

$$H' = \frac{d\,\bar{\sigma}}{d\,\varepsilon_p} = E\left\{\left[\frac{\lambda\,\bar{\varepsilon}_o}{2\,\varepsilon_p}\right]^{1/2} - 1.0\right\}$$

...(٣.١٣٩)

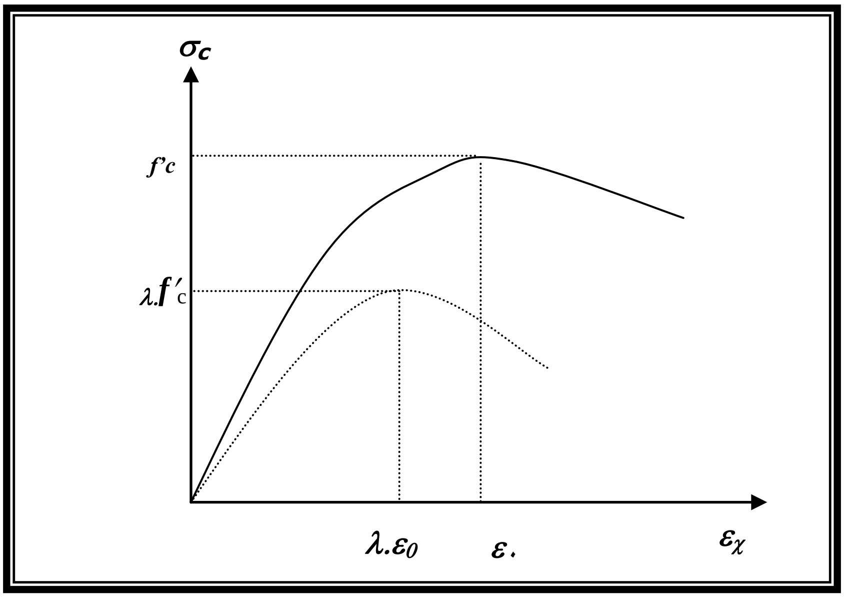

Fig.(٣.٢٠):Uniaxial Compressive Stress-Strain Relationship for Cracked Concrete

For a singly cracked sampling point, the compression reduction factor is given by:

$$\lambda = 1.0 - K_1 \frac{\varepsilon_1}{0.005} \leq 1.0 - K_1$$

...(٣.١٤٠)

where ε_1 is the transverse tensile strain in principal direction (١), the strain normal to the cracked plane. Also for doubly cracked sampling point, the reduction factor may be taken as:

$$\lambda = 1.0 - K_1 \frac{\left(\varepsilon_1^2 + \varepsilon_2^2\right)}{0.005} \leq 1.0 - K_1$$

...(٣.١٤١)

where ε_2 is the tensile strain normal to the second crack.

٣ . ١ ١ Modeling of Reinforcement

Compared to concrete, steel is a much simpler material to represent. Its stress-strain behavior can be assumed to be identical in tension and compression. In reinforced concrete members, reinforcing bars are normally long and relatively slender and therefore they can be assumed to be capable of transmitting axial forces only. In the current study, the uniaxial stress-strain behavior of reinforcement is simulated by an elastic-linear work hardening model, as shown in Fig. (٣. ٢١).

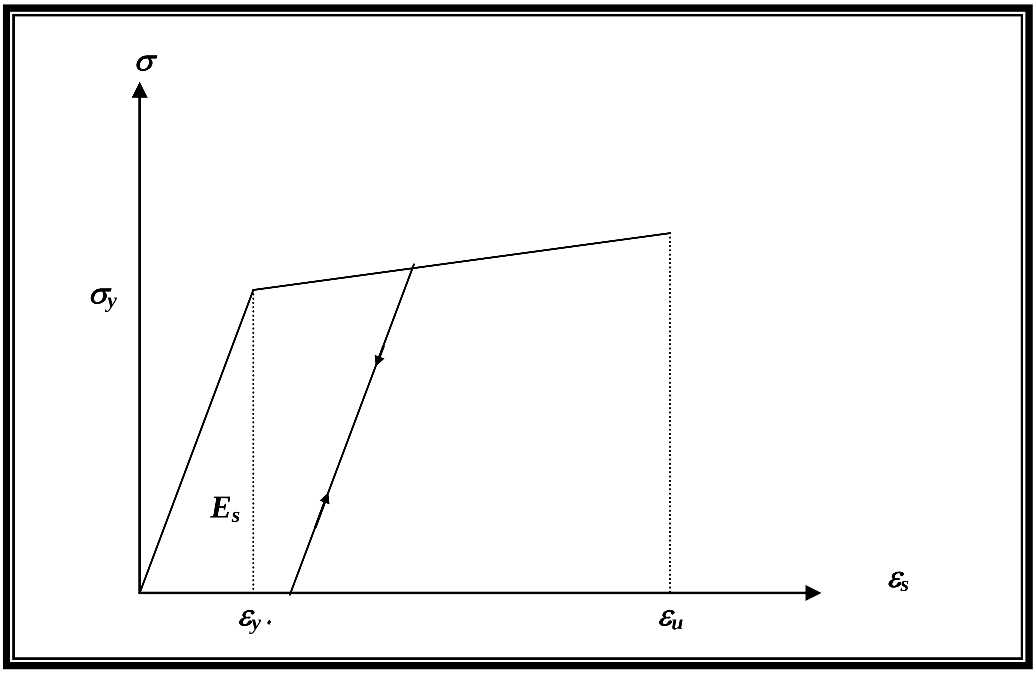

Fig.(٣.٢١) Stress-Strain Relationship of Steel Bars Used in the Analysis (Mohammed ٢٠٠١)

٣.١٢ The Employed Computer Programs

In the present research work, program ***P٣DNFEA*** **(program of Three-Dimensional Nonlinear Finite Element Analysis)**, which has been originally developed by AL-Shaarbaf and introduced in his Ph.D. thesis (١٩٩٠) is used. The main objective of the program is to analyze reinforced concrete members under general three-dimensional states of loading up to failure. The type of nonlinearity, which has been considered in this program, is the material nonlinearity. The major modification to the original program, which has been implemented by Mohammed (٢٠٠١), was the development of subroutines, which take into account the geometrical nonlinearity into consideration in three-dimensional problems by definition of large strain-displacement equations.

In the present work, the main modification to this program was the adding of ١٤-node brick element to analyze reinforced concrete members. The subroutine ***BRK١٤*** which is used to calculate the shape functions to ١٤-node brick element, was listed in Appendix [A].

In the present study, the ***Fortran PowerStation ٤.٠*** compiler produced by Microsoft Incorporation was used to operate the program under PC Pentium III with Intel ٦٥٠ MHz processor and ١٢٨ MB RAM.

CHAPTER FOUR

APPLICATIONS, RESULTS AND DISCUSSION

٤.١ INTRODUCTION

This chapter deals with the prediction of the behavior of reinforced concrete plate and shell structures using the finite element method and models presented in the previous chapter.

The main aim of this chapter is to study the validity, efficiency and the accuracy of the computational model and to demonstrate the versatility of the computer program used for the analysis of different types of structures. Some factors that affect the behavior of such structures are also studied. Comparison between the present analytical results and other theoretical and available experimental results are made to check the accuracy of the present method of analysis.

In the following sections, the analytical results obtained for the considered examples are discussed.

٤.٢ Reinforced Concrete Cylindrical Shell

A reinforced concrete cylindrical shell (shell no.٢) with edge beams was tested experimentally by Bouma et al. (١٩٦١). The dimensions and reinforcement details of the shell and the edge beams are illustrated in Fig. (٤.١). The applied load was uniformly distributed. This load and the dead weights of the shells with the edge beams are included in total applied load.

Several investigators such as [Arnesen et. al. (١٩٧٩), Ramm et. al. (١٩٨٤), and Thannon et. al. (١٩٨٧)] have analyzed the shell and thus comparison can be made with their models. Concrete and steel material properties and the additional material parameters are given in Table (٤. ١).

By utilizing symmetry properties, only one quarter of the shell is analyzed. The finite element meshes and boundary conditions are shown in Fig. (٤.٢).

Table (٤.١) Material Properties of Bouma's Cylindrical Shell

	Material properties and material parameters	symbol	Value
concrete	Young's modulus	E_c (N/mm^{٢})	٢٩٤٠٠
	Compression strength	$f'c$ (N/mm^{٢})	٣٠
	Tensile strength	f_t (N/mm^{٢})	١.٨٢
	Poisson's ratio	ν	٠.١٥
	Uniaxial crushing strain	ε_{cu}	٠.٠٠٣
Steel	Young's modulus	E_s (N/mm^{٢})	٢١٠٠٠٠
	Yield stress of shell reinforcement	f_y (N/mm^{٢})	٢٩٥
	Yield stress of beam reinforcement	f_y (N/mm^{٢})	٢٨٠
	Hardening parameter	H'	٠.٠
Tension stiffening parameters	Rate of stress release	$\alpha_{١}$	١٠.٠
	Sudden loss of stress at the instant cracking	$\alpha_{٢}$	٠.١
Shear retention parameters	Rate of decay of shear stiffness	$\gamma_{١}$	١٠.٠
	Sudden loss of shear stiffness at instant of cracking	$\gamma_{٢}$	٠.٥
	Residual shear stiffness due to dowel action	$\gamma_{٣}$	٠.١

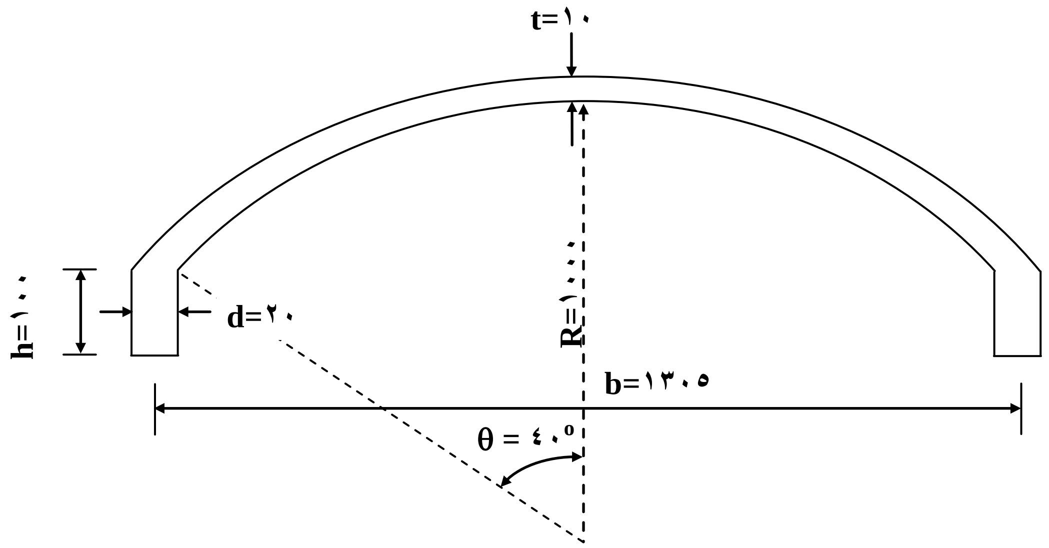

(a) Cylindrical shell cross section

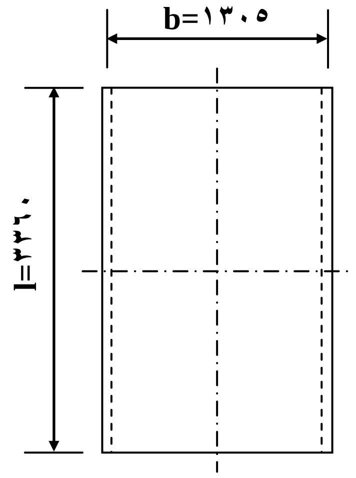

(b) Dimension of Cylindrical shell

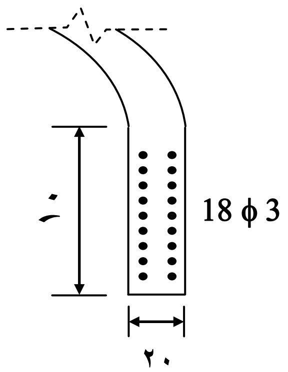

(c) Details of edge beam reinforcement

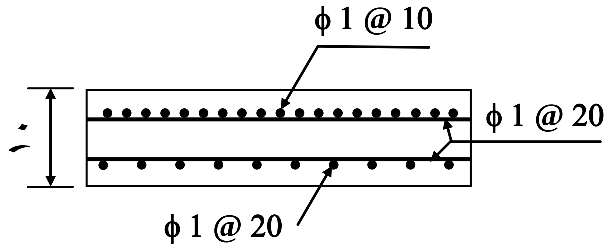

(d) Details of shell reinforcement

<u>All dimensions in mm</u>

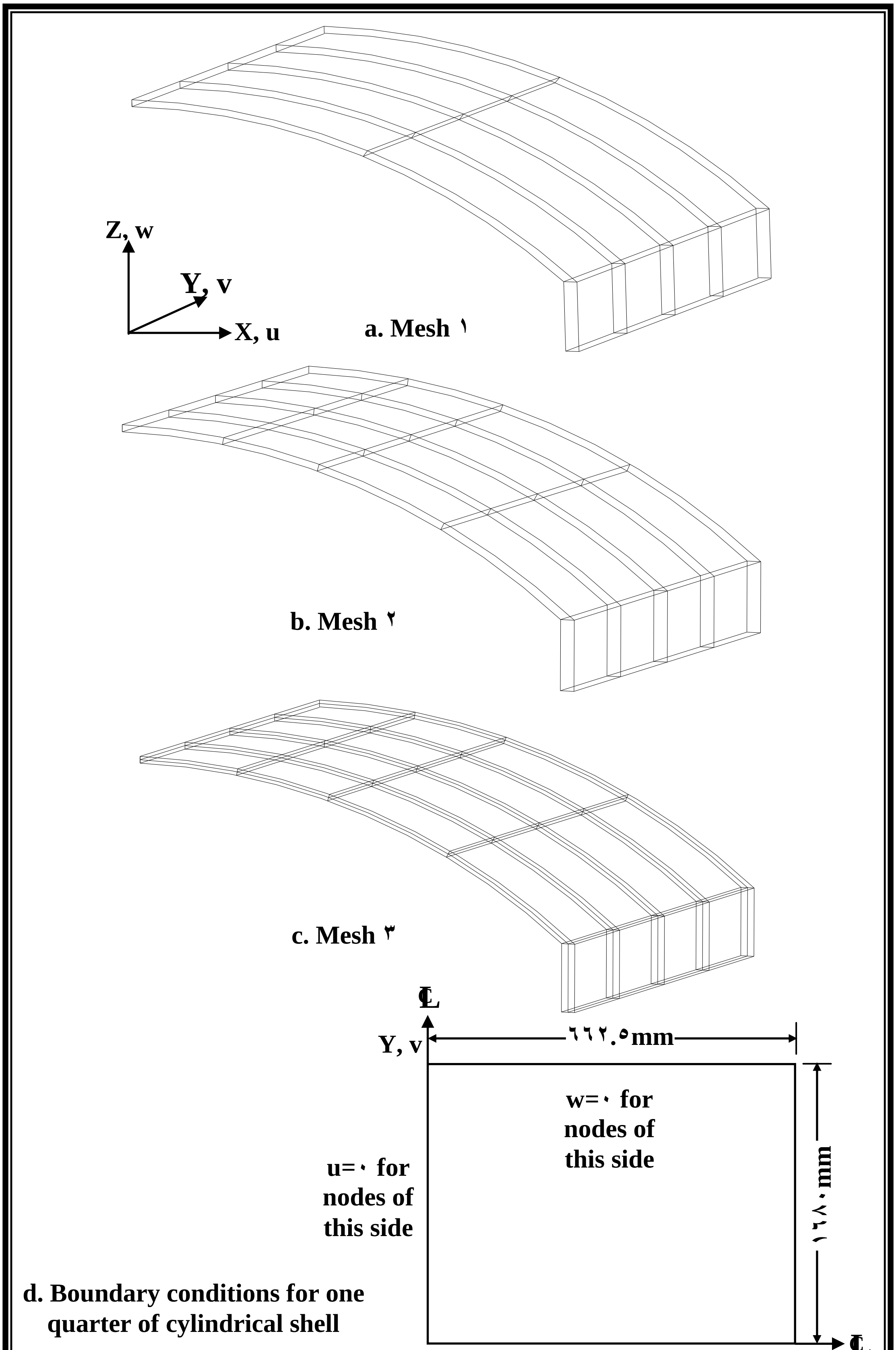
Z, w
Y, v
X, u
a. Mesh ١
b. Mesh ٢
c. Mesh ٣
℄
Y, v
٦٦٢.٥mm
w=٠ for
nodes of
this side
u=٠ for
nodes of
this side
١٦٨٠ mm
℄
d. Boundary conditions for one
quarter of cylindrical shell

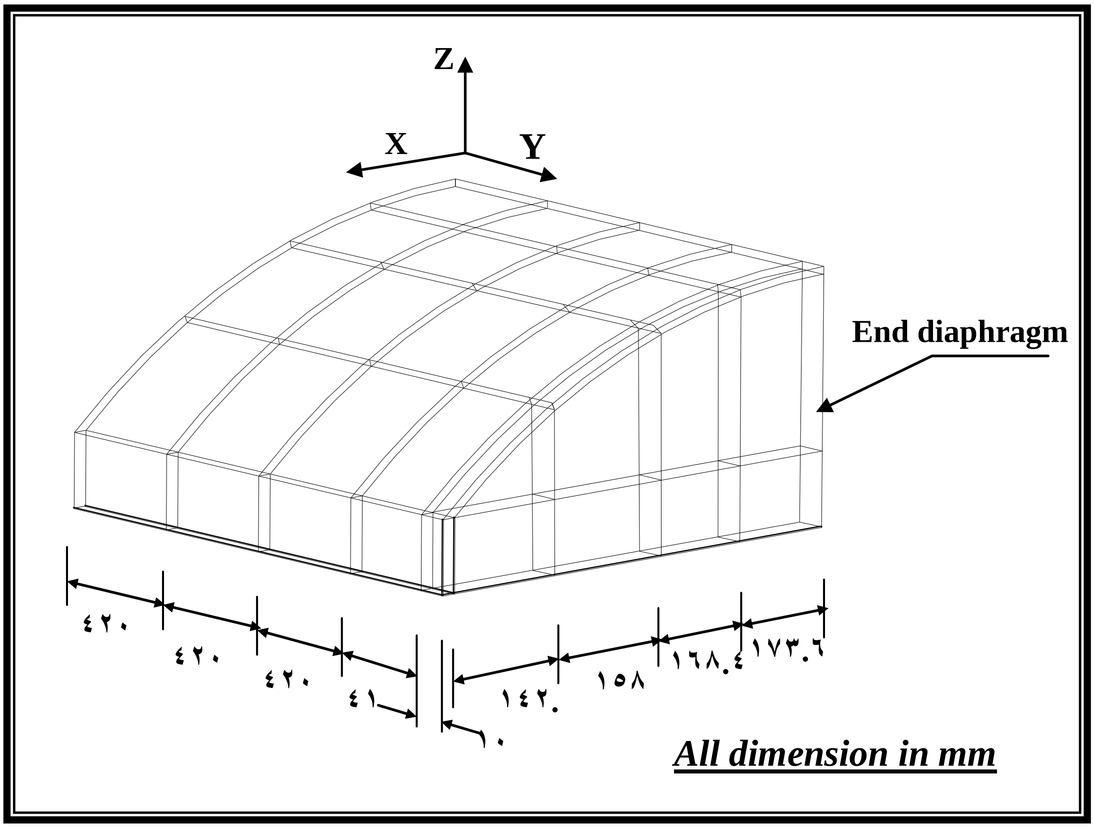

Fig. (٤.٣) Modeling of End Diaphragm for Bouma's Cylindrical Shell No.٢ (Mesh ٤)

٤.٢.١ Finite Element Results

The experimental, other theoretical pervious studies and the present finite element solutions as obtained from this study are compared in Fig. (٤.٤). In general, this figure shows good agreement for the finite element solution obtained from the present study compared with the experimental results throughout the entire range of behavior. It may be observed that the predicted ultimate load ٤٩.٣ kN was the nearest to the experimental ultimate load ٥٠.٨ kN. Also, the load-deflection behavior by using the degenarate two-dimensional finite element model supported by Thannon (١٩٨٨) is relatively closer to the experimental response but the predicated failure load is ٤٨.٠ kN.

Fig. (٤.٥) shows the deformation at midspan cross-section at failure load, this figure shows very good agreement with experimental and Thannon (١٩٨٨) results.

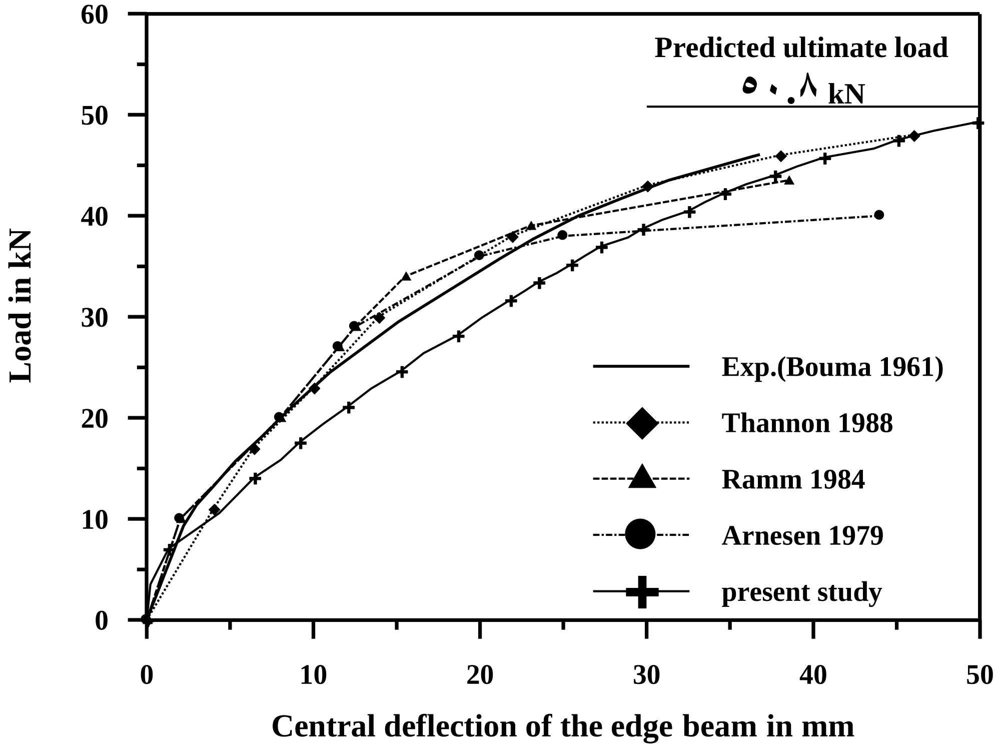

Fig. (٤.٤) Comparison of Load Deflection Curve for Bouma's Shell No.٢

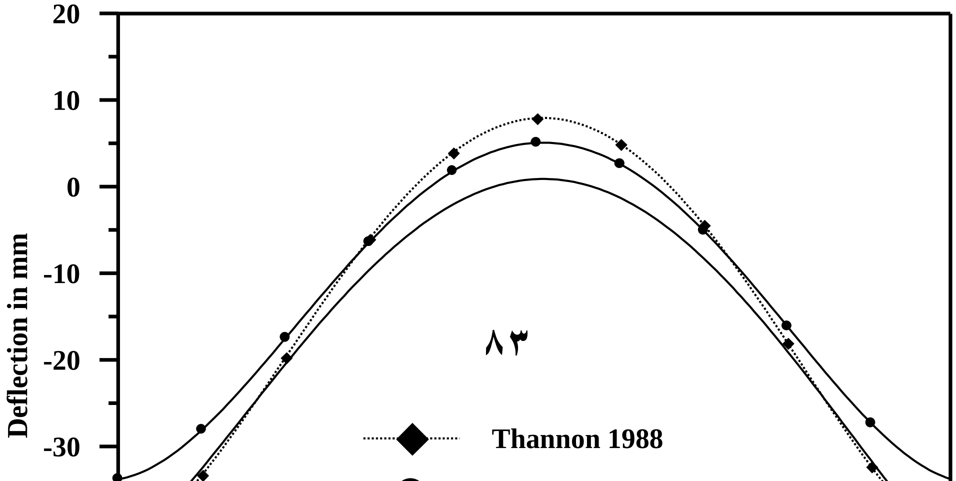

٤.٢.١.١ Effect of Mesh Refinement and Modeling of End Diaphragm

Three different meshes have been used as shown in Fig. (٤. ٢). As shown in Fig. (٤. ٢), mesh no. ١ represented one layer with twelve elements, mesh no. ٢ considered one layer with twenty elements, and mesh no. ٣ considered two layers each one has twenty elements.

Instead of modeling the end diaphragm, the end of the cylindrical shell is assumed simply supported in mesh no. ١, ٢, and ٣. The real representation for end diaphragm is considered in mesh no. ٤.

The comparison between the finite element solutions for different types of mesh and the experimental behavior is made in Fig. (٤. ٦). Fig. (٤. ٧) shows a good agreement with experimental results throughout the whole behavior by modeling end diaphragm. The end diaphragm modeling gives good results for two reasons:

١. The real representation for the geometry and the boundary conditions

٢. The increasing in the degrees of freedom due to increasing in the number of elements which modeled the cylindrical shell

Results and Discussion

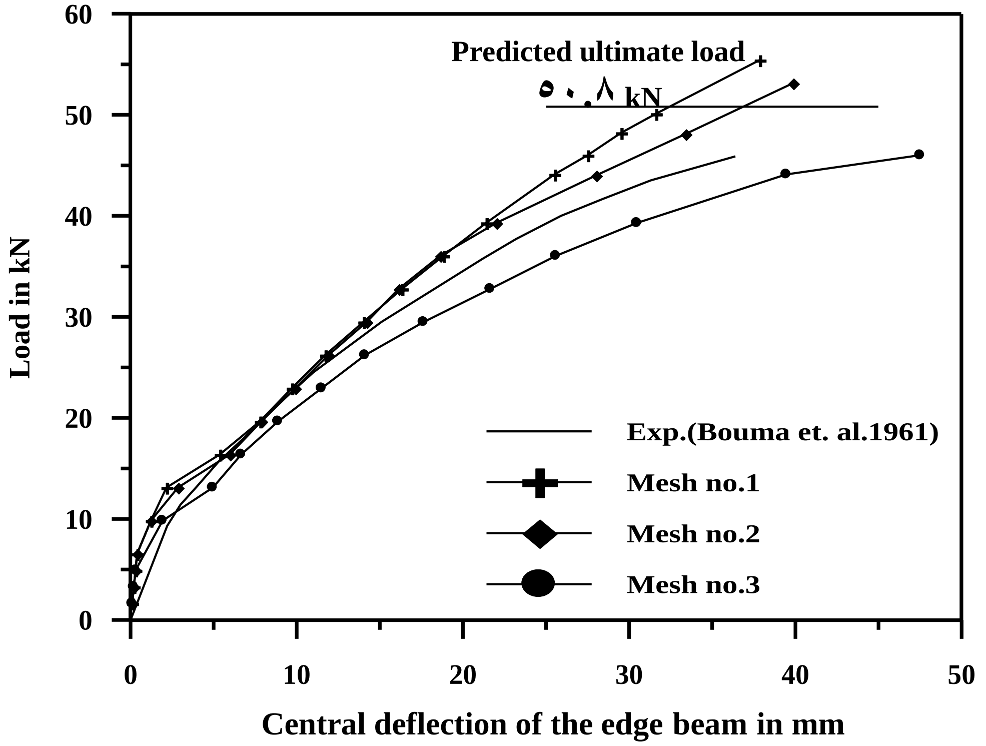

Fig. (٤.٦) Bouma's Shell No.٢, Effect of Mesh Type

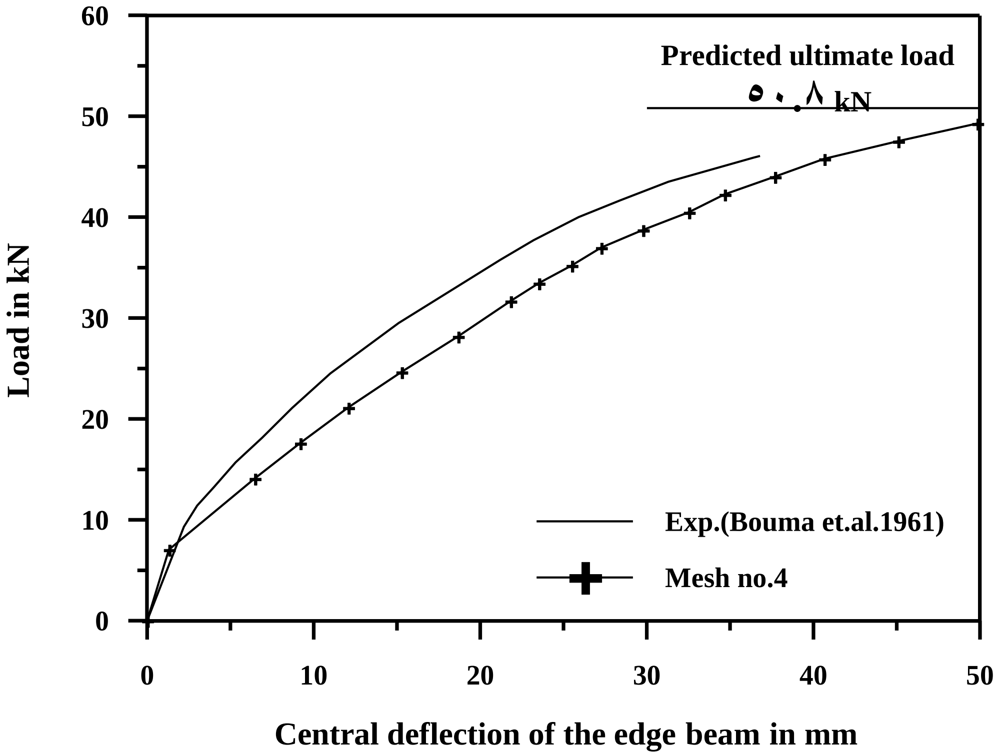

Fig. (٤.٧) Bouma's Shell No.٢, Effect of End Diaphragm Modeling

٤.٢.١.٢ Effect of Element Type

Fig. (٤.٨) shows the load-deflection curves obtained by using different types of element. These elements are ٢٠, ١٤ and ٨-node brick elements. This figure illustrates that the finite element results obtained by using ١٤ and ٨-node brick elements show stiffer response than the experimental results, while the ٢٠-node brick element offers good consistency with experimental results. The ٢٠-node brick element is popular due to its superior performance. The major advantage of this element over the other two elements, is that less number of elements can be used to reach to the real behavior of the structure, as well it has curve sides and therefore provides a better fit to the cylindrical shell [Cook (١٩٧٤), Moaveni (١٩٩٩)]. Therefore, the ٢٠-node brick element has been used in the present work.

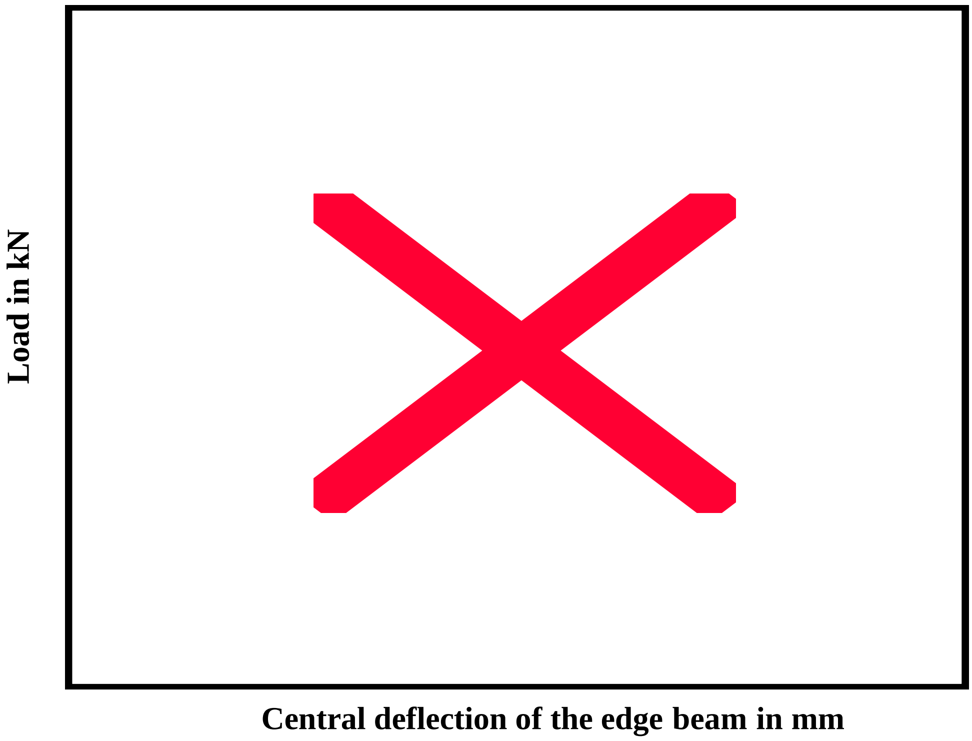

Fig. (٤.٨) Bouma's shell no.٢, Effect of Element Type on Load-Deflection Behavior

٤.٢.١.٣ Effect of Integration Rule

Fig. (٤.٩) shows the load-central deflection curve obtained by using different types of integration rule. Three rules are used : ٢٧, ١٥a, and the ٨-point integration rules. It can be seen from Fig. (٤.٩) that the results obtained by ١٥a-point integration rule agrees well with the experimental results. The ٢٧-point integration rule gives a stiffer response than ١٥a-point integration rule, while very softer response is obtained for the ٨-point integration rule. Rule ١٥a has advantage of having sampling points at the centers of the element faces. These locations are convenient sampling positions for the stress peak values (Cervera et. al. ١٩٨٦). Furthermore, the mismatch between two adjoining elements gives an estimate of the accuracy of the adopted mesh. The stiffer response produced by full integration (٢٧-point integration rule) is due to the shear locking phenomenon. Because the spread of points throughout the element is thought to be insufficient for nonlinear material analysis, the ٨-point integration rule gives far away results. For these reasons, the ١٥a-point integration rule element has been adopted in the present study.

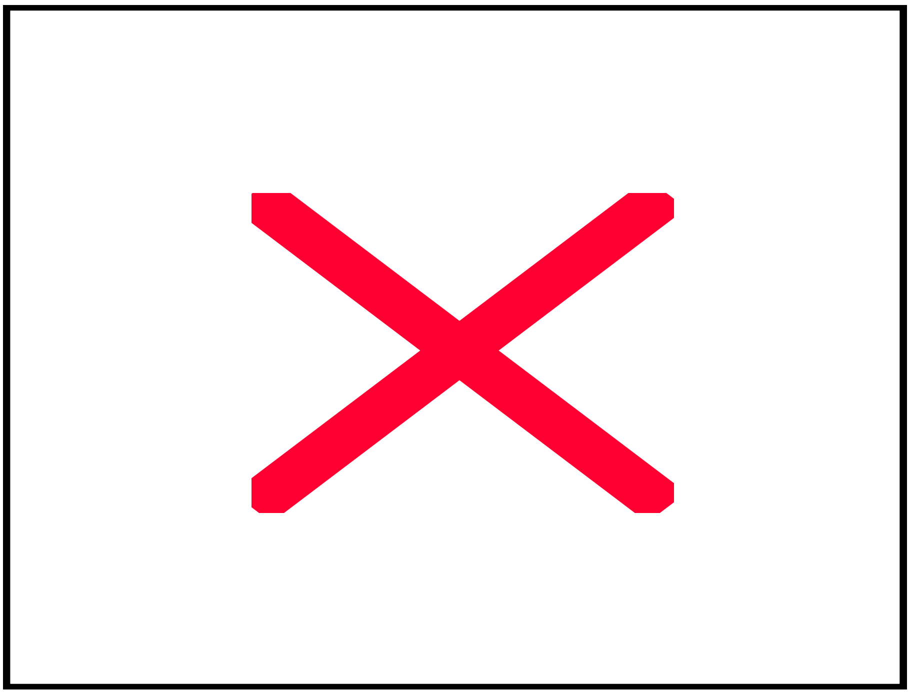

Fig. (٤.٩) Bouma's Shell No.٢, Effect of

٤.٢.١.٤ Effect of Geometric Nonlinearity

The effect of geometric nonlinearity is illustrated in Fig. (٤.١٠) and it is clear that the curve shows a closer agreement with experimental results when the geometric nonlinearity is considered and the failure load is significantly smaller than that found when geometrical nonlinearity is neglected. The results of the analysis based on geometrical nonlinearity revealed that the inclusion of geometric nonlinearity in the finite element analysis of cylindrical shell which exhibit large deformation before collapse plays an important role to improve the predicted load-deflection response. Therefore, the geometric nonlinearity is used in the present investigation.

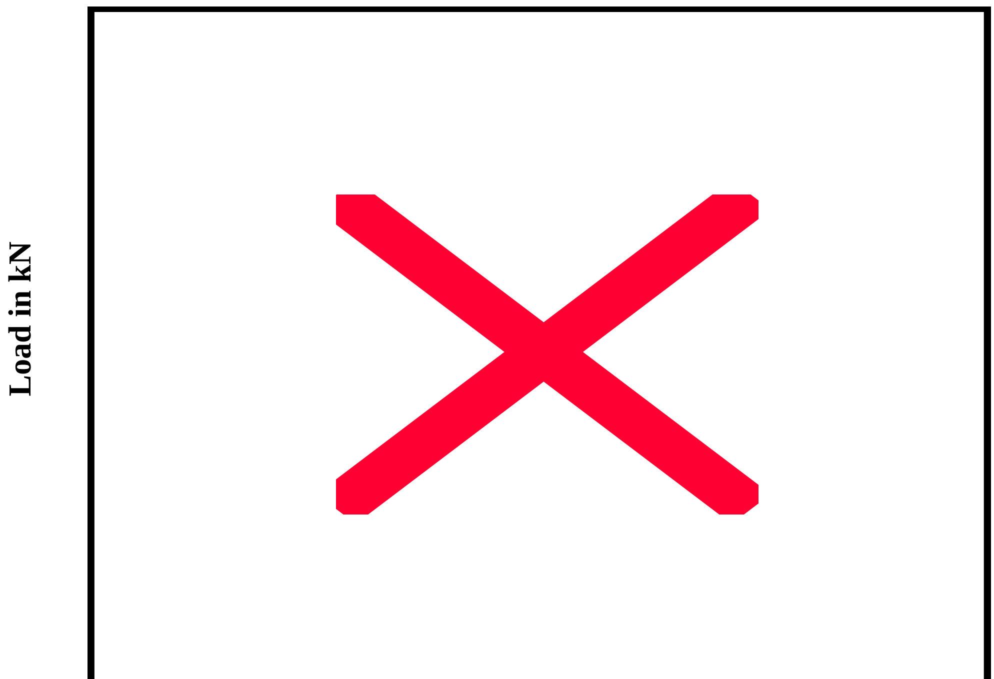

٤.٣ Reinforced Concrete Folded Plate

A concrete Folded Plate, ٣١٤.٨×٦٧.٣ cm in plan with ١٩ mm thickness and ٢٢.٩ cm rise, that was tested by Goble and Jendikis (١٩٦٦), has been analyzed. This structure had two edge beams (١٢.٧ cm deep by ٣.٨ cm width). No sufficient information about end diaphragms is given, therefore the diaphragms are not modeled in this study. Fig. (٤.١١) shows the geometry, reinforcement details, and the applied load.

During experiment the model has been tested in three loading-unloading (loading from zero to ١٣.٣٥ kN, followed by unloading then loading again from zero to ٢٦.٧ kN, followed by unloading and finally loading from zero up to failure). Due to symmetry, only one quarter of the folded plate is analyzed. The finite element meshes and boundary conditions used are shown in Fig. (٤.١٢). The details of the material properties of the folded plate are given in Table (٤.٢).

Table (٤.٢) Material Properties of Goble's Folded Plate

	Material properties and material parameters	**symbol**	**Value**
concrete	Young's modulus	E_c (N/mm٢)	٢٤٢٩٠
	Compressive strength	F´c (N/mm٢)	٢٤.٢
	Tensile strength	f_t (N/mm٢)	٢.٠٧

	Poisson's ratio	ν	٠.١٥
	Uniaxial crushing strain	ε_{cu}	٠.٠٠٣
Steel	Young's modulus	E_s (N/mm٢)	١٨٠٠٠٠
	Yield stress of shell reinforcement	f_y (N/mm٢)	٣٣١
	Yield stress of beam reinforcement	f_y (N/mm٢)	٣٣١
	Hardening parameter	H´	٠.٠
Tension stiffening parameters	Rate of stress release	α١	١٠.٠
	Sudden loss of stress at the instant of cracking	α٢	٠.١
Shear retention parameters	Rate of decay of shear stiffness	γ١	١٠.٠
	Sudden loss of shear stiffness at instant of cracking	γ٢	٠.٥
	Residual shear stiffness due to the dual action	γ٣	٠.١

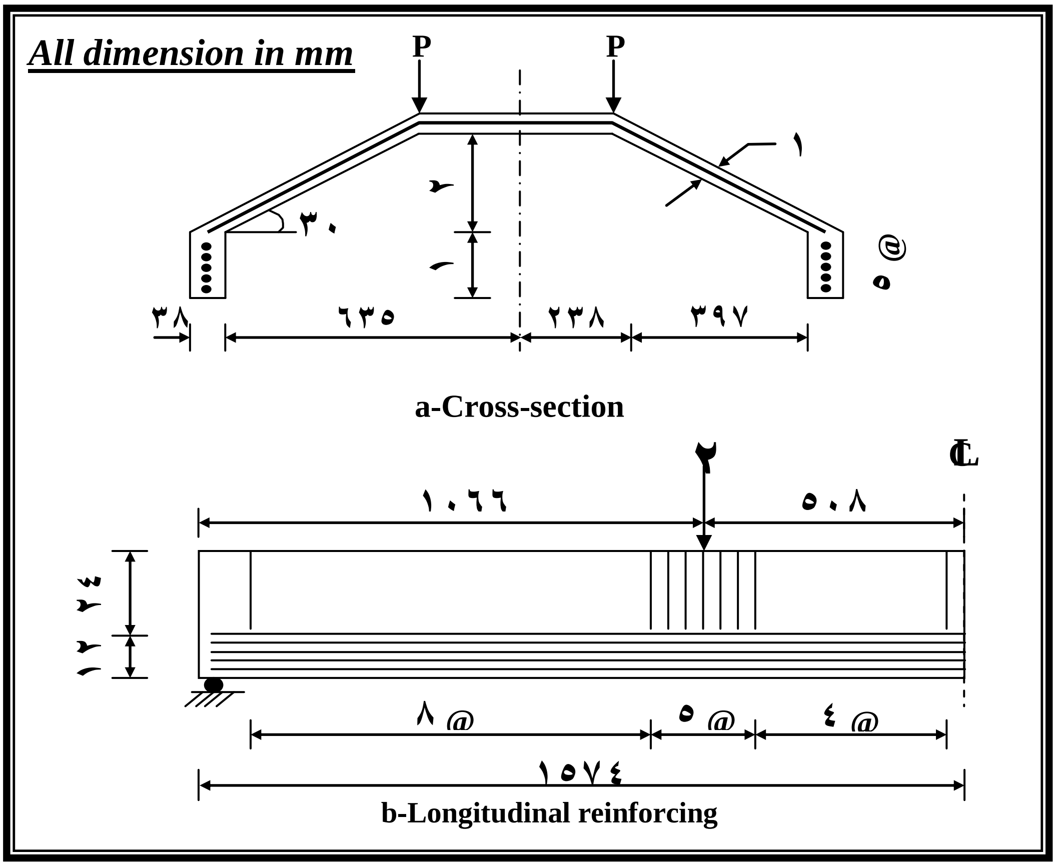

Fig (٤.١١) Geometry and Reinforcement Details of Goble's Folded Plate

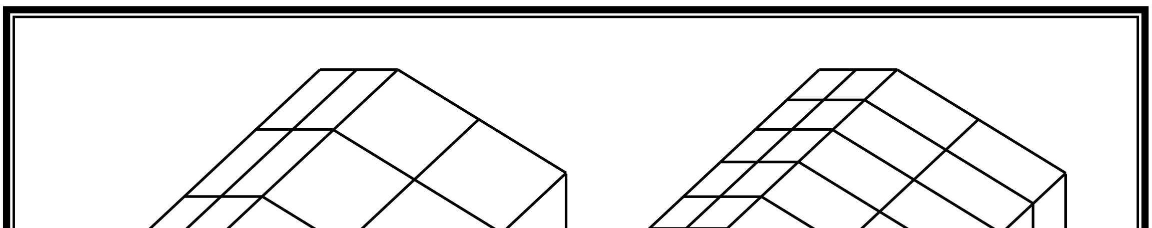

Results and Discussion

٤.٣.١ Finite Element Results

Fig. (٤.١٣) shows the comparison between the experimental, other theoretical studies and present finite element solutions obtained from this study. Only the ultimate load has been recorded in this test. In general, this figure shows good agreement for the finite element solution obtained from the present study compared with the experimental results. It may be detected that the predicted load ٣١.٦ kN was the nearest to the experimental ultimate load ٣٣.٨ kN. Also, the load-deflection behavior by using the degenerate two-dimensional finite element model supported by Thannon (١٩٨٨) was too far from the experimental response and the failure load produced was ٤٧.٦ kN. The large difference between the experimental and Thannon results is due to the non-real representation of steel reinforcement by using smeared layer of equivalent thickness through the shell element. This representation makes the steel layer work in two directions while this structure has only one direction reinforcement in the short direction of the slab.

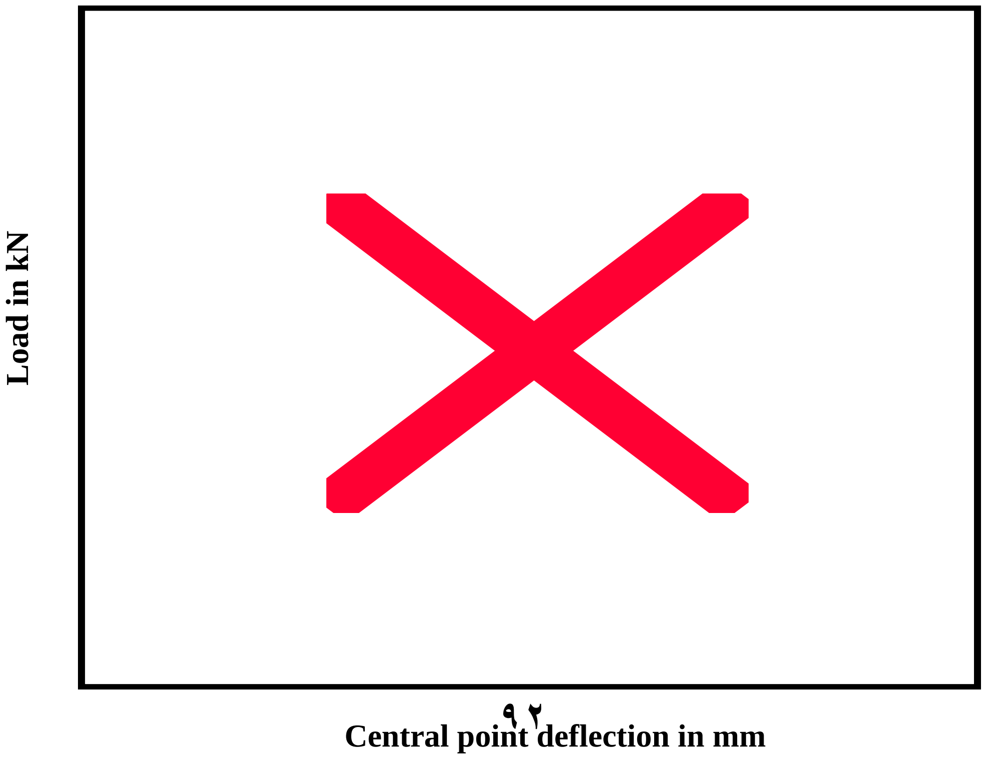

Fig. (٤.١٣) Comparison of Goble's Folded Plate

٤.٣.١.١ Effect of Mesh Refinement

Fig. (٤.١٣) shows three different meshes used to detect the best mesh. As shown in this figure, mesh no. ١ represented one layer with fifteen elements, mesh no. ٢ considered one layer with thirty elements, and mesh no. ٣ had two layers each one has fifteen elements.

The comparison between finite element solutions for different types of mesh and the experimental behavior is shown in Fig. (٤.١٤). This figure shows good agreement with the experimental results of mesh no.٣. It can be seen from Fig. (٤.١٢) that mesh No.٢ and mesh No. ٣ has twenty elements but the best results obtained from mesh no. ٣. Therefore, increasing in the number of concrete elements through the thickness improves the predicted response of the reinforced concrete folded plate. This is due to the fact that the sensitivity of the finite elements to trace cracking during all loading stages is increasing. As a result, mesh no.٣ is adopted for analysis of Goble’s Folded Plate in this study.

Load in kN

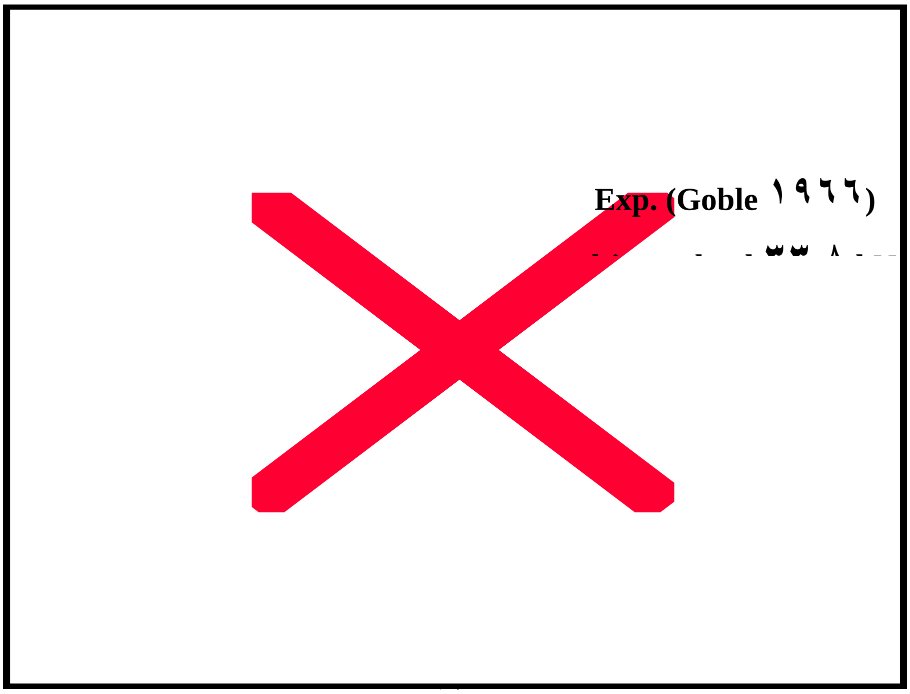

Central deflection in mm

Fig. (٤.١٤) Goble’s Folded Plate-Effect of Mesh

٤.٣.١.٢ Effect of Element Type

To study the effect of element type on the behavior of load-central deflection curves of the folded slab, three types of elements have been used to analyze this structure. These elements are٢٠, ١٤ and ٨-node brick elements.

As shown in Fig, (٤.١٥), the ١٤-node and ٨-node brick elements offer a stiffer load-deflection response compared with the results obtained by using the ٢٠-node brick element whose results are closer to the experimental results. It can be seen that good results can be obtained when the number of the nodes per element increases. The increasing in the number of nodes provides the element more degrees of freedom, which gives a softer load-deflection behavior to the structure. The good results that are submitted by ٢٠-node brick element are due to its high number of nodes. Therefore, this element is adopted in the analysis of the folded plate.

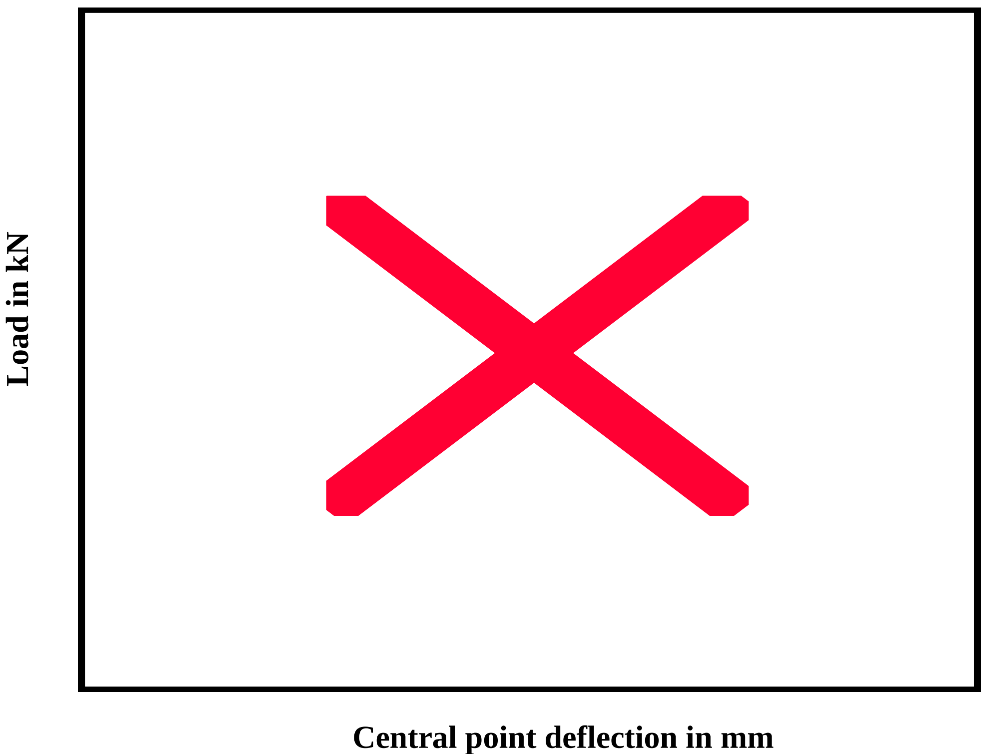

٤.٣.١.٣ Effect of Integration Rule

In Figure (٤.١٦), the effect of integration rule on the obtained behavior of load – central deflection curve of the folded plate is examined by using three types of integration rule. It is found that the ١٥a-point integration rule is more appropriate to estimate the ultimate load at failure than the other integration rules (٢٧-point and ٨-point). Because of the good distribution of the sampling points, the١٥a-point integration rule provided good results. Therefore, the ١٥a-point integration rule is used for the present research.

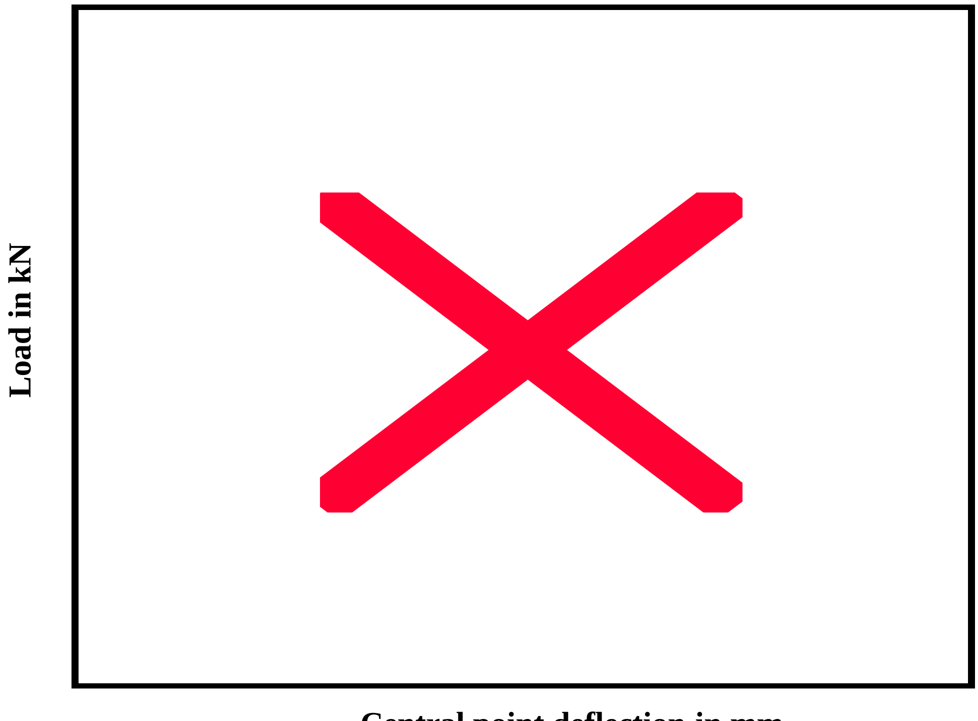

٤.٣.١.٤ Effect of Geometric Nonlinearity

The comparison between geometrical linear and geometrical nonlinear analysis is clearly shown in Fig. (٤.١٧). From these results it can be noticed that the response obtained by inclusion of geometrical nonlinearity is closer to the experimental ultimate load and it is vital for the reliable prediction of failure loads of this structure. From Fig. (٤.١٧) it can be noticed when the folded plate is submitted to large deformation especially before collapse, the analysis based on geometrical nonlinearity plays a major role to improve the analysis. For this reason the geometrical nonlinearity is used in the analysis of this study.

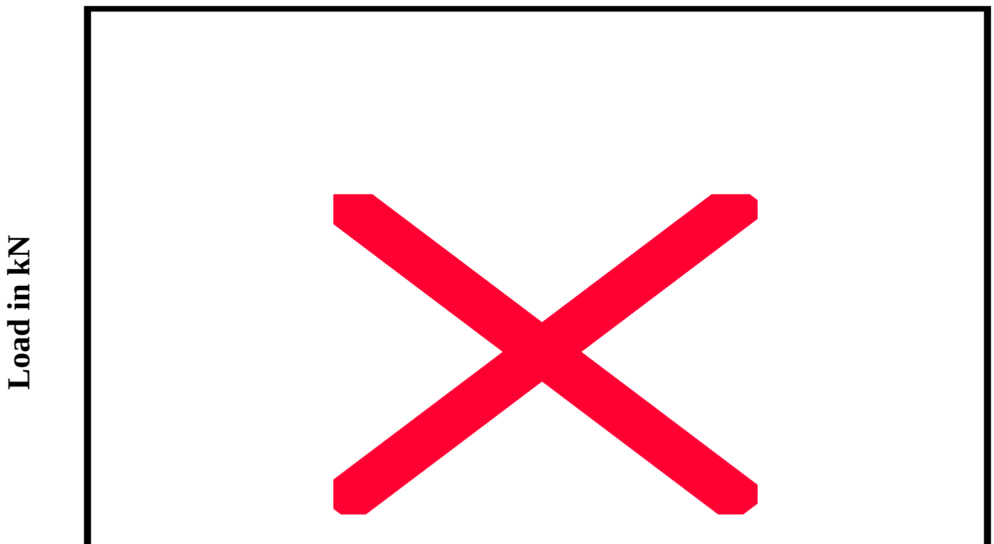

CHAPTER FIVE

PARAMETRIC STUDY

٥.١ INTRODUCTION

In this chapter, the influences of some parameters that affect the behavior of the cylindrical shell and the folded plate are studied. To achieve this aim, the reinforced concrete cylindrical shell and folded plate which were analyzed in chapter four have been chosen for the parametric studies to show the effects of various parameters such as the amount of steel reinforcement, the strength of concrete and some other parameters.

The geometric nonlinearity and material nonlinearity using the twenty-node brick element and ١٥a-point integration rule have been included in this study. For both cylindrical shell and folded plate, the span width and length are kept constant.

To complete the advantage of the present chapter, the predicted ultimate load for each parameter is listed in a single table.

٥.٢ Parametric Studies on Concrete Cylindrical Shell

To investigate the behavior of Bouma’s cylindrical shell under static load, some parameters that affect the behavior of this structure were studied. These parameters include the shell angle, shell thickness, reinforcement ratio, the strength of concrete, steel reinforcement, and edge beam height.

The effect of each parameter is briefly discussed in the following sections.

Parametric Study

٥.٢.١ Effect of Shell Angle

Fig. (٥.١) offers the effect of inplane membrane forces on the load carrying capacity and the enhancement in the behavior of the structure. The increase of curvature increases the membrane forces and acts to maximize the ultimate load and to decrease the deflection. Various shell angles are used which are, ٨٠°, ١٠٠°, ١٢٠°, ١٤٠°, ١٦٠°, and ١٨٠°. Fig. (٥.١) shows that the results obtained by using different angles give a good enhancement in the load carrying capacity and decrease in the deflection. The predicted collapse load increases from ٤٩.٣ kN for angle equals ٨٠° to ١٥٩.٣ kN for angle equals ١٨٠°. The deflection decreases from ٤٩.٨ mm to ٦.٨ mm for angle ١٨٠°, the ultimate load increases to ٣.٢٣ times ultimate load for angle equals ٨٠° and the deflection decreases to ٠.١٤ times ultimate deflection.

Because the variation in angle represents the main effect on membrane forces, this variation is considered as main parameter. Therefore, in the following sections the effect of angle change on the other parameters is studied briefly for shell angles ٨٠°, ١٠٠°, ١٢٠°, ١٤٠°, ١٦٠°, and ١٨٠°.

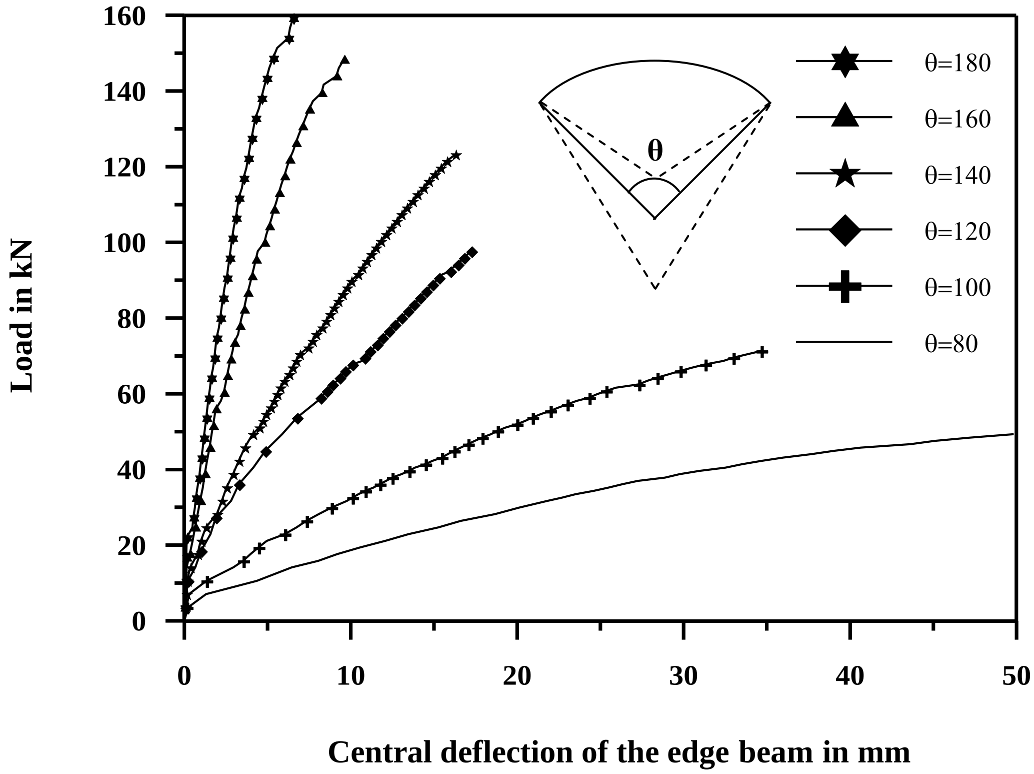

Fig. (٥.١) Effect of Increasing of Shell Angle on Load-Deflection Behavior

Parametric Study

٥.٢.٢ Effect of Shell Thickness

The effect of shell thickness on overall behavior is shown in Fig. (٥.٢). To investigate the effect of this parameter, five shells are analyzed with different thicknesses of (١٠, ١٥, ٢٠, ٢٥ and ٣٠ mm) respectively. The enhancement gained from increasing slab thickness is to increase the ultimate load carrying capacity and to decrease the deflection. The finite element results as shown in Fig. (٥.٢) shows the improvement in the behavior of these shells due to the increase in shell thickness. From these results it can be seen that as the shell thickness increases the load carrying capacity increases progressively.

It can be seen from Fig. (٥.٢) that as the shell thickness increases from ١٠ mm to ٣٠ mm, the ultimate load carrying capacity increases from ٤٩.٣ kN to ١٤٢.٦ kN and ultimate deflection decreases from ٤٩.٨ mm to ٣١.٤ mm. It can be noticed that the ultimate load for thicker shell increases to ٢.٨٩ times ultimate load and the deflection decreases to ٠.٦٣ times the ultimate deflection for shell thickness equal ١٠ mm.

To establish the effect of increasing shell thickness by using different shell angles, the five upper shells are repeated for different shell angles. Fig. (٥.٣) illustrates the improvement in ultimate load due to increase in the thickness, and the shell angle. A progressive increase happened in ultimate load capacity for higher shell angle. The ultimate load and the properties for each shell are listed in Table (٥.١).

Parametric Study

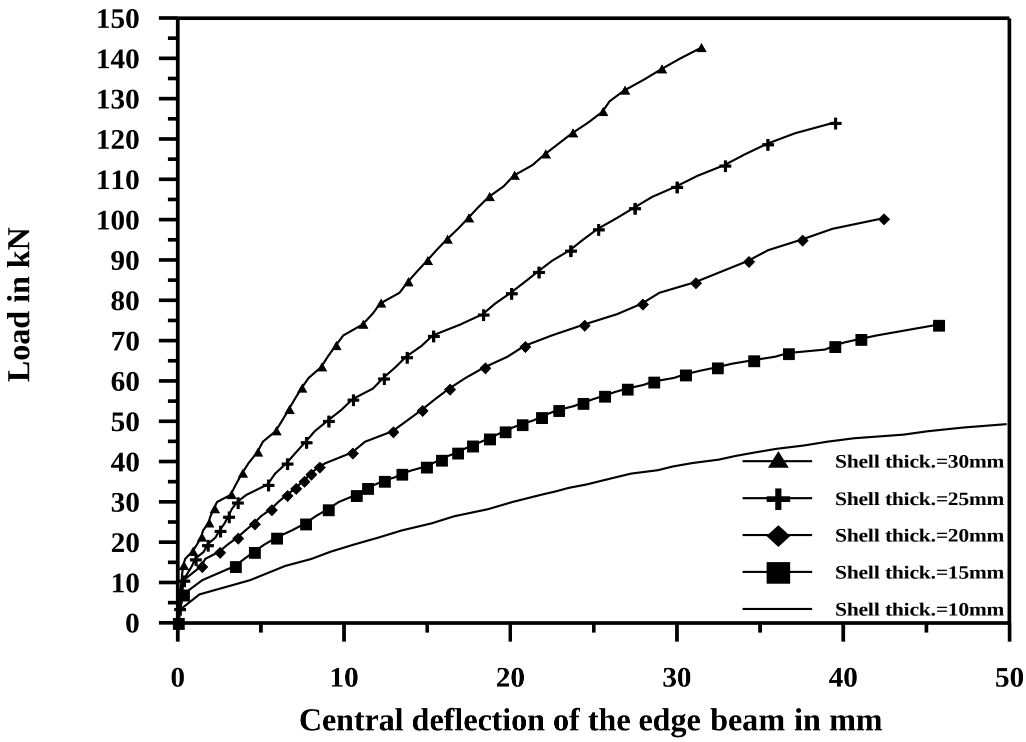

Fig. (٥. ٢) Effect of Shell Thickness on Load-Deflection Behavior

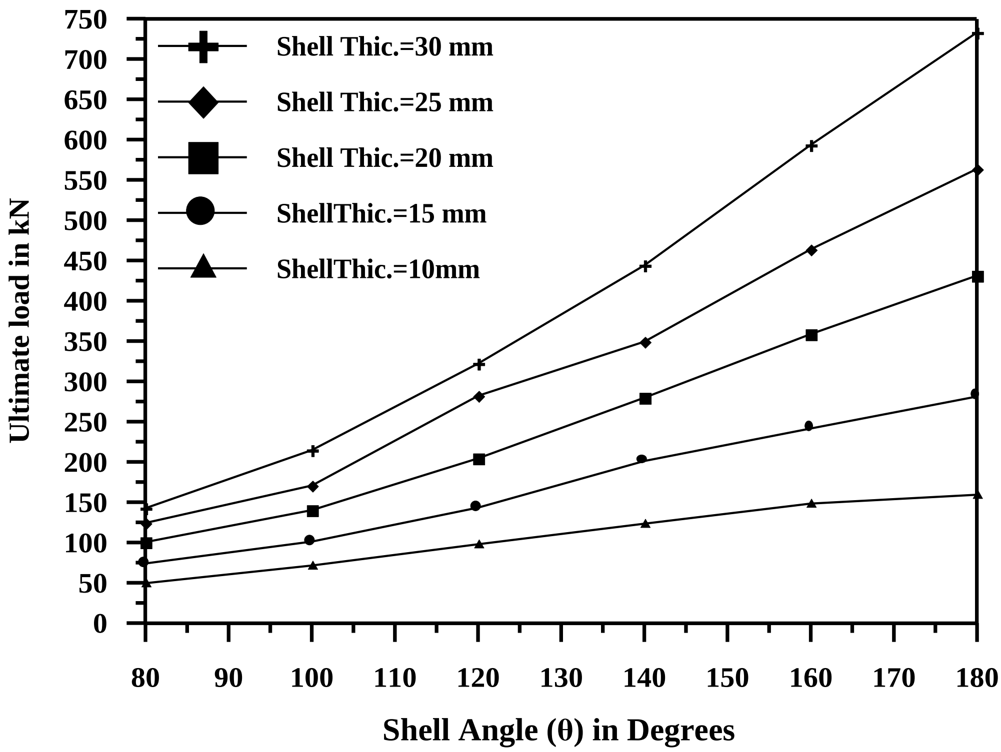

Fig. (٥. ٣) Effect of Shell Thickness on Load Carrying Capacity for Various Angles

٥.٢.٣ Effect of Edge Beam Height

To show the effect of edge beam height, seven shells are analyzed with different beam height of (٠.٠, ٥٠, ٧٠, ١٠٠, ١٣٠, ١٥٠ and ٢٠٠mm) respectively. The enhancement gained from increasing the height of edge beam is the increase in the ultimate load carrying capacity and the decrease in the deflection. Fig. (٥.٤) illustrates the enhancement in the behavior of these shells due to the increase in edge beam height, from this figure it can be found when the height of edge beam increases the load carrying capacity increases.

From Fig. (٥.٤) it can be noted that as the edge beam height increases from ١٠٠ mm to ٢٠٠ mm, the ultimate load carrying capacity increases from ٤٩.٣ kN to ٥٥.٢ kN and the ultimate deflection decreases from ٤٩.٨ mm to ٣٥.٦ mm. It can be noticed that the ultimate load for shell of larger edge beam increases to ١.١٢ times the ultimate load and the deflection decreases to ٠.٧١ times the ultimate deflection for edge beam height equal to ١٠٠ mm. When a shell without edge beam is used the ultimate load decreases to ٣٨.٧ and the deflection increases to ٦٦.٠ mm. Therefore, the load decreasing is equals to ٠.٧٨ times the ultimate load and the deflection increase equal to ١.٣٣ times the ultimate deflection for the edge beam height equal to ١٠٠ mm.

The effects of increasing edge beam height and using different shell angles are established by using the previous edge beams for different shell angles. Fig. (٥.٥) shows the behavior of the ultimate load due to increase or decrease in height of edge beam for different shell angles. It can be seen that the edge beam height becomes a very important parameter and the load carrying capacity

Parametric Study

increases progressively by enlarging the angle of shell. Table (٥.٢) shows the ultimate load for shells used to study this parameter.

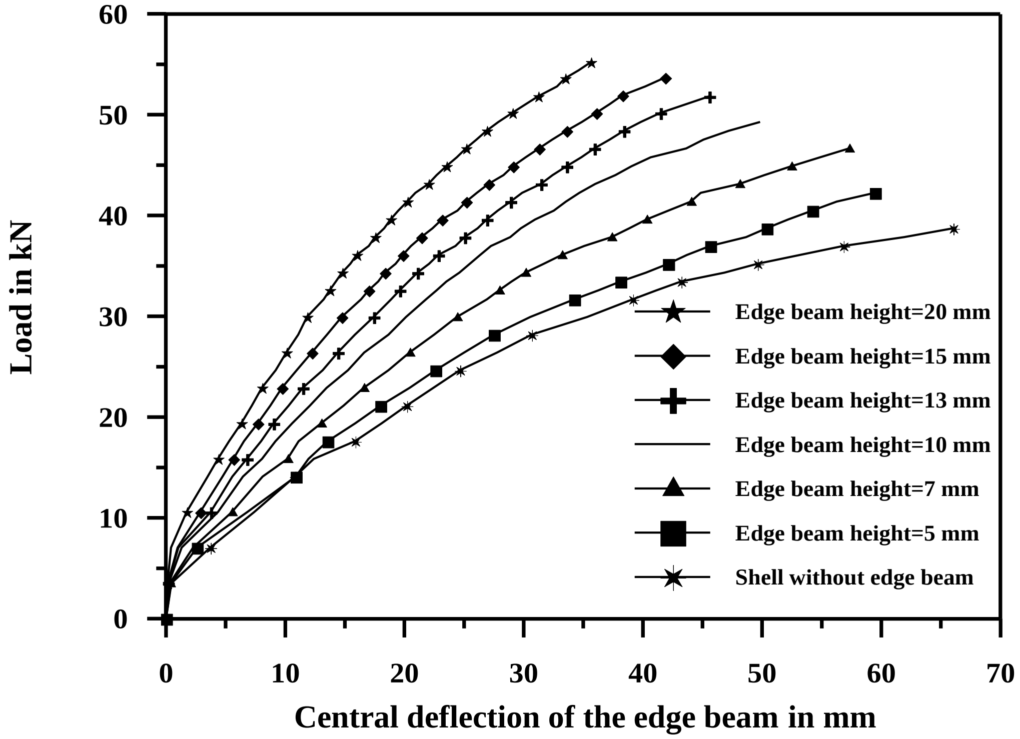

Fig. (٥.٤) Effect of Edge Beam Height on Load-Deflection Behavior

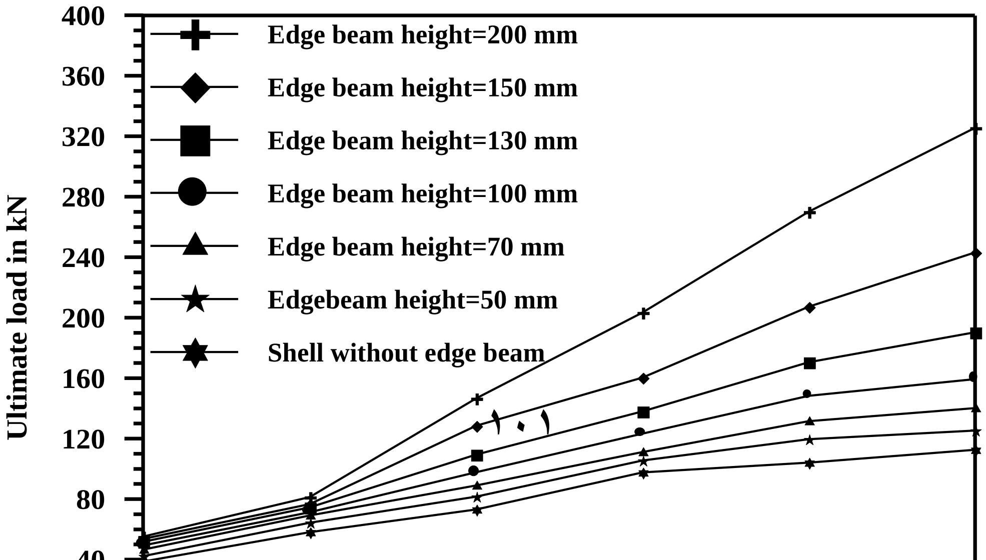

٥.٢.٤ Effect of Reinforcement Ratio

Three different types of steel reinforcement in Bouma's cylindrical shell are considered. They are longitudinal, short direction, and edge beam steel reinforcement. In the following three sections, the effect of these reinforcements are studied.

٥.٢.٤ .١ Effect Longitudinal Steel Reinforcement

To study the effect of this factor, seven reinforced concrete cylindrical shells are analyzed having longitudinal reinforcement ratios of (٢٥٪, ٥٠٪, ٧٥٪, ١٠٠٪, ١٢٥٪, ١٥٠٪, and ٢٠٠٪) times the original reinforcement respectively. As shown in Fig. (٥.٦), the finite element results obtained from analyzing these shells show a noticed rising in the load carrying capacity. It can be seen that increasing the reinforcement ratio to (٢٠٠٪) times the original reinforcement, the ultimate collapse load increase to ١.١٥ the times ultimate load and the ultimate deflection increases to ١.١١.

Different shell angles are used to find the effect of increasing reinforcement. Fig. (٥.٧) illustrates the improvement in ultimate load due to increase in the longitudinal reinforcement, and the shell angle. An increase is noticed in the ultimate load capacity by using different steel reinforcement in the way of increasing the shell angle. The ultimate load and the properties for each shell are listed in Table (٥.٣).

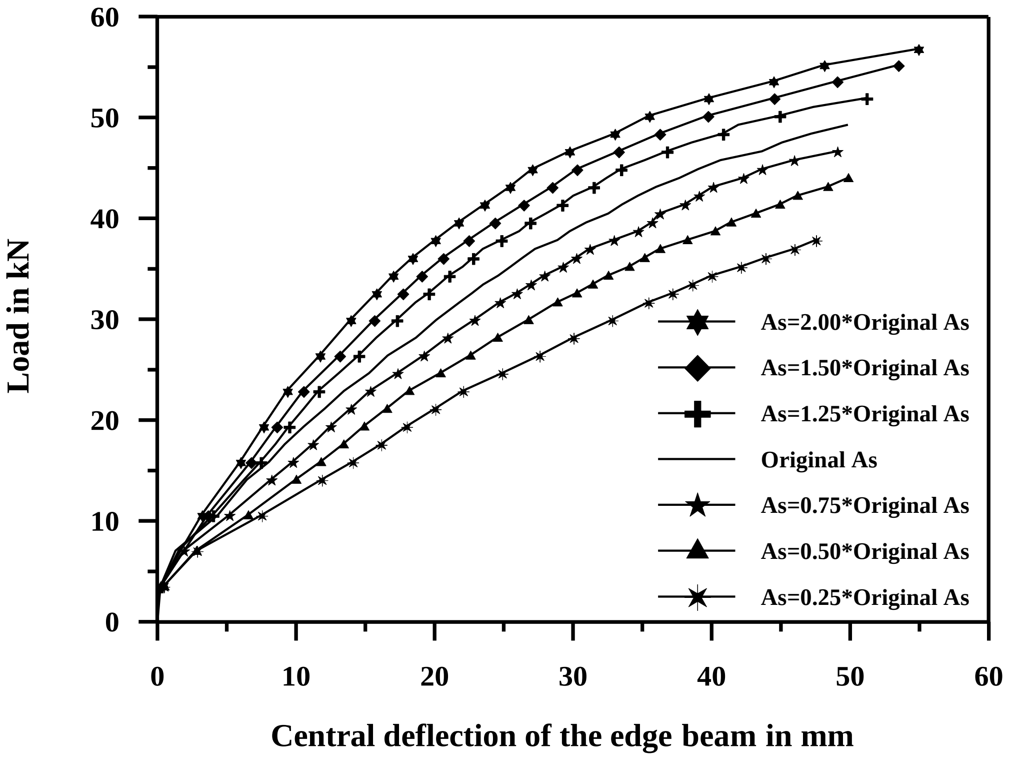

Fig. (٥.٦) Effect of Longitudinal Steel Reinforcement on Load-Deflection Behavior

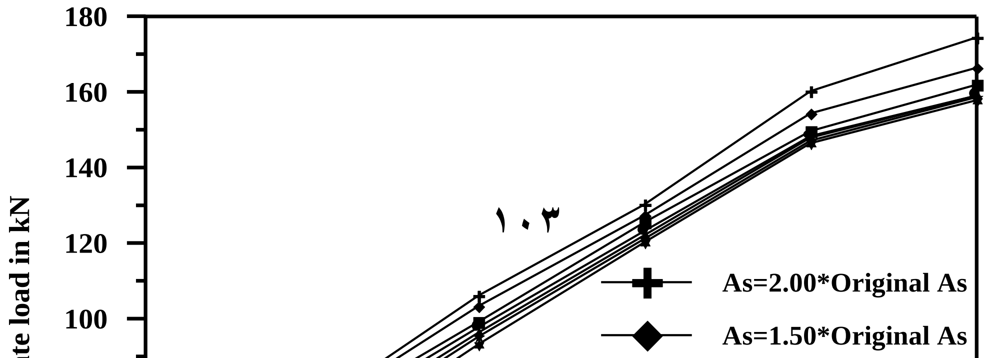

Parametric Study

٥.٢.٤ .٢ Effect of Transverse Steel Reinforcement

To establish the effect of increasing and decreasing the transverse reinforcement on the structure behavior, seven concrete cylindrical shells with transverse steel area equal to (٢٥٪, ٥٠٪, ٧٥٪, ١٠٠٪, ١٢٥٪, ١٥٠٪, and ٢٠٠٪) times the original steel area respectively are considered. Fig. (٥.٨) shows the finite element results obtained from analyzing these shells, a small improvement in the load carrying capacity is found. It can be noticed that increasing the reinforcement ratio to (٢٠٠٪), the ultimate collapse load increases to ١.٠٨ times the ultimate load for Bouma's cylindrical shell while the ultimate deflection increases to ١.٠٥.

The increasse in reinforcement becomes negligible when the shell angle increases. From Fig. (٥.٩) and Table (٥.٤) the relation between the variation of the amount of reinforcement and the increase in shell angle can be seen.

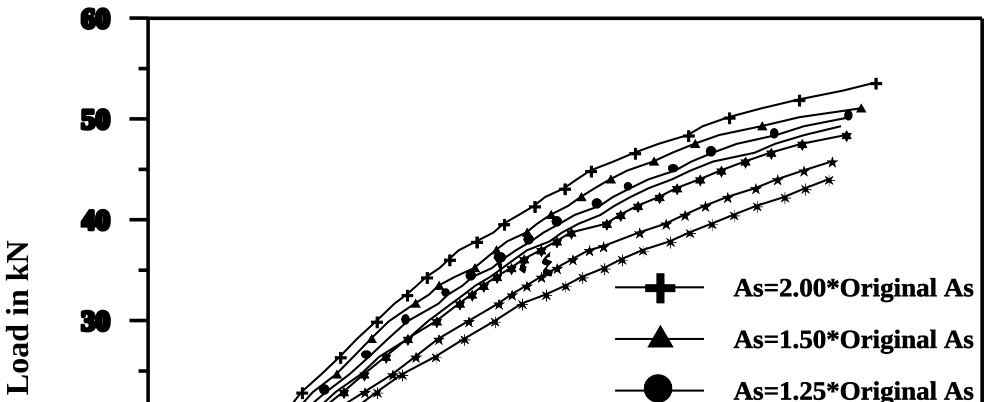

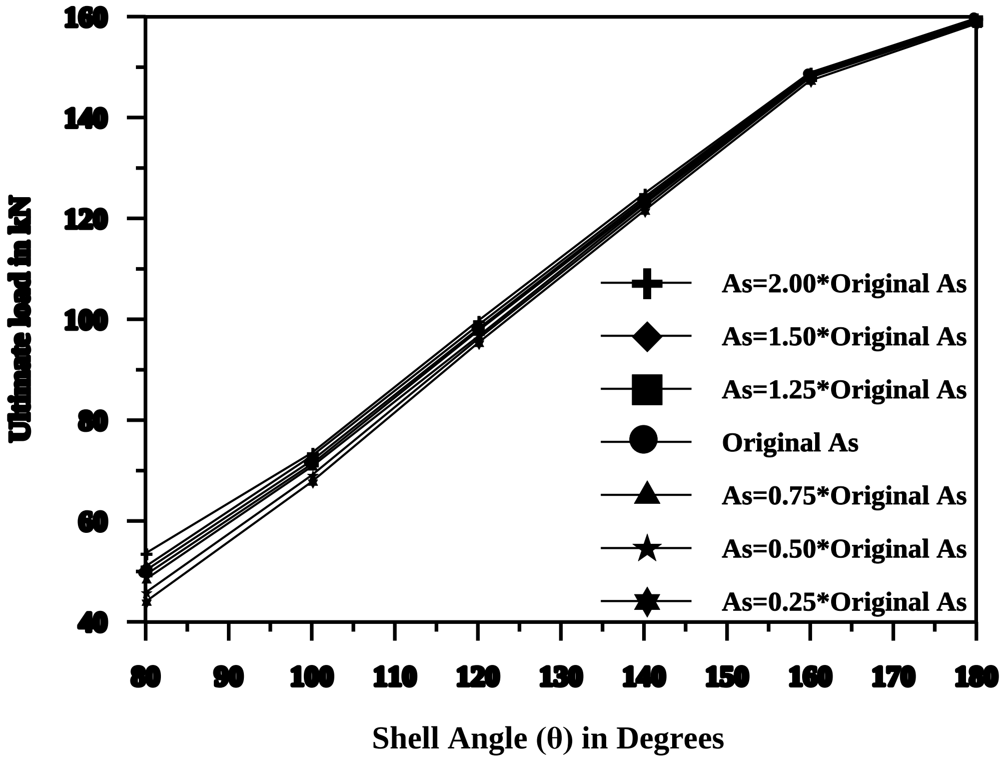

Fig. (٥.٩) Effect of Transverse Steel Reinforcement on Load Carrying Capacity for Various Angles

٥.٢.٤.٣ Effect of Edge Beam Reinforcement

Like longitudinal and transverse reinforcement seven concrete cylindrical shells with steel area for edge beam equals (٢٥٪, ٥٠٪, ٧٥٪, ١٠٠٪, ١٢٥٪, ١٥٠٪, and ٢٠٠٪) times the original steel area respectively, to study the effect of this parameter on structure behavior.

Fig. (٥.١٠) shows the ultimate loads obtained from analyzing these shells with different shell angles, a small improvement in the load carrying capacity is founded for angles equal to (٨٠°) and (١٠٠°). It can be noticed a very good enhancement in the behavior for large angles by increasing the edge beam reinforcement. Table (٥.٥) gives the ultimate loads the properties for each tested shell.

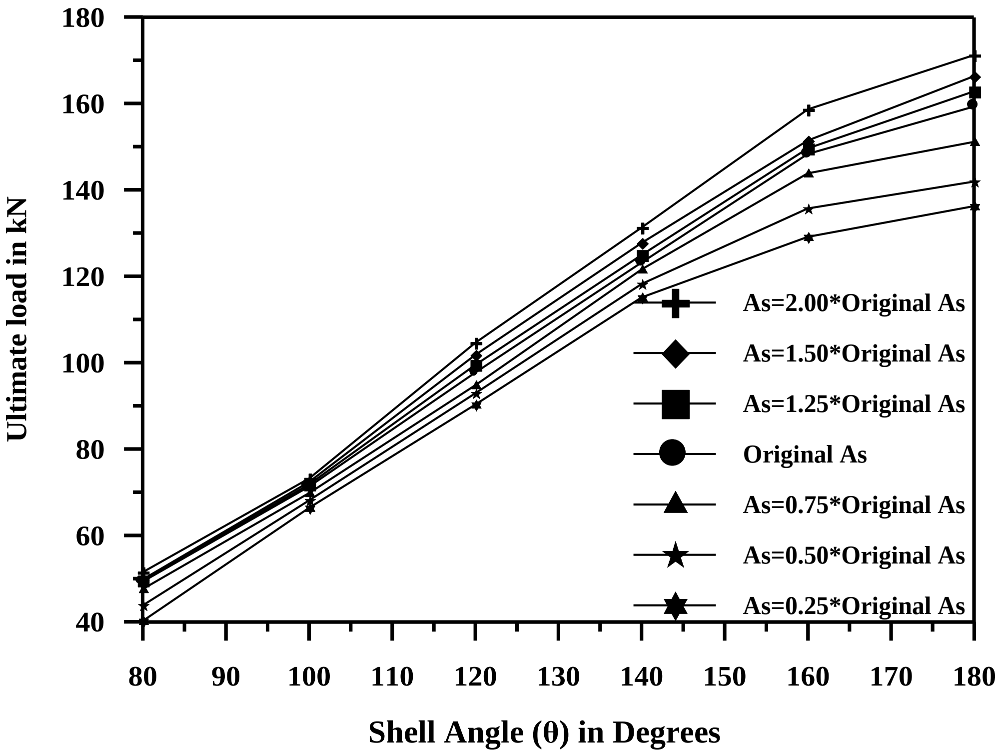

Fig. (٥.١٠) Effect of Edge Beam Steel Reinforcement on Load Carrying Capacity for Various Angles

٥.٢.٥ Effect of Concrete Compressive Strength

To determine the relation between concrete compressive strength and the improvement in load carrying capacity, different shells with compressive strength equal to (٢٠, ٢٥, ٣٠, ٣٥, ٤٠, ٤٥, and ٥٠ MPa) are used. Fig. (٥.١١) illustrates the enhancement in the behavior of these shells due to the increasing and decreasing in concrete compressive strength. From this figure it can be found as the concrete strength increases the load carrying capacity increases progressively.

Fig. (٥.١٢) shows the behavior of ultimate load due to increase or decrease in concrete compressive strength for different shell angles. It can be seen that the

Parametric Study

concrete compressive strength becomes very important parameter and the load carrying capacity increases progressively by enlarging the angle of shell. Table (٥.٦) shows the ultimate load and the properties for each shell used to study this parameter.

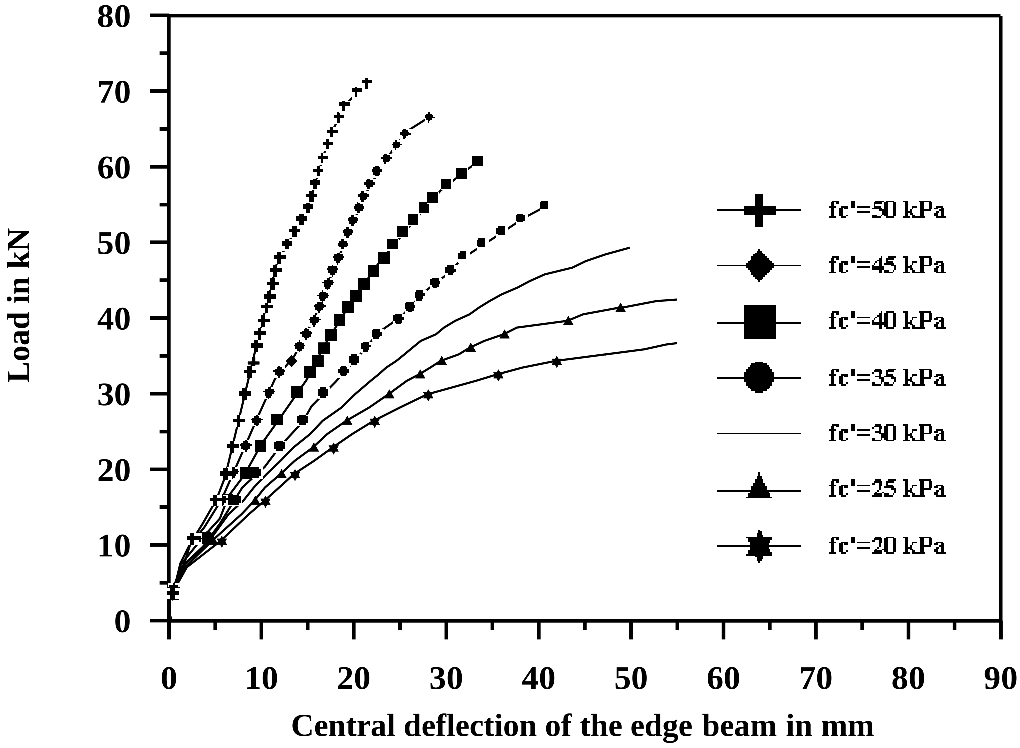

Fig. (٥.١١) Effect of Compressive Strength of Concrete on Load-Deflection Behavior

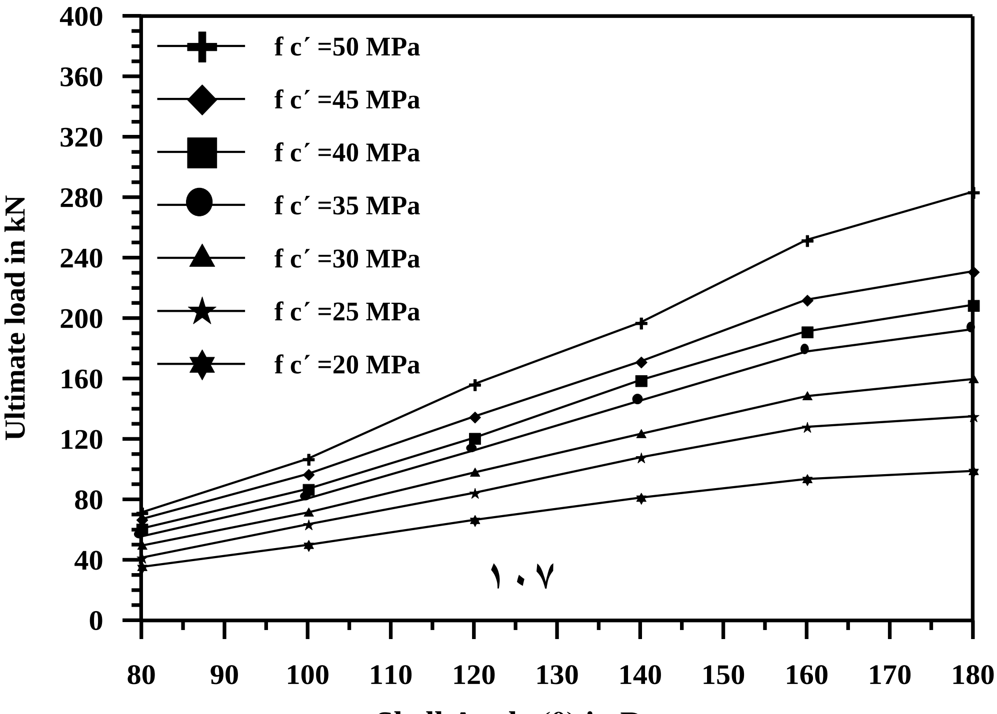

٥.٢.٦ Effect of Steel Grade

Different grade of steel used to establish the effect of this parameter on shell strength. Six shell angles are used to find the effect of increasing the steel strength.

Fig. (٥.١٣) illustrates the improvement in ultimate load due to increase in the yield stress of shell reinforcement, and the shell angle. An increasing noticed in ultimate load capacity for higher steel grades but this increasing may be constant for different shell angles. Table (٥.٧) illustrates the ultimate load and the properties for each shell used.

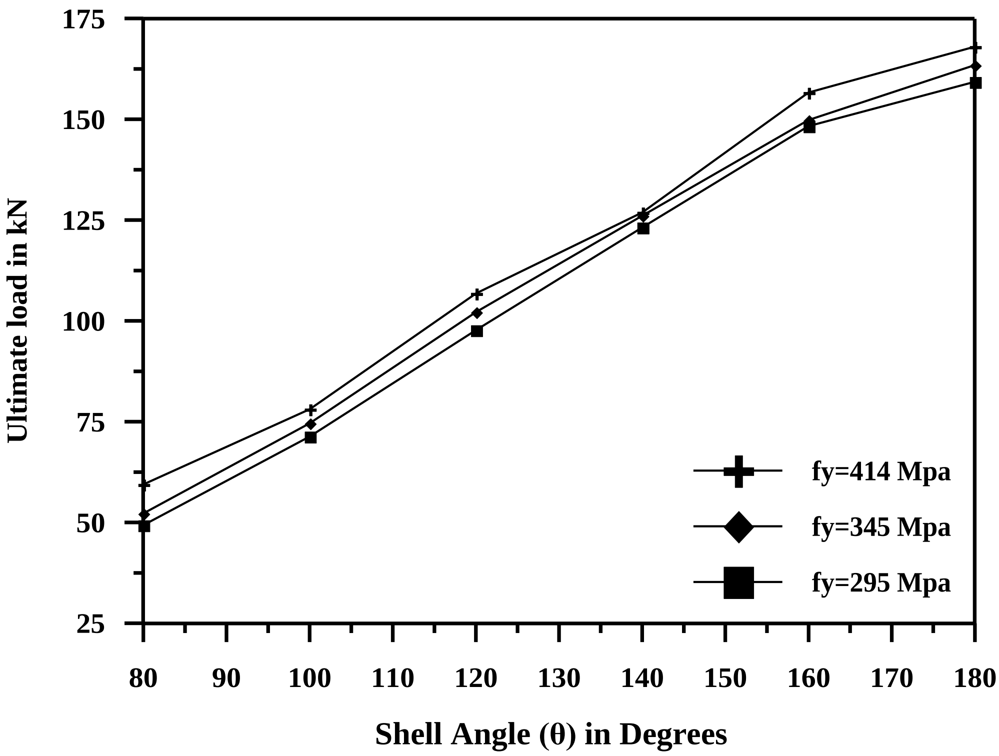

Fig. (٥.١٣) Effect of Yielding Strength of steel on Load Carrying Capacity for Various Angles

Table (٥.١) The Predicted Ultimate Loads in kN for Different Shell Thickness

fc' in kpa	fy in kPa	shell thic in mm	beam high. in mm	*pl*	*ps*	*pb*	shell angle(θ)					
							٨٠	١٠٠	١٢٠	١٤٠	١٦٠	١٨٠
٣٠	٢٥٩	١٠	١٠٠	٠.٠١١٨	٠.٠٠٧٨	٠.٠٦٣٦	٤٩.٣	٧١.٣	٩٧.٧	١٢٣.٢	١٤٨.٣	١٥٩.٣
٣٠	٢٥٩	١٥	١٠٠	٠.٠١١٨	٠.٠٠٧٨	٠.٠٦٣٦	٧٣.٩	١٠١.٢	١٤٣.٢	٢٠١	٢٤١.٤	٢٨١.١
٣٠	٢٥٩	٢٠	١٠٠	٠.٠١١٨	٠.٠٠٧٨	٠.٠٦٣٦	١٠٠.٣	١٤٠.١	٢٠٤.٤	٢٧٩.٦	٣٥٨.٥	٤٣١.٢
٣٠	٢٥٩	٢٥	١٠٠	٠.٠١١٨	٠.٠٠٧٨	٠.٠٦٣٦	١٢٤.١	١٧٠.٦	٣١٢.١	٣٤٩.٢	٤٦٣.٧	٥٦٣.٦
٣٠	٢٥٩	٣٠	١٠٠	٠.٠١١٨	٠.٠٠٧٨	٠.٠٦٣٦	١٤٢.٦	٢١٤.٧	٣٢٢	٤٤٣.٩	٥٩٣.٣	٧٣٢.٨

Parametric Study

Table (٥.٢) The Predicted Ultimate Loads in kN for Different Edge Beam heights

fc' in kpa	fy in kPa	shell thic in mm	beam high. in mm	*pl*	*ps*	*pb*	shell angle (θ)					
							٨٠	١٠٠	١٢٠	١٤٠	١٦٠	١٨٠
٣٠	٢٥٩	١٠	٠	٠.٠١١٨	٠.٠٠٧٨	٠.٠٦٣٦	٣٨.٧	٥٨.١	٧٣.١	٩٧.٦	١٠٤.١	١١٢.٦
٣٠	٢٥٩	١٠	٥٠	٠.٠١١٨	٠.٠٠٧٨	٠.٠٦٣٦	٤٢.٢	٦٤.٣	٨١.٦	١٠٥.٥	١١٩.٦	١٢٥.٣
٣٠	٢٥٩	١٠	٧٠	٠.٠١١٨	٠.٠٠٧٨	٠.٠٦٣٦	٤٦.٦	٦٩.١	٨٨.٩	١١١	١٣١.٥	١٤٠.٢
٣٠	٢٥٩	١٠	١٠٠	٠.٠١١٨	٠.٠٠٧٨	٠.٠٦٣٦	٤٩.٣	٧١.٣	٩٧.٧	١٢٣.٢	١٤٨.٣	١٥٩.٣
٣٠	٢٥٩	١٠	١٣٠	٠.٠١١٨	٠.٠٠٧٨	٠.٠٦٣٦	٥١.٨	٧٤.٥	١٠٩.٤	١٣٨	١٧٠.٥	١٩٠.٣
٣٠	٢٥٩	١٠	١٥٠	٠.٠١١٨	٠.٠٠٧٨	٠.٠٦٣٦	٥٣.٧	٧٦.٧	١٢٨.٥	١٦٠.٣	١٩٧.٢	٢٤٣.١
٣٠	٢٥٩	١٠	٢٠٠	٠.٠١١٨	٠.٠٠٧٨	٠.٠٦٣٦	٥٥.٢	٨١.٤	١٤٦.٦	٢٠٣.٤	٢٦٥.١	٣٢٥.٦

Table (٥.٣) The Predicted Ultimate Loads in kN for Different Longitudinal Steel Reinforcement

fc' in kpa	fy in kPa	shell thic in mm	beam high. in mm	*pl*	*ps*	*pb*	shell angle(θ)					
							٨٠	١٠٠	١٢٠	١٤٠	١٦٠	١٨٠
٣٠	٢٥٩	١٠	١٠٠	٠.٠٠٢٩٥	٠.٠٠٧٨	٠.٠٦٣٦	٣٧.٨	٦٣.٩	٩٣.٢	١٢٠.٢	١٤٦.٤	١٥٧.٨
٣٠	٢٥٩	١٠	١٠٠	٠.٠٠٥٩	٠.٠٠٧٨	٠.٠٦٣٦	٤٤	٦٦.٨	٩٥.٢	١٢١.١	١٤٧.١	١٥٨.٦
٣٠	٢٥٩	١٠	١٠٠	٠.٠٠٨٨٥	٠.٠٠٧٨	٠.٠٦٣٦	٤٦.٦	٦٨.٨	٩٦.٣	١٢٢.١	١٤٧.٩	١٥٩
٣٠	٢٥٩	١٠	١٠٠	٠.٠١١٨	٠.٠٠٧٨	٠.٠٦٣٦	٤٩.٣	٧١.٣	٩٧.٧	١٢٣.٢	١٤٨.٣	١٥٩
٣٠	٢٥٩	١٠	١٠٠	٠.٠١٤٧٥	٠.٠٠٧٨	٠.٠٦٣٦	٥١.٩	٧٣.٣	٩٩.١	١٢٥.٥	١٤٩.٦	١٦١.٩
٣٠	٢٥٩	١٠	١٠٠	٠.٠١٧٧	٠.٠٠٧٨	٠.٠٦٣٦	٥٤.٢	٧٥.١	١٠٣.٣	١٢٧.٣	١٥٤.٣	١٦٦.٤
٣٠	٢٥٩	١٠	١٠٠	٠.٠٢٣٦	٠.٠٠٧٨	٠.٠٦٣٦	٥٦.٨	٧٦.٢	١٠٦.١	١٣٠.٢	١٦٠.٢	١٧٤.٤

Table (٥.٤) The Predicted Ultimate Loads in kN for Different Transverse Steel Reinforcement

fc' in kpa	fy in kPa	shell thic in mm	beam high. in mm	*pl*	*ps*	*pb*	shell angle(θ)					
							٨٠	١٠٠	١٢٠	١٤٠	١٦٠	١٨٠
٣٠	٢٥٩	١٠	١٠٠	٠.٠١١٨	٠.٠٠١٩٥	٠.٠٦٣٦	٤٤	٦٧.٨	٩٥.٣	١٢١.٥	١٤٧.٣	١٥٨.٦
٣٠	٢٥٩	١٠	١٠٠	٠.٠١١٨	٠.٠٠٣٩	٠.٠٦٣٦	٤٥.٨	٦٩.١	٩٦.١	١٢٢.٢	١٤٧.٩	١٥٨.٩
٣٠	٢٥٩	١٠	١٠٠	٠.٠١١٨	٠.٠٠٥٨٥	٠.٠٦٣٦	٤٨.٤	٧٠.٨	٩٦.٦	١٢٢.٨	١٤٨.١	١٥٩.١

Parametric Study

٣٠	٢٥٩	١٠	١٠٠	٠.٠١١٨	٠.٠٠٧٨	٠.٠٦٣٦	٤٩.٣	٧١.٣	٩٧.٧	١٢٣.٢	١٤٨.٣	١٥٩.٣
٣٠	٢٥٩	١٠	١٠٠	٠.٠١١٨	٠.٠٠٩٧٥	٠.٠٦٣٦	٥٠.٢	٧٢	٩٨.١	١٢٣.٧	١٨٤.٤	١٥٩.٣
٣٠	٢٥٩	١٠	١٠٠	٠.٠١١٨	٠.٠١١٧	٠.٠٦٣٦	٥١	٧٢.٩	٩٨.٨	١٢٤.٢	١٤٨.٧	١٥٩.٥
٣٠	٢٥٩	١٠	١٠٠	٠.٠١١٨	٠.٠١٥٦	٠.٠٦٣٦	٥٣.٦	٧٣.٥	٩٩.٧	١٢٤.٩	١٤٨.٩	١٥٩.٧

Table (٥.٥) The Predicted Ultimate Loads in kN for Different Edge Beam Steel Reinforcement

fc' in kpa	fy in kPa	shell thic in mm	beam high. in mm	*pl*	*ps*	*pb*	shell angle(θ)					
							٨٠	١٠٠	١٢٠	١٤٠	١٦٠	١٨٠
٣٠	٢٥٩	١٠	١٠٠	٠.٠١١٨	٠.٠٠٧٨	٠.٠١٥٩	٤٠.٢	٦٦.٤	٩٠.٣	١١٥.١	١٢٩.١	١٣٦.٢
٣٠	٢٥٩	١٠	١٠٠	٠.٠١١٨	٠.٠٠٧٨	٠.٠٣١٨	٤٣.٨	٦٨.١	٩٢.٩	١١٨.٢	١٣٥.٧	١٤١.٩
٣٠	٢٥٩	١٠	١٠٠	٠.٠١١٨	٠.٠٠٧٨	٠.٠٤٧٧	٤٧.٦	٦٩.٨	٩٤.٨	١٢١.٦	١٤٣.٨	١٥١.١
٣٠	٢٥٩	١٠	١٠٠	٠.٠١١٨	٠.٠٠٧٨	٠.٠٦٣٦	٤٩.٣	٧١.٣	٩٧.٧	١٢٣.٢	١٤٨.٣	١٥٩.٣
٣٠	٢٥٩	١٠	١٠٠	٠.٠١١٨	٠.٠٠٧٨	٠.٠٧٩٥	٤٩.٦	٧١.٨	٩٩.٥	١٢٤.٩	١٤٩.٦	١٦٢.٨
٣٠	٢٥٩	١٠	١٠٠	٠.٠١١٨	٠.٠٠٧٨	٠.٠٩٥٤	٤٩.٨	٧٢.٤	١٠١.٨	١٢٧.٧	١٥١.٤	١٦٦.٣
٣٠	٢٥٩	١٠	١٠٠	٠.٠١١٨	٠.٠٠٧٨	٠.١٢٧٢	٥١.٥	٧٣.٢	١٠٤.٦	١٣١.٣	١٥٨.٦	١٧١.٢

Table (٥.٦) The Predected Ultimate Loads in kN for Different Concrete Compressive Strength

fc' in kpa	fy in kPa	shell thic in mm	beam high. in mm	*pl*	*ps*	*pb*	shell angle(θ)					
							٨٠	١٠٠	١٢٠	١٤٠	١٦٠	١٨٠
٢٠	٢٥٩	١٠	١٠٠	٠.٠١١٨	٠.٠٠٧٨	٠.٠٦٣٦	٣٥.٢	٤٩.٩	٦٦.٤	٨٠١.١	٩٣.٤	٩٨.٨
٢٥	٢٥٩	١٠	١٠٠	٠.٠١١٨	٠.٠٠٧٨	٠.٠٦٣٦	٤١.٤	٦٣.٥	٨٤.٣	١٠٧.٨	١٢٧.٩	١٣٥.٠
٣٠	٢٥٩	١٠	١٠٠	٠.٠١١٨	٠.٠٠٧٨	٠.٠٦٣٦	٤٩.٣	٧١.٣	٩٧.٧	١٢٣.٢	١٤٨.٣	١٥٩.٦
٣٥	٢٥٩	١٠	١٠٠	٠.٠١١٨	٠.٠٠٧٨	٠.٠٦٣٦	٥٥.٤	٨٠.٦	١١٢.٤	١٤٥.٤	١٧٧.٩	١٩٢.٦
٤٠	٢٥٩	١٠	١٠٠	٠.٠١١٨	٠.٠٠٧٨	٠.٠٦٣٦	٦٠.٧	٨٦.٩	١٢٠.٧	١٥٨.٩	١٩١.٢	٢٠٨.٧
٤٥	٢٥٩	١٠	١٠٠	٠.٠١١٨	٠.٠٠٧٨	٠.٠٦٣٦	٦٦.٩	٩٦.٩	١٣٤.٨	١٧١.٢	٢١٢.١	٢٣١.٠

Table (٥.٧) The Predicted Ultimate Loads in kN for Different Steel Grades

fc' in kpa	fy in kPa	shell thic in mm	beam high. in mm	*pl*	*ps*	*pb*	shell angle(θ)					
							٨٠	١٠٠	١٢٠	١٤٠	١٦٠	١٨٠

Parametric Study

٣٠	٢٥٩	١٠	١٠٠	٠.٠١١٨	٠.٠٠٧٨	٠.٠٦٣٦	٤٩.٣	٧١.٣	٩٧.٧	١٢٣.٢	١٤٨.٣	١٥٩.٣
٣٠	٣٤٥	١٠	١٠٠	٠.٠١١٨	٠.٠٠٧٨	٠.٠٦٣٦	٥٢.٢	٧٤.٦	١٠٢.٢	١٢٦.١	١٤٩.٨	١٦٣.٤
٣٠	٤١٤	١٠	١٠٠	٠.٠١١٨	٠.٠٠٧٨	٠.٠٦٣٦	٥٩.٤	٧٨.١	١٠٦.٨	١٢٦.٩	١٥٦.٦	١٦٨

٥.٣ Mathematical Formula for Prediction of Ultimate Load Capacity for Cylindrical Shell

The following expression to find the ultimate load for cylindrical shell structures of the considered span width ratio, is suggested in the present study because of the preceding parametric study using STATISTIC program version ٥.٠:

$$P = -١١٩ + (-٣٧٦٥٧.٧٥٥٧ * f\acute{c}^{(-٠.٠٠٠٣)} - ٩٤٧.٨٢٢٨ * fy^{(-٣.٢٤٤٣)} + ٢٩.٢٣١٩ * t + ٠.٠٣٦٩ * hb^{(١.٦٦٤)} + ١٩٠٧.٩٦٨٩ * pl^{(٠.٠٠٠٧)} + ٣٥٣٣٣.٣٠٨١ * pb^{(٠.٠٠٠١)} + ٧٥.٨٩٩٦ * ps) * \sin(٠.٤٥٨ * th - ٣٩.٤١٩) + ١٨٧.٠٨١ * \log_{١٠}(t * ١.٠٣١٢) * pl^{(٠.٠٢٠٦)} \quad ...(٥.١)$$

where ,

P is the ultimate load in kN
fć is the concrete compresive strength in kPa
fy is the yielding stress of steel reinforcement in kPa
t is the thickness of the cylindrical shell in mm
hb is the edge beam height in mm
pl, is the steel reinforcement ratio in long direction
ps is the steel reinforcement ratio in short direction
pb is the steel reinforcement ratio in edge beam
th is the shell angle in degree
Coefficient of correlation (R=٠.٨٨)

As shown in Fig. (٥.١٤), good results obtained from the comparison between the finite element results and the result optioned from proposed mathematical formula.

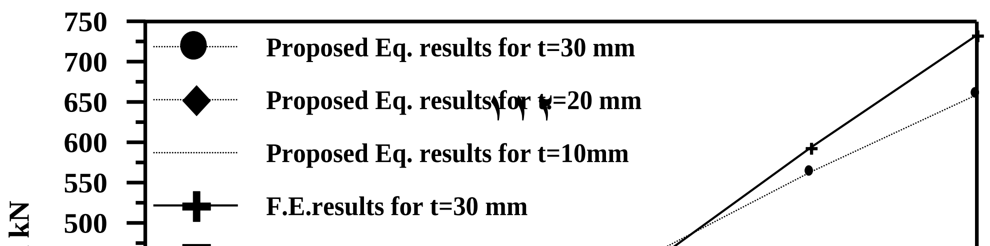

Parametric Study

٥.٤ Parametric Studies on concrete Folded Plate

To establish the behavior of reinforced concrete folded plate; some parameters that affect the behavior of this structure have been studied. These parameters are the inclination angle, plate thickness, the plate reinforcement ratio, the concrete compressive strength, and steel grade. The discussion of the effect of these parameters, are made in the later sections.

٥.٤.١ Effect of longitudinal steel reinforcement

In the practice in one-way slaps, minimum steel reinforcement provided in addition to the main reinforcement to distribute the loads and the cracks provided by temperature and shrinkage stresses (Nilson and Winter ١٩٨٨). Therefore, minimum reinforcement added to long direction of folded plate. This

Parametric Study

reinforcement can be obtained from the following equation (ACI Committee ٣١٨ ١٩٩٥)

$$\rho_{min} = \frac{0.0018*400}{f_y} \qquad ...(٥.٢)$$

This ratio is (٠.٠٠١٨) and it's provided by (Ø ٢ @ ٧٥ mm)

Figure (٥.١٥) shows the influence of reinforcement ratio on the behavior of folded plate. The finite element results obtained from analyzing this folded plate show a significant enhancement in the load carrying capacity. It can be noticed that the ultimate collapse load increase to ١.٣٢ times the ultimate load for folded plate without minimum longitudinal reinforcement. Then this reinforcement is used in the following sections.

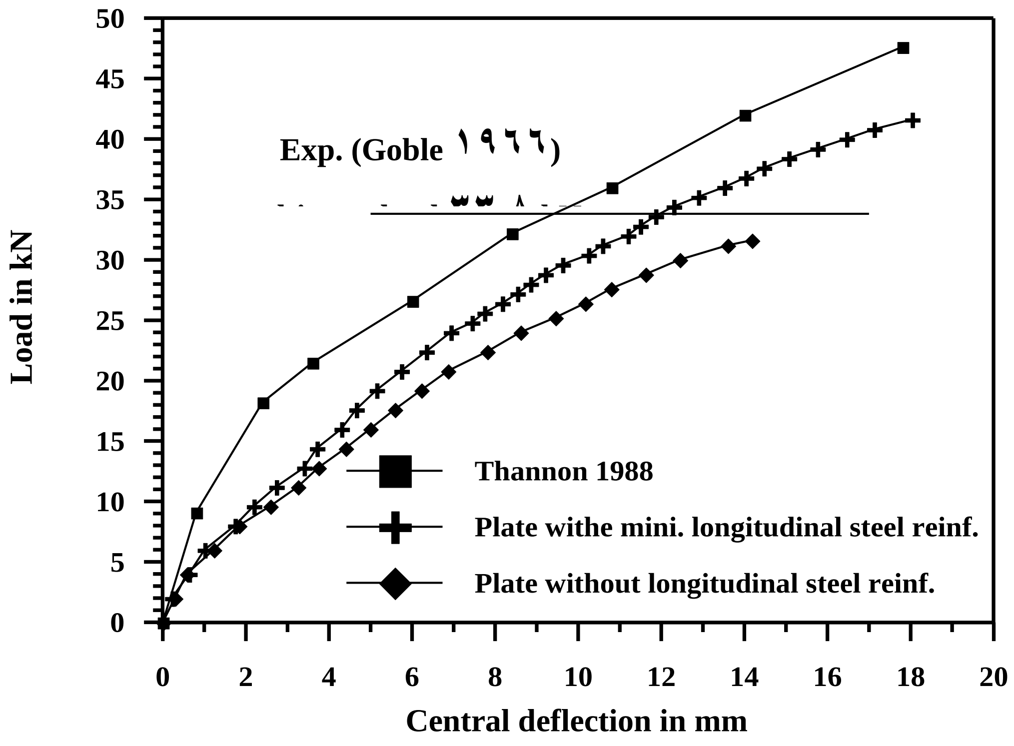

Fig. (٥.١٥) Goble's Folded Plate-Effect of Longitudinal Reinforcement on Load-Deflection Behavior

Parametric Study

٥.٤.٢ Effect of Inclination Angle

In order to study the effect of inclination angle (θ) on load-deflection behavior, four different values of θ are used. These values of inclination angle are ٢٠°, ٣٠°, ٤٥°, and ٦٠°. The results obtained from the finite element analysis are shown in Fig. (٥.١٦). From This figure it's clear that when inclination angle increases from ٣٠° to ٤٥° or ٦٠°, the ultimate collapse load is significantly decreased. When inclination angle equals ٢٠°, Gobl's folded plate will be change to V-shaped folded plate. By using this folded plate the membrane force is significantly increased, and from fig. (٥.١٦) the collapse ultimate load for θ equals ٢٠° is rapidly increased.

As result, the inclination angle plays major role to represent the load-deflection behavior and ultimate load. Therefore, the effect of angle change on the other parameters is studied briefly in the following sections by using for angles ٢٠°, ٣٠°, ٤٥°, and ٦٠°. Constant rise, width, and length of the folded plate used in all parametric study.

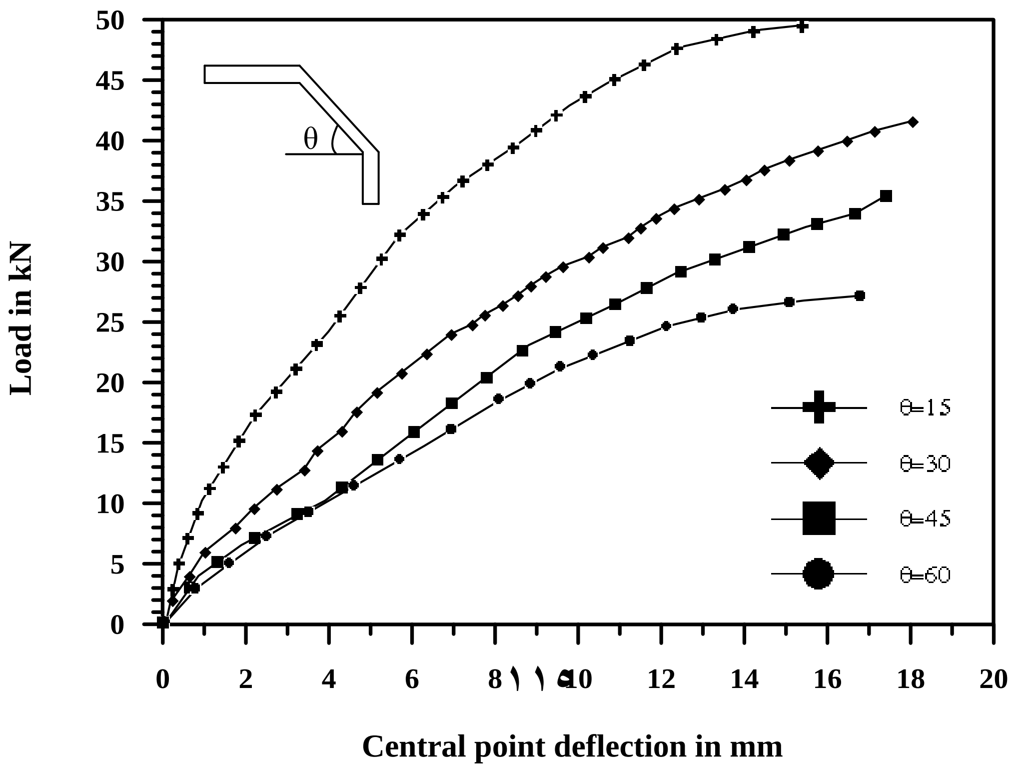

Fig. (٥.١٦) Goble's Folded Plate Effect of

٥.٤.٣ Effect of Reinforcement Ratio

In addition to minimum reinforcement that added to the folded slab in section (٥.٤.١), Goble's folded had two type of reinforcement; the main reinforcement in the plate (short direction reinforcement) and the second one is the edge beam reinforcement. The main and edge beam reinforcement are discussed in the following two sections.

٥.٤.٣.١ Effect Maim Reinforcement

To establish the effect on increasing short direction reinforcement on the structure behavior, Four folded plates with main reinforcement steel area equals (١٠٠٪, ١٥٠٪, ١٧٥٪, and ٢٠٠٪) times the original steel area respectively.

Fig. (٥.١٧) shows the variation of ultimate load with different steel ratio for various inclination angles. This figure shows significant increasing in ultimate load capacity for higher steel ratio when inclination angle is increased. From table (٥.٨) the amount of reinforcement, the increasing in inclination angle and ultimate loads can be noted.

٥.٤.٣.٢ Effect Edge Beam Reinforcement

Different amounts of steel reinforcement have been used in the finite element analysis to establish this aim. The amount of edge beam reinforcement are ١.٥٠, ١.٧٥, and ٢.٠٠ times the actual reinforcement. Fig. (٥.١٨) shows the effect of amount of edge beam reinforcement on the collapse load for different angles.

Parametric Study

The ultimate load capacity of the folded plate shows an increase in its value with the increase in amount of steel reinforcement for various angles.

The ultimate loads obtained from studying this parameter and the properties of different folded plates are listed in table (٥.٩).

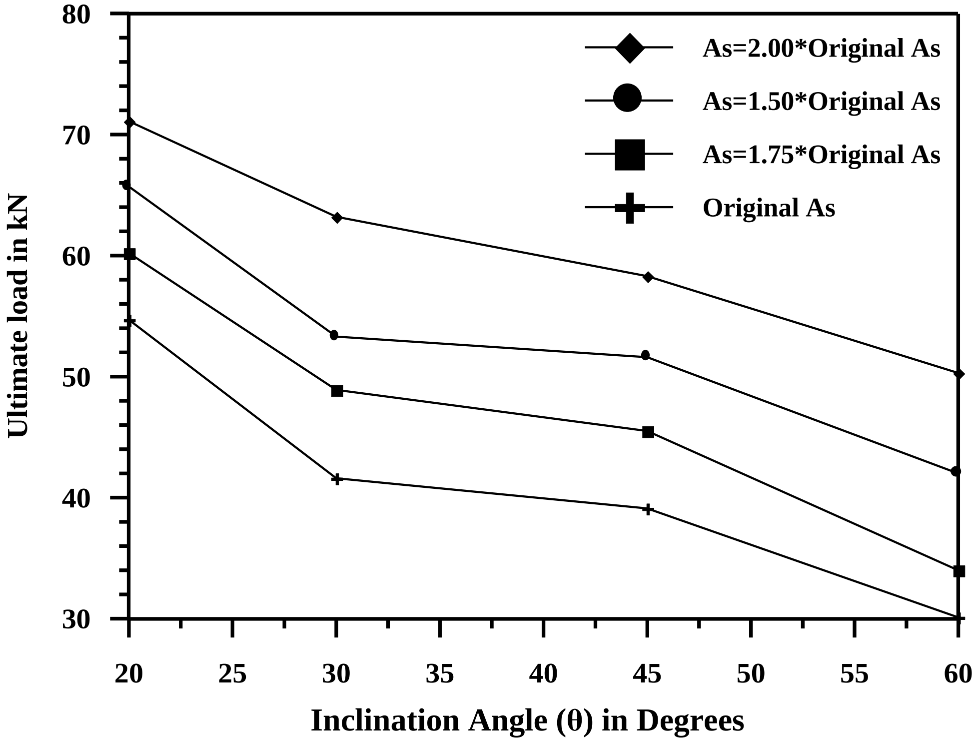

Fig. (٥.١٧) Effect of Short Direction Steel Reinforcement on Load Carrying Capacity for Various Angles

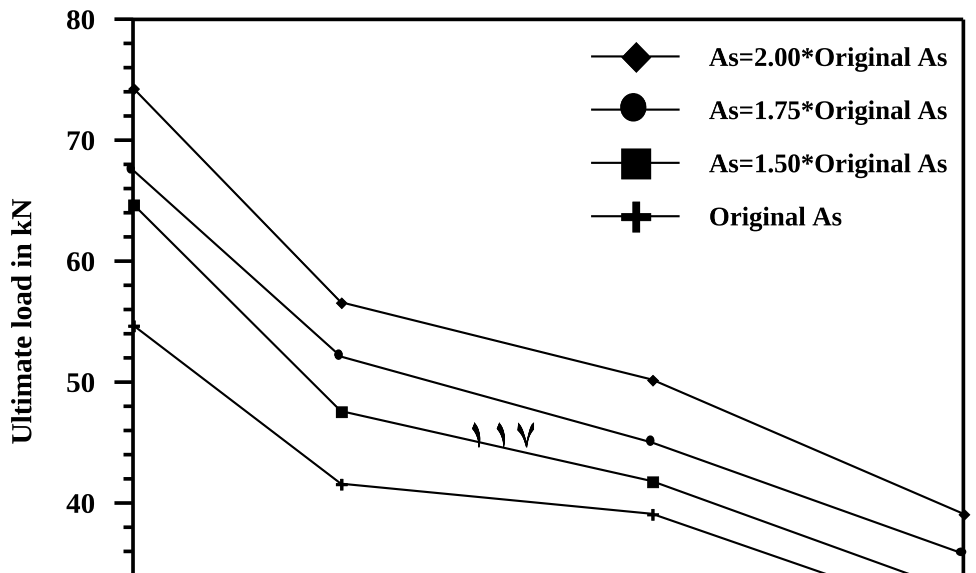

٥.٤.٤ Effect of Folded Plate Thickness

The folded plate thickness is another important factor that affects the behavior of this structure. In order to investigate the effect of plate thickness on the load carrying capacity and load-deflection relationship of folded plates. Four folded plates with different thickness for various inclination angles are analyzed with the other parameters kept constant.

In Figure (٥.١٩), the effect of plate thickness on the overall behavior of the folded plate is demonstrated .The finite element results obtained from analyzing these shells as shown in Figure (٥.١٩), which reveals that the stiffness of the folded plate increases as the thickness increased. Also, the predicted collapse load is clearly increased as the thickness increases. The predicted collapse loads for these folded plates and its properties as given in Table (٥.١٠).

Parametric Study

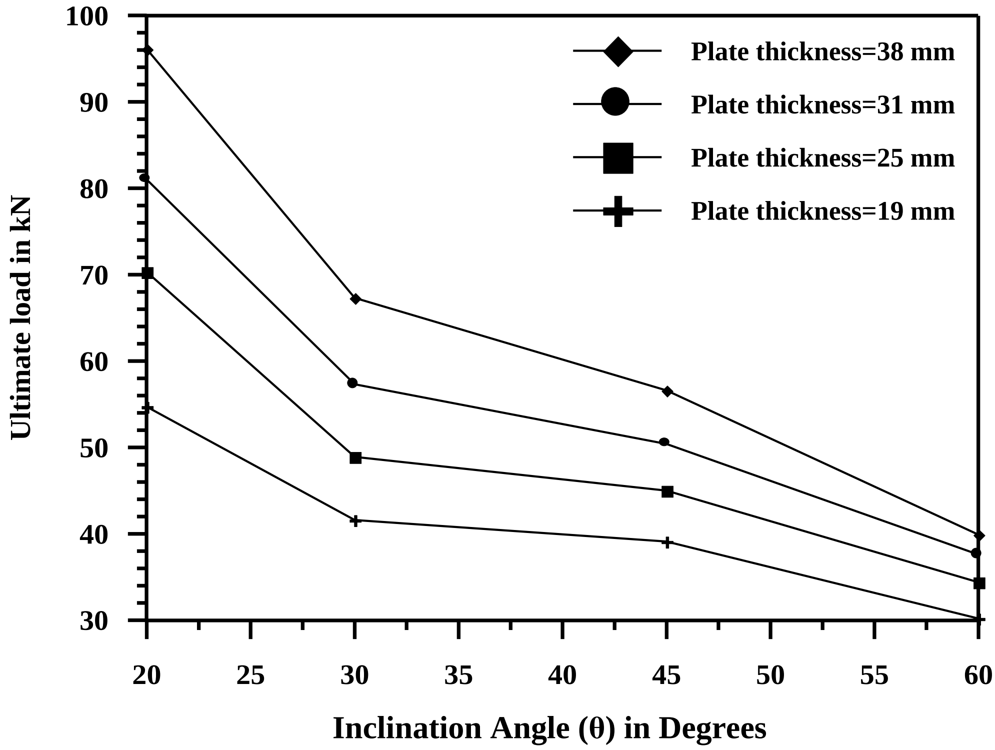

Fig. (٥.١٩) Effect of Folded Plate Thickness on Load Carrying Capacity for Various Angles

٥.٤.٥ Effect of Edge Beam Height

Different beam heights are used to show this aim. These different heights are (٠.٠, ١٢٧, ١٥٠ and ٢٠٠mm) respectively. The enhancement gained from increasing the height of edge beam is to increase the ultimate load carrying capacity.

Fig. (٥.٢٠) shows the different behavior of the ultimate load due to increase or decrease in the height of edge beam and for different inclination angles. It can be seen that the edge beam height becomes a very important parameter and the load carrying capacity increases progressively for small inclination angle. Table (٥.١١) shows the ultimate load for the folded plate used to study this parameter in addition to its properties.

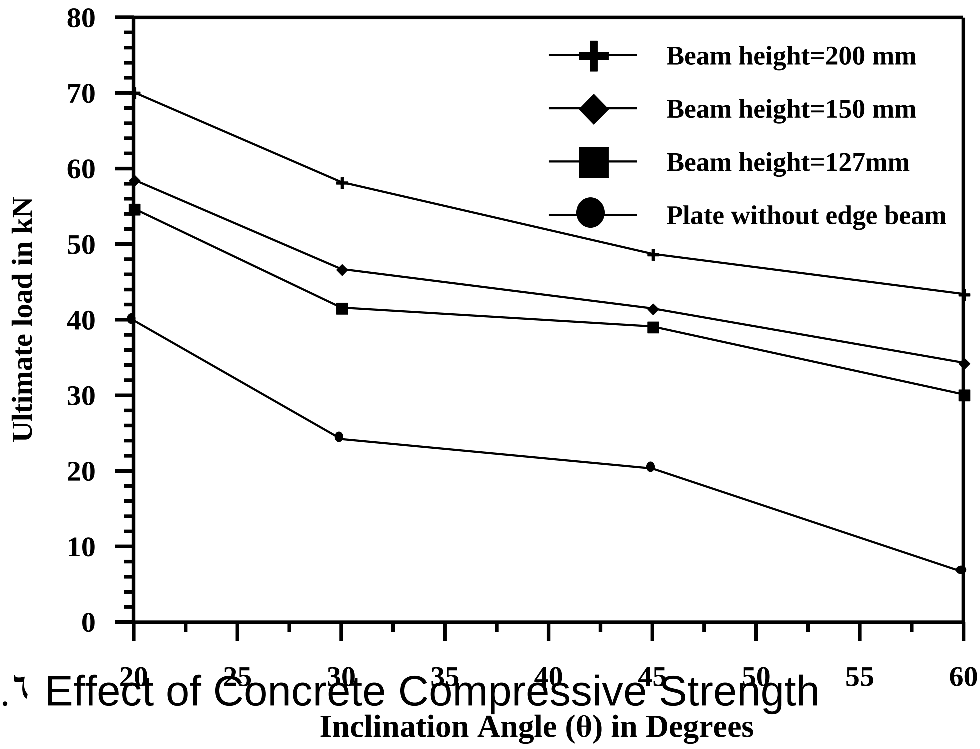

Fig. (٥.٢٠) Effect of Edge Beam Height on Load Carrying Capacity for Various Angles

٥.٤.٦ Effect of Concrete Compressive Strength

To investigate the effect of concrete compressive strength on the improvement in load carrying capacity, the folded plate with compressive strength equal to (٢٤.٢, ٣٠, ٤٠, and ٥٠ MPa) is used.

Fig. (٥.٢١) shows the behavior of ultimate load due to increase in concrete compressive strength for different inclination angles. It can be seen that the load carrying capacity increases with increasing of concrete compressive strength for different inclination angles. Table (٥.١٢) shows the ultimate load and the properties for each folded plate used to study this parameter.

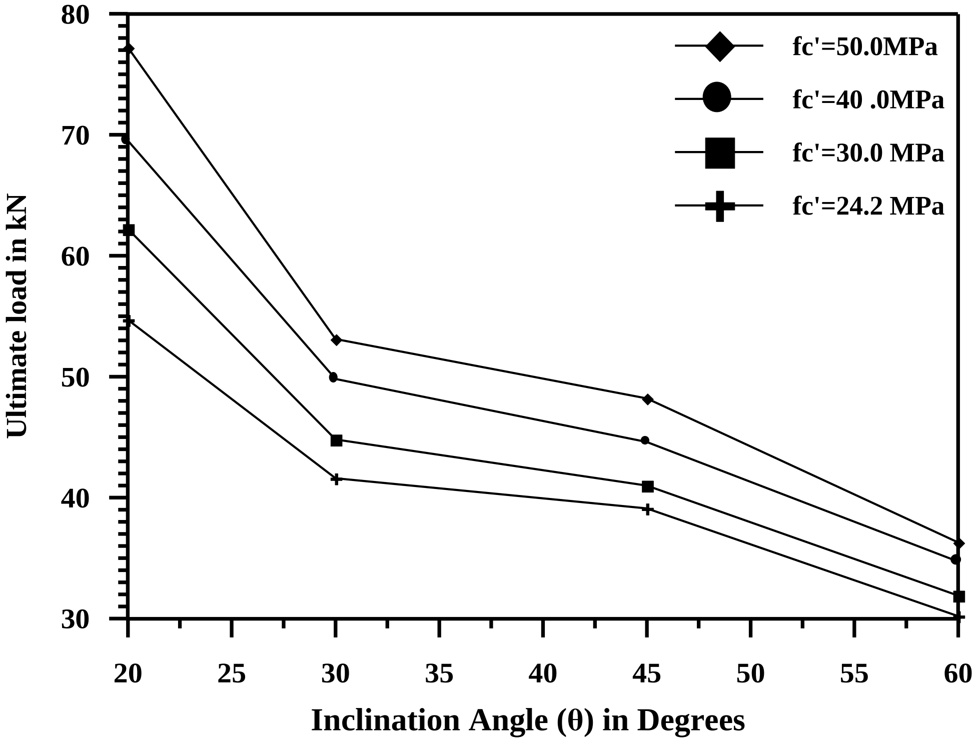

Fig. (٥.٢١) Effect of Concrete Compressive Strength on Load Carrying Capacity for Various Angles

٥.٤.٧ Effect of Steel Grade

In order to present an idea about the effect of increasing the yield stress of steel reinforcement on ultimate collapse load, Goble's folded plate is analyzed for different steel grades. The values of steel grade used to study this parameter are ٣٤٥ and ٤١٤ MPa in addition to the original steel grade (٣٣١ MPa).

The effects of using different inclination angles for different steel grades are shown in Fig. (٥.٢٢). This figure shows a significant increase in predicted ultimate load when the steel grade increases. The predicted collapse loads and the properties for different folded plates used to study this aim are given in Table (٥.١٣).

Parametric Study

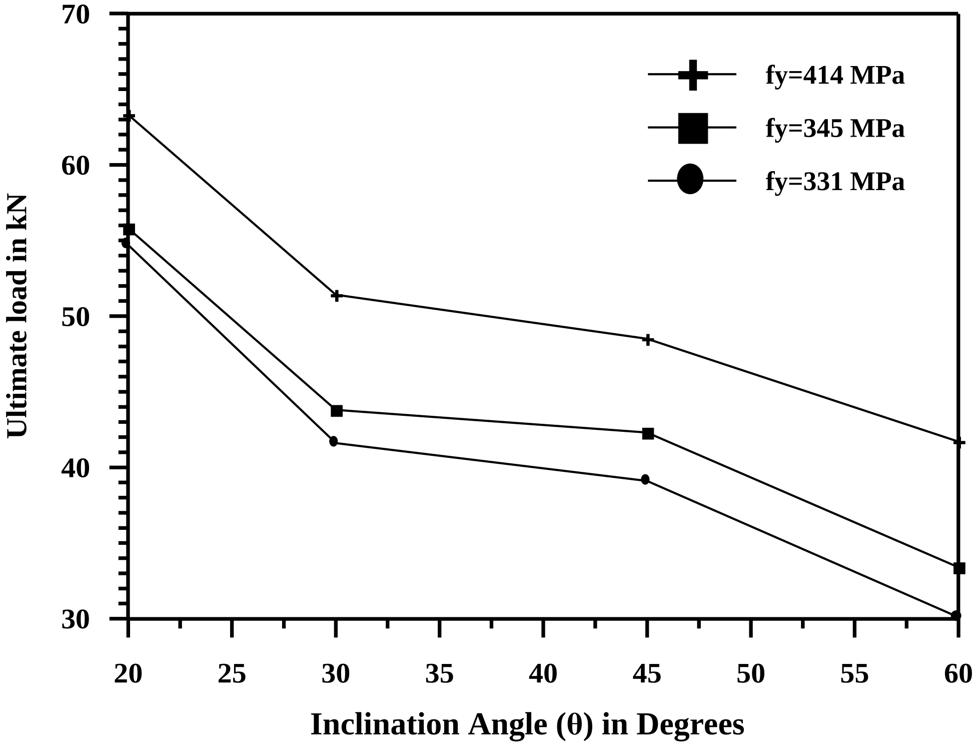

Fig. (٥.٢٢) Effect of Yield Stress of Steel Reinforcement on Load Carrying Capacity for Various Angles

Table (٥.٨) The Predicted Ultimate Load in kN for Different Short Direction Steel Reinforcement

fc' in kpa	fy in kPa	plate thic in mm	beam high. in mm	*pl*	*ps*	*pb*	inclination angle(θ)			
							٢٠	٣٠	٤٥	٦٠
٢٤.٢	٣٣١	١٩	١٢٧	٠.٠٠١٨	٠.٠٢٢٢	٠.٠٣٢٨	٥٤.٧	٤١.٦	٣٩.١	٣٠.٢
٢٤.٢	٣٣١	١٩	١٢٧	٠.٠٠١٨	٠.٠٣٣٣	٠.٠٣٢٨	٦٠.٢	٤٨.٩	٤٥.٥	٣٤
٢٤.٢	٣٣١	١٩	١٢٧	٠.٠٠١٨	٠.٠٣٨٥	٠.٠٣٢٨	٦٥.٧	٥٣.٣	٥١.٦	٤٢
٢٤.٢	٣٣١	١٩	١٢٧	٠.٠٠١٨	٠.٠٤٤٤	٠.٠٣٢٨	٧١.١	٦٣.٢	٥٨.٣	٥٠.٣

Table (٥.٩) The Predicted Ultimate Load in kN for Different Edge Beam Steel Reinforcement

fc' in	fy in kPa	plate	beam	*pl*	*ps*	*pb*	inclination angle(θ)

Parametric Study

kpa		thic in mm	high. in mm				٢٠	٣٠	٤٥	٦٠
٢٤.٢	٣٣١	١٩	١٢٧	٠.٠٠١٨	٠.٠٢٢٢	٠.٠٣٢٨	٥٤.٧	٤١.٦	٣٩.١	٣٠.٢
٢٤.٢	٣٣١	١٩	١٢٧	٠.٠٠١٨	٠.٠٢٢٢	٠.٠٤٩٢	٦٤.٧	٤٧.٦	٤١.٨	٣٢.٥
٢٤.٢	٣٣١	١٩	١٢٧	٠.٠٠١٨	٠.٠٢٢٢	٠.٠٥٧٤	٦٧.٥	٥٢.١	٤٥	٣٥.٨
٢٤.٢	٣٣١	١٩	١٢٧	٠.٠٠١٨	٠.٠٢٢٢	٠.٠٦٥٦	٧٤.٣	٥٦.٦	٥٠.٢	٣٩.١

Table (٥.١٠) The Predicted Ultimate Load in kN for Different Plate Thickness

fc' in kpa	fy in kPa	plate thic in mm	beam high. in mm	*pl*	*ps*	*pb*	inclination angle(θ)			
							٢٠	٣٠	٤٥	٦٠
٢٤.٢	٣٣١	١٩	١٢٧	٠.٠٠١٨	٠.٠٢٢٢	٠.٠٣٢٨	٥٤.٧	٤١.٦	٣٩.١	٣٠.٢
٢٤.٢	٣٣١	٢٥	١٢٧	٠.٠٠١٨	٠.٠٢٢٢	٠.٠٣٢٨	٧٠.٣	٤٨.٩	٤٥	٣٤.٤
٢٤.٢	٣٣١	٣١	١٢٧	٠.٠٠١٨	٠.٠٢٢٢	٠.٠٣٢٨	٨١	٥٧.٣	٥٠.٤	٣٧.٦
٢٤.٢	٣٣١	٣٨	١٢٧	٠.٠٠١٨	٠.٠٢٢٢	٠.٠٣٢٨	٩٦.١	٦٧.٣	٥٦.٦	٣٩.٩

Table (٥.١١) The Predicted Ultimate Load in kN for Different Edge Beam Heights

fc' in kpa	fy in kPa	plate thic in mm	beam high. in mm	*pl*	*ps*	*pb*	inclination angle(θ)			
							٢٠	٣٠	٤٥	٦٠
٢٤.٢	٣٣١	١٩	٠	٠.٠٠١٨	٠.٠٢	٠.٠٣	٣٩.٩	٢٤.٢	٢٠.٣	٦.٦

					٢٢	٢٨				
٢٤.٢	٣٣١	١٩	١٢٧	٠.٠٠١٨	٠.٠٢ ٢٢	٠.٠٣ ٢٨	٥٤.٧	٤١.٦	٣٩.١	٣٠.٢
٢٤.٢	٣٣١	١٩	١٥٠	٠.٠٠١٨	٠.٠٢ ٢٢	٠.٠٣ ٢٨	٥٨.٥	٤٦.٧	٤١.٥	٣٤.٣
٢٤.٢	٣٣١	١٩	٢٠٠	٠.٠٠١٨	٠.٠٢ ٢٢	٠.٠٣ ٢٨	٧٠.١	٥٨.٢	٤٨.٧	٤٣.٤

Table (٥.١٢) The Predicted Ultimate Load in kN for Different Concrete Compressive Strength

fc' in kpa	fy in kPa	plate thic in mm	beam high. in mm	*pl*	*ps*	*pb*	inclination angle(θ)			
							٢٠	٣٠	٤٥	٦٠
٢٤.٢	٣٣١	١٩	١٢٧	٠.٠٠١٨	٠.٠٢	٠.٠٣	٥٤.٧	٤١.٦	٣٩.١	٣٠.٢
٣٠	٣٣١	١٩	١٢٧	٠.٠٠١٨	٠.٠٢	٠.٠٣	٦٢.٢	٤٤.٨	٤١	٣١.٩
٤٠	٣٣١	١٩	١٢٧	٠.٠٠١٨	٠.٠٢	٠.٠٣	٦٩.٥	٤٩.٨	٤٤.٦	٣٤.٧
٥٠	٣٣١	١٩	١٢٧	٠.٠٠١٨	٠.٠٢	٠.٠٣	٧٧.٢	٥٣.١	٤٨.٢	٣٦.٣

Table (٥.١٣) The Predicted Ultimate Load in kN for Different Steel Grades

fc' in kpa	fy in kPa	plate thic in mm	beam high. in mm	*pl*	*ps*	*pb*	inclination angle(θ)			
							٢٠	٣٠	٤٥	٦٠
٢٤.٢	٣٣١	١٩	١٢٧	٠.٠٠١٨	٠.٠٢٢٢	٠.٠٣٢٨	٥٤.٧	٤١.٦	٣٩.١	٣٠.٢
٢٤.٢	٣٤٥	١٩	١٢٧	٠.٠٠١٨	٠.٠٢٢٢	٠.٠٣٢٨	٥٥.٨	٤٣.٨	٤٢.٣	٣٣.٤
٢٤.٢	٤١٤	١٩	١٢٧	٠.٠٠١٨	٠.٠٢٢٢	٠.٠٣٢٨	٦٣.٣	٥١.٤	٤٨.٥	٤١.٧

٥.٥ Mathematical Formula for Prediction of Ultimate Load Capacity for Folded Plate

Parametric Study

Based on finite element results, an equation to estimate the ultimate load for folded plate structures of the considered shape is suggested in the present study by using STATISTIC program as follows:

P = -٤٤٠ + (-٢٥٧.٢٣*fć $^{(-٠.٠١٨٤)}$ **+ ١٨٥.٣٧٣*fy** $^{(-٢٢.٢٥٦)}$ **+ ٨٢٨.٠٦٨*t** $^{(-٠.١٢٢)}$
+ ٠.٠٨٥*hb $^{(٠.٩٢٤)}$ **-٣٧٦.٥٤٨ * *pb*** $^{(-٠.٠١٢)}$ **- ٠.١٥٤٤* *ps*** $^{(-١.٠٥٨٣٦)}$**)*log**$_{١٠}$**(١٧.٤٤٣٨*th) +٩.٥٣٧*log**$_{١٠}$**(t** $^{(٥٢.٩١٤)}$**)**
...(٥.٣)

where , **P** is the ultimate load in kN
fć is the concrete compresive strength in kPa
fy is the yielding stress of steel reinforcement in kPa
t is the thickness of the folded plate in mm, **hb** is the edge beam height in mm
ps, is the steel reinforcement ratio in short direction
pb is the steel reinforcement ratio in edge beam
th is the shell angle in degree
Coefficient of correlation (R=٠.٩٦)

Fig. (٥.٢٣) shows good results obtained from the comparison between the finite element results and the result optioned Eq. **(٥.٣)** for different folded plate thickness.

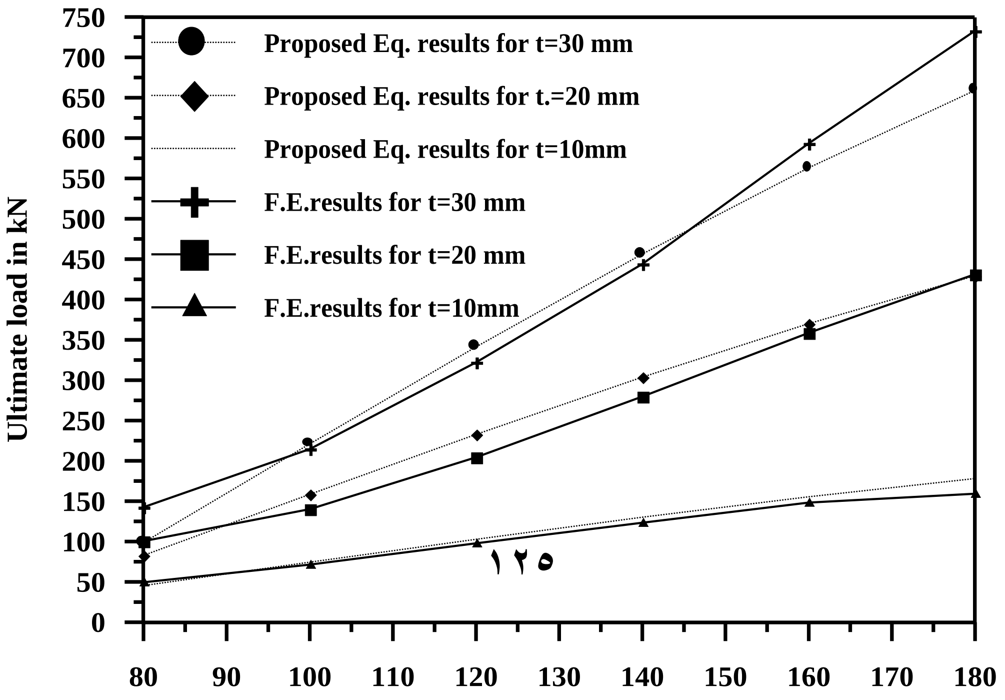

CHAPTER SIX

CONCLUSIONS AND RECOMMENDATIONS FOR FURTHER WORK

٦.١ Conclusions

Based on the results obtained from the finite element procedure, which have been carried out throughout the present work, the following conclusions can be drawn:

١. The finite element results obtained for the reinforced concrete shell and the reinforced concrete folded plate show that the computational model adopted in this study is suitable for prediction of the load-deflection behavior and collapse load. The numerical results obtained from the different case studies reveal that the predicted load-deflection curves and collapse loads are in good agreement with the available experimental results.

٢. It was found that using isoparametric ٢٠-node brick element is proved to be efficient for folded plate and cylindrical shell structural discretiztion. The numerical tests carried out for the two structures show that the inclusion of the geometric nonlinearity together with material nonlinearity in the finite element model significantly improve the predicted load-deflection behavior and collapse load at all stages of loading.

٣. The effect of the type of the integration rule was found to have a significant effect on the predicted behavior and the computed collapse load. The ١٥a-point integration rule showed better agreement with experimental results

٤. A significant enhancement is found in the finite element results for the mesh contains end diaphragm.

٥. It was noticed that modeling the steel bars as axial members embedded in the brick element gives better results than the smeared layers of equivalent thickness throughout the shell element approach.

٦. For the cases analyzed, the results showed that the shell angle was the most pronounced factor that affected the load-deflection behavior and load carrying capacity of the shell due to the presence of membrane action. Also, the inclination angle in folded plate played a major parameter that affects load carrying capacity.

٧. From the parametric studies carried out on the cylindrical shell and the folded plate, it was found that the increase of thickness was a pronounced effect on load-deflection behavior.

٨. According to the results obtained, it can be concluded that the increase of edge beam height gives a noticed increase in the collapse load especially for higher shell angles. Also, the absence or the decrease in the edge beam height decreases the failure load.

٩. It was found that in cylindrical shells, the effect of steel reinforcement is not a significant parameter on the load carrying capacity. This can be attributed to the presence of membrane action in this structure, while for the folded plate the collapse load showed a significant increase when then main reinforcement increases.

١٠. The finite element results show that as the compressive strength of concrete increases the ultimate collapse load increases progressively for the cylindrical shell and the folded plate shows less increase.

٦.٢ Recommendations for Further Work

Some suggestions are given below for possible improvement of the formulation and extension of this investigation:

Recommendations for Further Work

١. The inclusions of strain softening behavior of concrete and using a numerical procedure such as the arc-length method or displacement control. This can improve the structural response beyond the ultimate load level and increase its accuracy.

٢. Extension of the material model adopted in the present study to include the long-term effect on the concrete behavior (creep and shrinkage) as well as cyclic loading.

٣. Wider studies on folded plates and cylindrical shells with variable span length and width and different boundary conditions in addition to the parameters that were studied in this work.

٤. Finding an empirical equation, which takes into account the above suggestions to evaluate the ultimate load capacity for these types of structures.

٥. Making more experimental studies on cylindrical shells and folded plates with different boundary conditions and comparing the results with the present numerical results.

APPENDIX

A

Subroutine BRK١٤ used to calculate shape function and it's derivative for ١٤-node brick element.

```
      SUBROUTINE BRK١٤(FUN,IFUN,DER,IDER,JDER,X,Y,Z,ITEST)
      IMPLICIT REAL*٨ (A-H,O-Z)
      DIMENSION FUN(IFUN),DER(IDER,JDER)
      ITEST=٠
      A=X-١.٠
      AA=١.٠+X
      B=Y-١.٠
      BB=١.٠+Y
      C=Z-١.٠
      CC=١.٠+Z
      XY=X*Y
      XZ=X*Z
      YZ=Y*Z
C
   FUN(١)=٠.١٢٥*((XY+XZ+YZ+٢.٠*(X+Y+Z+١.٠))*A*B*C
   DER(١,١)=٠.١٢٥*(٢.٠*XY+٢.٠*XZ+٤.٠*X+YZ+Y+Z)*B*C
   DER(٢,١)=٠.١٢٥*(٢.٠*XY+XZ+X+٢.٠*YZ+٤.٠*Y+Z)*A*C
   DER(٣,١)=٠.١٢٥*(XY+٢.٠*XZ+X+٢.٠*YZ+Y+٤.٠*Z)*A*B
C
   FUN(٢)=٠.١٢٥*((XY-XZ+YZ+٢.٠*(-X+Y-Z-١.٠))*A*BB*C
   DER(١,٢)=٠.١٢٥*(٢.٠*XY-٢.٠*XZ-٤.٠*X+YZ+Y-Z)*BB*C
   DER(٢,٢)=٠.١٢٥*(٢.٠*XY-XZ-X+٢.٠*YZ+٤.٠*Y-Z)*A*C
   DER(٣,٢)=٠.١٢٥*(XY-٢.٠*XZ-X+٢.٠*YZ+Y-٤.٠*Z)*A*BB
C
   FUN(٣)=٠.١٢٥*((XY+XZ-YZ+٢.٠*(X-Y-Z-١.٠))*AA*B*C
   DER(١,٣)=٠.١٢٥*(٢.٠*XY+٢.٠*XZ+٤.٠*X-YZ-Y-Z)*B*C
   DER(٢,٣)=٠.١٢٥*(٢.٠*XY+XZ+X-٢.٠*YZ-٤.٠*Y-Z)*AA*C
   DER(٣,٣)=٠.١٢٥*(XY+٢.٠*XZ+X-٢.٠*YZ-Y-٤.٠*Z)*AA*B
C
   FUN(٤)=٠.١٢٥*((XY-XZ-YZ+٢-)*٠.X-Y+Z+١.٠))*AA*BB*C
   DER(١,٤)=٠.١٢٥*(٢.٠*XY-٢.٠*XZ-٤.٠*X-YZ-Y+Z)*BB*C
   DER(٢,٤)=٠.١٢٥*(٢.٠*XY-XZ-X-٢.٠*YZ-٤.٠*Y+Z)*AA*C
   DER(٣,٤)=٠.١٢٥*(XY-٢.٠*XZ-X-٢.٠*YZ-Y+٤.٠*Z)*AA*BB
C
   FUN(٥)=-٠.١٢٥*((XY-XZ-YZ+٢.٠*(X+Y-Z+١.٠))*A*B*CC
   DER(١,٥)=-٠.١٢٥*(٢.٠*XY-٢.٠*XZ+٤.٠*X-YZ+Y-Z)*B*CC
   DER(٢,٥)=-٠.١٢٥*(٢.٠*XY-XZ+X-٢.٠*YZ+٤.٠*Y-Z)*A*CC
   DER(٣,٥)=-٠.١٢٥*(XY-٢.٠*XZ+X-٢.٠*YZ+Y-٤.٠*Z)*A*B
C
   FUN(٦)=-٠.١٢٥*((XY+XZ-YZ+٢.٠*(-X+Y+Z-١.٠))*A*BB*CC
   DER(١,٦)=-٠.١٢٥*(٢*٠.XY+٢.٠*XZ-٤.٠*X-YZ+Y+Z)*BB*CC
   DER(٢,٦)=-٠.١٢٥*(٢.٠*XY+XZ-X-٢.٠*YZ+٤.٠*Y+Z)*A*CC
   DER(٣,٦)=-٠.١٢٥*(XY+٢.٠*XZ-X-٢.٠*YZ+Y+٤.٠*Z)*A*BB
C
   FUN(٧)=-٠.١٢٥*((XY-XZ+YZ+٢.٠*(X-Y+Z-١.٠))*AA*B*CC
   DER(١,٧)=-٠.١٢٥*(٢.٠*XY-٢.٠*XZ+٤.٠*X+YZ-Y+Z)*B*CC
   DER(٢,٧)=-٠.١٢٥*(٢.٠*XY-XZ+X+٢.٠*YZ-٤.٠*Y+Z)*AA*CC
```

```
      DER(٣,٧)=-٠.١٢٥*(XY-٢.٠*XZ+X+٢.٠*YZ-Y+٤.٠*Z)*AA*B
C
      FUN(٨)=-٠.١٢٥*((XY+XZ+YZ+٢.٠*(-X-Y-Z+١.٠))*AA*BB*CC
      DER(١,٨)=-٠.١٢٥*(٢.٠*XY+٢.٠*XZ-٤.٠*X+YZ-Y-Z)*BB*CC
      DER(٢,٨)=-٠.١٢٥*(٢.٠*XY+XZ-X+٢.٠*YZ-٤.٠*Y-Z)*AA*CC
      DER(٣,٨)=-٠.١٢٥*(XY+٢.٠*XZ-X+٢.٠*YZ-Y-٤.٠*Z)*AA*BB
C
      FUN(٩)=-٠.٥*AA*A*B*C
      DER(١,٩)=-BB*B*C*X
      DER(٢,٩)=-AA*A*C*Y
      DER(٣,٩)=-٠.٥*AA*A*BB*B
C
      FUN(١٠)=٠.٥*AA*A*BB*B*CC
      DER(١,١٠)=BB*B*CC*X
      DER(٢,١٠)=AA*A*CC*Y
      DER(٣,١٠)=٠.٥*AA*A*BB*B
C
      FUN(١١)=-٠.٥*AA*A*B*CC*C
      DER(١,١١)=-B*CC*C*X
      DER(٢,١١)=-٠.٥*AA*A*CC*C
      DER(٣,١١)=-AA*A*B*Z
C
      FUN(١٢)=٠.٥*AA*A*BB*CC*C
      DER(١,١٢)=BB*CC*C*X
      DER(٢,١٢)=٠.٥*AA*A*CC*C
      DER(٣,١٢)=AA*A*BB*Z
C
      FUN(١٣)=-٠.٥*A*BB*B*CC*C
      DER(١,١٣)=-٠.٥*BB*B*CC*C
      DER(٢,١٣)=-A*CC*C*Y
      DER(٣,١٣)=-A*BB*B*Z
C
      FUN(١٤)=٠.٥*AA*BB*B*CC*C
      DER(١,١٤)=٠.٥*BB*B*CC*C
      DER(٢,١٤)=AA*CC*C*Y
      DER(٣,١٤)=AA*BB*B*Z
C
      RETURN
      END
```

REFERENCES

١. Abbasi, M. S. A., Baluch, M. H., Azad, A. K., and Abdel-Rahman, H. H., "**Nonlinear Finite Element Modeling of Failure Modes in Reinforced Concrete Slabs** ", Int. J. of Computers and Structures, Vol. ٤٢, No. ٣, ١٩٩٢, pp. ٨١٥-٨٢٣.

٢. Abdel-Rahman, H.H. and Hinton, E., "**Nonlinear Finite Element Analysis of Reinforced Concrete Stiffened and Cellular Slabs**", J. of Computer and Structures, Vol.٢٣,No.٣,١٩٨٦, pp. ٣٣٣-٣٥٠.

٣. ACI-Committee ٣١٨, " **Building Code Requirements for Structural Concrete (ACI ٣١٨M-٩٥)** ", American Concrete Institute, Detroit, Michigan, ١٩٩٥.

٤. Ahmad, S., Irons, B.M. and Zienkiewicz, O.C., "**Analysis of Thick and Thin Shell Structures by Curved Finite Elements** ", Inter. J. Num. Meth. Engng., Vol.٢, No.٣, ١٩٧٠, pp.٤١٩-٤٥١.

٥. Al-Khuza'y, A. N. A., " **Nonlinear Finite Element Analysis of Reinforced Concrete Shells and Ribbed Shells** ", M.Sc. Thesis, University of Technology, ٢٠٠١.

٦. Al – Mahaidi, R. S. H.. " **Nonlinear Finite Element Analysis of Reinforced Concrete Deep Members** " Structural Engineering Research Report No. ٣٨, Department of Civil Engineering, University of Alberta, ١٩٧١.

٧. Argyris, J. H. and Kelsey, S., " **Structural Analysis by the Matrix Force Method with Applications to Aircraft Wings** ", Wiss. Ges. Luftfahrt Jahrb. , ١٩٥٦, pp. ٨٠٥-٨٢٣.

٨. Arnesen, A., Sorensen, S. and Bergan, P. G., " **Nonlinear Analysis of Reinforced Concrete** ", Int. J. of Computers and Structures, Vol. ١٢, No. ٤, ١٩٨٠, pp. ٥٧١-٥٧٩.

٩. ASCE Committee on Concrete and Masonary Structures. "**A State of The Art Report on The Finite Element Analysis of Reinforced Concrete**" Task Committee on Finite Element Analysis of Reinforced Concrete Structures, ASCE Special Publication, ١٩٨١. [mentioned in Husain (٢٠٠٢)]

References

١٠. Al-Shaarbaf, I. A. S., " **Three-Dimensional Nonlinear Finite Element Analysis of Reinforced Concrete Beams in Torsion** ", Ph.D. Thesis, University of Bradford, ١٩٩٠.

١١. Baka, H. A., " **Nonlinear Finite Element Analysis of Flat and Slightly Curved Concrete Slabs Using Shell Element** ", M.Sc. Thesis, University of Babylon, ٢٠٠٢.

١٢. Bathe, K. J.," **Finite Element Procedures** " Prentice – Hall, Inc., ١٩٩٦.

١٣. Bathe, K.J. and Bolourchi, S., "**A Geometrical and Material Nonlinear Plate and Shell Element** ", J. of Computers and Structures, Vol.١١, ١٩٨٠, pp.٢٣-٤٨.

١٤. Bathe, K. J. and Ho, L.W. "**A Simple and Effective Element for Analysis of General Shell Structures** ", J. of Computers and Structures, Vol.١٣, ١٩٨١, pp. ٦٧٣-٦٨١.

١٥. Bathe, K. J., Ramaswamy, S., " **On Three – Dimensional Nonlinear Analysis of Concrete Structures** " Nuclear Engineering and Design, Vol. ٥٢, ١٩٧٩, pp. ٣٨٥ – ٤٠٩.

١٦. Bergan, P. G., and Holand, I., " **Nonlinear Finite Element Analysis of Concrete Structures** ", Comp. Meth. in App. Mech. and Eng., Vol. ١٧/١٨, Part I, Jan., ١٩٧٩, pp. ٤٤٣-٤٦٧.

١٧. Bouma, A. L., Van Riel, A. C.,Van Coten, H. and Beranek, W. J., "**Ivestigation on Models of Eleven Cylindrical Shells Made of Reinforced and Prestressed Concrete** ", Proceedings of the Symposium on Shell Research, Delft, Sept.١٩٦١, pp. ٧٩-١٠١.

١٨. Bresler, B. and Pister, K.S., " **Strength of Concrete under Combined Stresses** ", ACI Journal Vol.٣٠, No.٩, Sept., ١٩٥٨, pp.٣٢١-٣٤٥.

١٩. Buyukozturk, O., " **Nonlinear Analysis of Reinforced Concrete Structures**", Int. J. of Computers and Structures, Vol. ٧, No. ١, ١٩٧٧, pp. ١٤٩-١٥٦.

٢٠. Cervera, M., Hinton, E. and Hassan, O., " **Nonlinear Analysis of Reinforced Concrete Plate and Shell Structures Using ٢٠-Noded Isoparametric Brick Element** ", J. of Computers and Structures, Vol. ٢٥, No. ٦, ١٩٨٧.pp.٨٤٥-٨٦٩

References

٢١. Chen, W. F., " **Plasticity in Reinforced Concrete** ", McGraw-Hill Book Co., New York, ١٩٨٢.

٢٢. Chen, W. F., and Saleeb, A. F., " **Constitutive Equations for Enginerring Materials: Elasticity and Modeling** ", Vol. ١, John Wiley and Sons, New York, ١٩٨٢.

٢٣. Cook, R. D., " **Concept and Application of Finite Element Analysis** ", John Wiley and Sons, Inc., New York. ١٩٧٤.

٢٤. Dawe, D. J., " **Matrix and Finite Element Displacement Analysis of Structures** ", Clarendon Press, Oxford, U.K., ١٩٨٤.

٢٥. Edwards, N. P., and Billington, D, P., " **FE Analysis of Tucker High School Roof using Nonlinear Geometry and Creep** ", J. of Str. Eng., ASCE, Vol. ١٢٤, No. ٩, Sep., ١٩٩٨, pp. ٩٨٤-٩٩١.

٢٦. Guice, L. K., Slawson, T.R., and Rhomberg, E. J., " **Membrane Analysis of Flat Plate Slabs** ", ACI Structural J., Jan.-Feb., ١٩٨٩, pp.٨٣-٩٢.

٢٧. Goble, G. G., " **Reinforced Concrete Folded Plate Behavior** ", Large Span Shells, Proceedings, IASS Congress, USSR, Leningrad, (Sept. ٦-٩, ١٩٦٦) [mentioned in Thannon ١٩٨٨].

٢٨. Hand, F. R., Pecknold, D. A., and Schnobrich, W. C., " **Nonlinear Layered Analysis of Reinforced Concrete Plates and Shells** ", J. of Str. Div., ASCE, Vol. ٩٩, No. ST٧, July, ١٩٧٣, pp. ١٤٩١-١٥٠٥.

٢٩. Hrenikoff, A., **"Solution of Problems in Elasticity by the Framework Method**", J. Appl. Mech., Vol.٨, ١٩٤١, pp.١٦٩-١٧٥.

٣٠. Hu, H.T. and Schnobrich, W.C., " **Nonlinear Analysis of Cracked Reinforced Concrete** ", ACI Struct. J., Vol.٨٧, No.٢ March April, ١٩٩٠, pp.١٩٩-٢٠٧.

٣١. Huang, H.C., " **Implementation of Assumed Strain Degenerated Shell Element** ", J. of Computer and Structures, Vol.٢٥, No.١, ١٩٨٧, pp.١٤٧-١٥٥.

٣٢. Irons, B. M., " **Quadrature Rule for Brick Based Finite Elements** ", Int. J. for Num. Meth. in Eng., Vol. ٣, No. ٢, April-June, ١٩٧١, pp. ٢٧٥-٢٩٠.

٣٣. Kabir, A.F, " **Nonlinear Analysis of Reinforced Concrete Panels, Slabs and Shells for Time Dependent Effects** ", Ph.D. Dissertation, Division of

Structural Engineering and Structural Mechanics, University of California, Berkeley, UC-SESM Report, No.٧٦-٦, Dec.١٩٧٦.

٣٤. Kupfer, H.B. and Gerstle, K.H., “ **Behavior of Concrete Under Biaxial Stresses** ”, ASCE J. of Engineering Mechanics Division, Vol.٩٩, No.EM٤, August ١٩٧٣, pp.٨٥٣-٨٦٦.

٣٥. Lin, C.S. and Scordelis, A.C., “ **Nonlinear Analysis of Reinforced Concrete Shells of General Form** ”, J. of the Structural Division, ASCE, Vol.١٠١, No.ST٣, March ١٩٧٥, pp.٥٢٣-٥٣٨.

٣٦. Mawenya, A.S, and Davies, J.D., “ **Finite Element Bending Analysis of Multiplayer Plates** ”, Int. J. of Numerical Methods in Engineering, Vol.٨, ١٩٧٤, pp. ٢١٥-٢٢٥.

٣٧. Mehta, R. P., “ **Concrete Structures: Purposes and Materials** ” Prentice – Hall, Inc.,New Jersey, ١٩٨٦.

٣٨. Mirza, S.A., Hatzinikdas, M. and McGregor, J.G., “ **Statistical Description of Strength in Concrete** ”,ASCE Journal of Structural Engineering Division Vol.١٠٥,No.st٦, June, ١٩٧٩, pp.١٠٢١-١٠٣٧.

٣٩. Moaveni, S., “**Finite Element Analysis Theory and Application with ANSYS**” Prentice – Hall, Inc., New Jersey, ١٩٩٩.

٤٠. Mohamed, M. S., “ **A Finite Element and Experimental Study of Reinforced Concrete in Torsion** ” Ph. D. thesis, University of Glasgow, ١٩٨٦.

٤١. Mohammed, A. Z., “ **Nonlinear Finite Element Analysis of Reinforced Concrete Folded Plates** ”, M.Sc. Thesis, University of Al-Nahrein, ٢٠٠١.

٤٢. Mohammed, N. S., “ **Nonlinear Finite Element Analysis of Ferrocement Roofing Elements** ”, M.Sc. Thesis, University of Technology, ١٩٩٨.

٤٣. Neville, A.M., “ **Properties of Concrete** ”, Pitman Publishing Book, London, ١٩٨١.

٤٤. Nilson, A. H., “ **Finite Element Analysis of Reinforced Concrete** ”, Published by the American Society of Civil Engrineers, New York, ١٩٨٢.

٤٥. Nilson, A. H.and Winter, G., “ **Design of Concrete Structures** ”, McGraw-Hill Book Co., New York, ١٩٨٨.

References

٤٦. Owen, D.R.J., Thannon, A.Y and Bicanic, N. " **Finite Element Model for Ultimate Load Analysis of Reinforced Concrete Stiffened Shells and Folded Slabs** ". CCES-٨٨ International Conference in Computational Engineering Science, (١٠-١٤ April ١٩٨٨), Paper ٣٠ii.

٤٧. Owen, D. R. J, and Hinton, E., " **Finite Element in Plasticity : Theory and Practice** ", Pineridge Press, Swansea, U.K., ١٩٨٠.

٤٨. Phillips, D. V., and Zienkiewicz, O. C., " **Finite Element Nonlinear Analysis of Concrete Structures** ", Proc. Inst. of Civ. Engr., Part ٢, Vol. ٦١, Mar., ١٩٧٦, pp. ٥٩-٨٨.

٤٩. Scanlon, A., " **Time Dependent Deflections of Reinforced Concrete Slabs**" Ph. D. thesis, University of Alberta, ١٩٧١. [mentioned in Al – Shaarabaf (١٩٩٠)]

٥٠. Scanlon, A. and Murry, D.W., " **Time-Dependent Reinforced Concrete Slab Deflection** ", ASCE J. of Structure Divisions, Vol.١٠٠, ST٩, ١٩٧٤, pp.١٩١١-١٩٢٤.

٥١. Schnobrich, W.C., " **Behavior of Reinforced Concrete Structures Predicted by Finite Element Method** ", Computer and Structures, Vol.٧, ١٩٧٧, pp.٣٦٥-٣٧٦.

٥٢. Scordelis, A.C., "**Finite Element Analysis of Reinforced Concrete Structures**", Proc. Special Conference on the Finite Element Method in civil Eng., pp.٧١-١١٣. McGill, University of Montreal, Canada, June ١٩٧٢.

٥٣. Smith, I., M. and Griffiths, D. V., " **Programming the Finite Element Method** ", ٣rd Edition, John Wiley & SONS Ltd., ١٩٩٨.

٥٤. Smith, I., M. and Kidger, D. J., " **Elastoplastic Analysis Using The ١٤-node Brick Element Family** ", Int. J. Num. Meth. Eng., ٣٥, ١٩٩٢. pp.١٢٦٣-١٢٧٥

٥٥. Suidan, M.T. and Schnobrich, W.C., "**Finite Element Analysis of Reinforced Concrete**", J. of Stut. Div., ASCE, Vol.٩٩, No.ST-١٠, October ١٩٧٣, pp.٢١٠٩-٢١٢٢.

٥٦. Tasuji, M. E., Slate, F. O., and Nilson, A. H., " **Stress-Strain Response and Fracture of Concrete in Biaxial Loading** ", J. of ACI, Vol. ٧٥, No. ٧, July, ١٩٧٨, pp. ٣٠٦-٣١٢.

References

٥٧. Thannon, A.Y, Bicanic, N and Owen, D.R.J., " **Ultimate Load Analysis of Eccentrically Stiffened Shell Structures** ", IABSE Colloquium, in Computational Mechanics of Concrete Structure-Advances and Applications, Proceedings, Delft, (١٩٨٧), pp.٣٦٧-٣٨٢.

٥٨. Thannon, A.Y., " **Ultimate Load Analysis of Reinforced Concrete Stiffened Shells and Folded Slabs Used in Architectural Structures** ", Ph.D. Thesis, University College of Swansea, ١٩٨٨.

٥٩. Timoshenko, S. P. and Goodier, J. N., " **Theory of Elasticity** ", McGraw-Hill, New York, ١٩٥١

٦٠. Tirupathi, R. Chandrupatla and Ashok D. Belegundu, "**Introduction to Finite Elements in Engineering**", Prentice-Hall, U.S.A., ١٩٩٦.

٦١. Turner, M. J., Clough, R. W., Martin, H. C. and Topp, L. J., "**Stiffness and Deflection Analysis of Complex Structures** ", J. Aeronaut. Soc., Vol.٢٣, No.٩, ١٩٥٦, pp.٨٠٥-٨٢٣. [mentioned in Al-Khuza'y (٢٠٠١)]

٦٢. Usama, A., " **Nonlinear Finite Element Analysis of One-Way Partially Restrained Slabs** ", M.Sc Thesis, University of Baghdad, March, ١٩٩٧.

٦٣. Valliappan, S., and Doolan, T. F., " **Nonlinear Stress Analysis of Reinforced Concrete** ", J. of Str. Div., ASCE, Vol. ٩٨, No. ST٤, Apr., ١٩٧٢, pp. ٨٨٥-٨٩٧.

٦٤. Zienkiewicz, O. C., " **The Finite Element Method** ", ٣rd Edition, McGraw-Hill Book Co., New York, ١٩٧٧.

٦٥. Ziekiewicz, O.C. Taylor, R.L. and Too, J.M., " **Reduced Integration Technique in General Analysis of Plates and Shells** ", Int. J. Num. Meth. Eng., Vol.٣, No.٢, ١٩٧١, pp.٢٧٥-٢٩٠.